SOIL MECHANICS AND BITUMINOUS MATERIALS
RESEARCH LABORATORY

DESIGN CONSIDERATIONS FOR ASPHALT PAVEMENTS

by

C. L. MONISMITH

D. B. McLEAN

and

N. OGAWA

REPORT NO. TE 73-5

to

THE TRANSPORTATION LABORATORY
DIVISION OF HIGHWAYS
STATE OF CALIFORNIA
DEPARTMENT OF TRANSPORTATION

PREPARED IN COOPERATION WITH
THE UNITED STATES DEPARTMENT OF TRANSPORTATION
FEDERAL HIGHWAY ADMINISTRATION

TE73-5
DNA

DEPARTMENT OF CIVIL ENGINEERING
INSTITUTE OF TRANSPORTATION AND TRAFFIC ENGINEERING

University of California · Berkeley

ClibPDF - www.fastio.com

TECHNICAL REPORT STANDARD TITLE PAGE

1 REPORT NO.	2 GOVERNMENT ACCESSION NO.	3. RECIPIENT'S CATALOG NO.
4 TITLE AND SUBTITLE Design Consideration for Asphalt Pavements		5 REPORT DATE December 1973 6 PERFORMING ORGANIZATION CODE 19301-633153
7 AUTHOR(S) Monismith, C.L., McLean, D. B., and Ogawa, N.		8 PERFORMING ORGANIZATION REPORT NO. TE 73-5
9 PERFORMING ORGANIZATION NAME AND ADDRESS Office of Research Services University of California Berkeley, California 94720		10 WORK UNIT NO. 11 CONTRACT OR GRANT NO D-6-1
12. SPONSORING AGENCY NAME AND ADDRESS Department of Transportation Division of Highways Sacramento, California 95807		13 TYPE OF REPORT & PERIOD COVERED Interim 1-1-13 to 12-31-73 14. SPONSORING AGENCY CODE RTA 13945-191202 UCB

15 SUPPLEMENTARY NOTES

Conducted in cooperation with U. S. Department of Transportaton, Federal Highway Administration.

16 ABSTRACT

This report describes some research which has been completed to permit estimation of the accumulation of permanent deformation from repeated traffic loading in asphalt-bound layers resting directly on subgrade.

Constitutive relationships which attempt to define the distortion characteristics of a fine-grained soil as a function of water content, dry density, stress state, and number of stress repetitions are presented. In addition such relationships for asphalt concrete as a function of time of loading, temperature, and stress state are developed.

The data for the asphalt concrete have been incorporated in analysis procedures using both layered elastic and viscoelastic theory to represent pavement response to load to illustrate a preliminary framework by means of which rutting in the asphalt bound layer can be estimated.

17 KEY WORDS	18 DISTRIBUTION STATEMENT
Asphalt Concrete Pavements Permanent deformation Subgrade soil Layered elastic analysis	unlimited

19 SECURITY CLASSIF (OF THIS REPORT)	20. SECURITY CLASSIF. (OF THIS PAGE)	21 NO OF PAGES	22. PRICE
Unclassified	unclassified		

HMRT - 1242 (ORIG 9/72)

ClibPDF - www.fastio.com

Soil Mechanics and Bituminous Materials
Research Laboratory

DESIGN CONSIDERATIONS FOR ASPHALT PAVEMENTS

A Report on an investigation

by

C. L. Monismith
Professor of Civil Engineering
and Research Engineer

D. B. McLean
E. W. Brooker and Associates
Calgary, Alberta, Canada
formerly, Research Assistant

and

N. Ogawa
Engineer
Japanese Public Highway Corporation
Tokyo, Japan
formerly, Research Assistant

to
The Transportation Laboratory
Division of Highways
State of California
Department of Transportation

Under
Research Technical Agreement 13945-191202 UCB
HPR-DR-1(9) D 0601

Prepared in Cooperation with
The United States Department of Transportation
Federal Highway Administration

Report No. TE 73-5, Office of Research Services
University of California, Berkeley, California
December 1973

ClibPDF - www.fastio.com

INTRODUCTION

Previous research (e.g., that reported in TE 70-5 (1)) has provided some suggested guidelines for improved pavement and asphalt mix design to assist in minimizing the fatigue mode of distress. One of the recommendations stated that as much asphalt as practicable should be used to insure proper fatigue resistance but not so much that rutting might be induced. To develop, in turn, some guidelines for mix design for specific situations (particularly for pavements with thick asphalt-bound layers) it would appear desirable to have a predictive method whereby from laboratory tests the amount of rutting could be predicted in a manner similar to that for fatigue cracking. Research described in this report has been directed to that end.

A subsystem which provides the framework to predict the distortion (rutting) mode of distress is shown in Fig. 1. This report describes some research which has been completed to provide the necessary data to assist in making this subsystem implementable. Specifically, data and procedures are presented which are part of the sections shown as Blocks 9, 10 and 11 in Fig. 1.

For the structural analysis phase (Block No. 9) two methods to estimate stresses and strains are presented, one using elastic theory and the other viscoelastic layer theory.

Constitutive relationships which attempt to define the distortion characteristics of a fine-grained soil as a function of water content, dry density, stress state and number of stress repetitions and an asphalt concrete as a function of time of loading, temperature and stress state (Block 10) are presented. The data for the asphalt concrete have been incorporated in the analysis procedures to illustrate a preliminary framework by means of which rutting in an asphalt-bound layer can be estimated (Block 11).

ClibPDF - www.fastio.com

REPEATED LOAD TESTS ON YGNACIO VALLEY SUBGRADE SOIL

This section describes the results of tests performed on a fine-grained subgrade soil to ascertain the influence of compaction and stress conditions on the accumulation of permanent strain with repeated stress applications.

Equipment

The tests were performed using repeated load equipment similar to that described in Report TE 71-8 (2) capable of accommodating 2.8 in. diameter by 6 in. high specimens*.

Axial and radial deformations were measured by means of LVDT's attached to each specimen. Axial deformations were measured in the central 3 in. of the specimen height; radial deformations were measured at mid height.

To minimize the influence of creep deformations on the measured radial strains, the LVDT's for these measurements were suspended from the upper clamps of the vertical measuring device with four flexible springs and bonded to the membrane with epoxy resin.

Material and Specimen Preparation

One material has been tested thus far -- a silty clay** representative of the subgrade from a portion of Ygnacio Valley Road, Contra Costa County (Report TE 70-5 (1) contains a more detailed description of this material).

The density vs. water content relationship determined in the modified AASHO compaction test is shown in Fig. 2. As noted in the figure, specimens

---

* Appendix D contains a brief description of the equipment for the convenience of the reader.

** Liquid limit = 35, plasticity index 15.

ClibPDF - www.fastio.com

were prepared at dry densities in the range 90 to 95% of the maximum value obtained in the modified AASHO compaction test and at water contents in the range 16 to 20 percent. For convenience these conditions have been labeled as shown in Fig. 2. By selecting the three conditions shown in this figure it was planned to cover a range in soil conditions that might be obtained in-situ.

Static compaction was used to prepare the specimens since it is thought to induce structures at high degrees of saturation similar to those obtained by field compaction dry of the line of optimums and subsequently soaked (3).

Test Procedures

The test program to date has consisted of: (1) tests in which samples were subjected to single values of deviator stress (in the range 5 to 20 psi)* repeatedly applied, generally for 10,000 stress applications although some specimens were subjected to 100,000 stress applications; and (2) tests with sequential loading to ascertain the influence of stress history on the accumulation of permanent deformation.

In the stress history tests, two different conditions were utilized:

(1) Increasing sequence -- with 10,000 applications each of 5 psi, 10 psi, and 20 psi.

(2) Variable sequence:

(a) 2,000 applications each with 3 psi, 5 psi, and 10 psi

(b) 2,000 applications each with 5 psi, 3 psi, and 10 psi

(c) 2,000 applications each with 10 psi, 5 psi, and 3 psi.

---

* This range in axial stresses was selected in part because measurable values of permanent deformation could be obtained with the recording equipment which was used.

ClibPDF - www.fastio.com

For convenience all specimens were tested at a confining pressure of 5 psi*. Repeated loads were applied at a frequency of 20 repetitions per minute and with a load duration of 0.1 sec. Time-of-loading discussions (e.g., in Report TE 72-4 (4) and by Barksdale (5) for a reasonable range in pavement thicknesses) would indicate this to be representative of traffic traveling at velocities in the range 20 to 40 miles per hour.

Test Results

Relationships between axial, radial, and volumetric strain** and number of stress applications for specific stress levels are shown in Figs. 3 through 12 on semi logarithmic plots. Some difficulties were experienced in measuring radial strains, in part due to specimen creep. Thus the values at larger stress repetitions may be slightly smaller than were experienced by the specimens. Results of Figs. 3-12 can also be plotted as shown in Figs. 13 through 15; a linear relationship between strain and N on the log-log plot appears quite reasonable. Appendix A contains a summary of the data obtained to date.

---

* This pressure is higher than exists in-situ. Normally static confining pressures in the upper part of the subgrade will be in the range of 1 to 1.5 psi. The value of 5 psi was selected because the pressure regulators available for the test program provided more precise control in this range than at the lower values.

** Volumetric strain was determined from the relation:

$$\varepsilon_{vol.} = \varepsilon_1 - 2\varepsilon_3$$

where: ε_1 and ε_3 are the measured axial and radial strains respectively.

ClibPDF - www.fastio.com

To illustrate the change in accumulation of permanent deformation with load repetitions, change of strain per cycle has been plotted versus the number of stress applications. These results are shown in Figs. 16 through 18.

The influence of stress history is illustrated in Figs. 19 through 21 for conditions where specimens were subjected to stress sequences in which the lower stresses were first applied. Results without conditioning at a lower stress level are also shown. As Seed et al had reported earlier (6, 7), these data illustrate the influence of stress history on the accumulation of permanent strain.

To ascertain whether such effects are predictable from the results of tests performed at particular stress levels, a few tests were performed in which the axial stress levels 3, 5, and 10 psi were varied in the sequences noted in the previous section. These results are shown in Fig. 22. Again, the influence of stress history is apparent since the three specimens were all subjected to a total of 6000 stress applications.

Analyses

Plastic strain vs. stress applications. To develop constitutive relationships which will be useful for analysis and design purposes, the data of Figs. 3 through 12 have been plotted on log-log plots as shown in Figs. 13 through 15. An equation of the form:

$$\varepsilon^p = AN^b \qquad (1)$$

where:

ε^p = permanent strain

N = number of stress applications

A, b = experimentally determined coefficients

was used to fit the data using least squares procedures. From the data

ClibPDF - www.fastio.com

presented in these figures it is apparent that the linear relationship (on the log-log plot) can be used to represent the data reasonably well.

Table 1 contains a listing of the coefficients for a series of specimens tested at a range in water contents and dry densities and at deviator stresses ranging from 3 to 20 psi. Although the data are comparatively few, it is possible that the exponent b is dependent only on soil type while the coefficient A is a function of stress level and placement conditions.

As stated earlier, the majority of the specimens were subjected to 10,000 stress applications. To ascertain the appropriateness of equation (1) to predict response at larger numbers of stress repetitions, a few specimens were subjected to 100,000 applications. The equations shown on the curves in Fig. 23 were developed for the data obtained from the first 10,000 stress repetitions. Comparisons between measured deformations and estimated values shown in the figure indicate the suitability of this approach.

Pleastic strain vs. applied stress. Subgrades of well-designed pavements are subjected to comparatively small stresses from conventional traffic loads; e.g., Fig. 24 illustrates the results of computations for a two layer pavement of asphalt concrete resting directly on subgrade and subjected to a 9,000 lb. load on dual tires*. At stiffnesses in the asphalt-bound layer larger than 200,000 psi, the vertical compressive stresses in the subgrade are less than five psi and approach 0.5 psi at

---

* The computations shown in Fig. 24 were obtained by means of the Chevron program contained in Reference (1).

ClibPDF - www.fastio.com

Table 1 Summary of Permanent Deformation Determinants on Ygnacio Valley Subgrade Soil

Specimen Conditions		Repeated deviator stress-psi	Coefficients in $\varepsilon^p = AN^b$	
Water Content - percent	Dry density*- lb per cu. ft.		A $\times 10^{-4}$	B
16.7	112	5	0.168	0.184
16.8	112	10	0.306	0.185
16.5	112	20	1.28	0.156
19.8	107	3	0.378	0.212
19.3	107	5	1.22	0.145
19.7	107	10	4.57	0.193
19.3	107	20	39.5	0.185
16.4	107	5	0.0467	0.332
16.5	107	10	0.746	0.163
16.1	107	20	1.73	0.154

*Nearest 1 lb per cu. ft.

ClibPDF - www.fastio.com

high asphalt concrete stiffnesses for a comparatively weak subgrade. At these stress levels, measurement of permanent deformation is not as precise as at higher stresses. Accordingly, if the permanent deformation at lower stresses could be deduced from measurements at higher stresses, such measurement difficulties could be minimized.

Konder et al. (8) and Duncan and Chan (9) have suggested that stress vs. strain data obtained from static triaxial tests can be approximated by a hyperbola. Similarly, Barksdale (10) has presented data indicating the applicability of such a relationship to the plastic strain vs. stress data at a specific number of load applications for granular materials.

Based on this concept, an equation of the following form was used to develop a relationship between applied stress and plastic strain at a particular number of stress applications for the fine-grained soil studied in this investigation:

$$\Delta\sigma_a = \frac{\varepsilon_a^p}{\ell + m\varepsilon_a^p} \tag{2}$$

where:

$\Delta\sigma_a$ = repeated axial stress

ε_a^p = cumulative permanent axial strain at a specific number of stress applications

ℓ,m = experimentally determined coefficients

Equation (2) may also be expressed as:

$$\frac{\varepsilon_a^p}{\Delta\sigma_a} = \ell + m\varepsilon_a^p \tag{3}$$

If $\frac{\varepsilon_a^p}{\Delta\sigma_a}$ is plotted as a function of ε_a^p, a straight line is obtained. The intercept of this line with the $\frac{\varepsilon_a^p}{\Delta\sigma_a}$ axis yields the value of ℓ while the value m corresponds to the slope of the line.

ClibPDF - www.fastio.com

Using least squares techniques, the experimental data were analyzed according to equation (3). Having deduced the coefficients ℓ and m by this procedure, the equations were then plotted in the form of equation (2). Comparison of actual data at 10,000 stress applications and the hyperbolic relationship are shown in Fig. 25 for the data shown in Figs. 13, 14, and 15*. It would appear that such a relationship is a useful way of representing the data of permanent strain vs. applied stress so that permanent strains at small stress levels can be deduced from tests at larger stress levels where the strains can be more precisely measured with relatively simple equipment of the type used in this investigation.

The relationships shown in Fig. 25 can also be used to estimate the accumulation of permanent deformations for different stresses resulting from wheel loads of varying intensities.

Cumulative loading. Data have already been presented (Fig. 22) which were obtained by applying stresses of different magnitudes and in different sequences. Since the actual stress sequence is not known in the field, it would appear desirable to have some way by means of which the results of such cumulative loading could be predicted from the results of simple loading tests, e.g., Figs. 13 - 15.

At present, at least two methods are available to obtain the cumulative permanent strain from the results of simple loading tests: (1) a "time-hardening" procedure, and (2) a "strain-hardening" procedure; both are illustrated schematically in Fig. 26.

---

* Appendix B also contains such curves for combined data obtained in the study.

ClibPDF - www.fastio.com

In the "time-hardening" method (Fig 26), if the specimen is loaded for N_1 repetitions of stress state $\bar{\sigma}_1$, the resulting permanent strain will be $\varepsilon_1^p(N)$. The equivalent number of repetitions, N_2', at stress state $\bar{\sigma}_2$, which would have given the same permanent strain is obtained as shown in Fig. 26. If further N_2 applications of load $\bar{\sigma}_2$ are applied, the total strain will follow the path as shown in Fig. 26.

The "strain-hardening" procedure, also illustrated in Fig. 26, requires determination of the ε_1^p after N_1 repetitions of stress $\bar{\sigma}_1$. The number of repetitions at effective stress $\bar{\sigma}_2$ is then taken equal to N_1, and a further N_2 applications are applied. Total permanent strain is the sum ε_1^p and ε_2^p.

Both approaches were used to predict the responses shown in Fig. 22 from test data at single stress levels. Figs. 27, 28 and 29 show comparisons of the experimental results which those predicted by both methodologies. In these figures, it is seen that neither method provides solutions which agree quantitatively with the experiment results. Interestingly, however, the predicted results are in qualitative agreement; further, the predicted results bracket the actual data. More detailed examination indicates that the time-hardening method provides better agreement if the stress levels are successively increased, whereas the strain hardening method provides closer agreement if the loads are successively decreased.

LABORATORY TESTS ON ASPHALT CONCRETE

To develop a reasonable measure of the permanent deformation characteristics of asphalt-bound materials requires that the materials be tested under representative service conditions which include the use of realistic stress-states, times of loading, and temperatures. Appendix C contains a summary of analyses developed to determine such representative conditions.

ClibPDF - www.fastio.com

To simulate the different loading conditions which might occur, the repeated load triaxial compression equipment developed by Dehlen (11) was utilized. This equipment permits independent application of axial and radial stresses in repeated loading. While the equipment and test procedures were briefly described in Report No. TE 72-4 (4), a description is included in Appendix D for convenience.

Creep testing has also been performed on the asphalt concrete as a part of this study. Creep compliances determined from this type of test can be used in a procedure developed by the Federal Highway Administration to estimate the accumulation of permanent deformations (12). This procedure is also described in Appendix D.

Materials

The aggregate consisted of a crushed Watsonville granite combined to a 1/2 in. maximum medium grading as shown in Fig. 30.

An 85-100 penetration asphalt cement supplied by the Chevron Research Company, with the characteristics shown in Table 2 was mixed with the aggregate using procedures described earlier (1). Stabilometer tests indicated that an asphalt content of 6 percent (by weight of aggregate) would produce an asphalt concrete mix with a stabilometer value greater than 37, which according to the State of California Specifications would satisfy the stability requirements for a Type A material*.

---

* The other specification requirements were not checked although, as noted subsequently, the void contents of the 4 in. by 8 in. cylindrical specimens were greater than 4 percent - one of the design requirements.

ClibPDF - www.fastio.com

Specimen Preparation

Asphalt concrete specimens were compacted at 230°F using a Triaxial Institute (or California) Kneading Compactor. During the compaction process, material was supplied continuously to the sample mold. This procedure reduces density variations which occur in specimens compacted in lifts and eliminates weaknesses which may occur at compaction interfaces. Compacted specimens were approximately 4 in. in diameter by 9 in. in height. Poorly compacted material at the top and base of the sample was removed by trimming each specimen to a height of approximately 8 in. Fig. 31 illustrates the jig used for trimming. This jig was also used to drill holes for the LVDT mounts. The compaction schedule (number of tamps and tamping pressure) was evolved by a trial and error procedure. The procedure was varied until the range of variation of bulk specific gravity within a specimen was consistently less than 0.02. (NOTE: This variation was measured by sawing a specimen into four discs, each about 2 in. high, and measuring the bulk specific gravity of each disc.)

Prior to repeated load or creep tests aluminum end caps were bonded to all specimens using an epoxy adhesive. To insure proper axial alignment and parallelism of the caps a device illustrated in Fig. 32 was used.

Special precautions were required to preclude leakage of the cell fluid through the membrane into the specimen. End caps were cleaned and polished prior to reuse, thus ensuring a tight seal between the caps and the membrane. Epoxy was used to attach the inner membrane to the specimen in the vicinity of the LVDT connection. A second membrane was then placed over the first. Leakage through the outer membrane was controlled by placement of a special sealant between the LVDT mounting block and the membrane.

ClibPDF - www.fastio.com

TABLE 2

PROPERTIES OF ASPHALT CEMENT

Initial Properties*		
Penetration	at 77°F, dmm	92
	at 39°F, dmm	33
Viscosity	at 140°F, Kp	1.33
	at 275°F, CS	2.76
Rolling Thin Oven Test		
	loss (wt.), percent	0.19
	penetration retained, percent	57.6
	viscosity at 140°F, Kp	3.34
	viscosity at 275°F, CS	4.29
Recovered Properties**		
Penetration at 77°F, dmm		- mean 41.3 - range 41-43
Softening Point (Ring and Ball), °F		- mean 131.7 - range 131-132.5

---

* Tests performed by Chevron Research, Richmond, California

** Tests performed by California Division of Highways, Materials and Research Section, Sacramento, California

ClibPDF - www.fastio.com

Mixture Characteristics

Two groups of specimens were prepared. The first group (62 specimens) exhibited the following characteristics:

	Bulk Specific Gravity			Air Void Content		
	Mean Value	Standard Deviation	Coef.of Variation percent	Mean Value Percent	Standard Deviation	Coef.of Variation percent
Specimens 1-62	2.484	0.011	0.5	4.7	0.43	9.1
Specimens 63-87	2.428	0.004	0.1	6.9	0.14	2.0

A second group, prepared using a different supply of the granite, exhibited slightly different characteristics for the same gradation, asphalt content, and compaction procedure. Characteristics of these specimens are also shown in the above summary.

Test Program

Repeated load and creep tests were conducted at temperatures of 67°, 85° and 100°F. Appendix D also contains a summary of the various test conditions. For the repeated load tests three loading conditions have been utilized; these have been termed:

(1) extension tests: zero axial stress; compressive radial stress

(2) unconfined compression tests; compressive axial stress, zero radial stress.

(3) tension tests: tensile axial stress, compressive radial stress.

Loading conditions for the creep tests included:

(1) unconfined compression tests

(2) extension tests.

ClibPDF - www.fastio.com

Laboratory Test Results

Repeated Load Test Data

Stiffness characteristics. Stiffness characteristics were determined from the applied stress conditions and measured recoverable deformation by means of the following equations (13):

$$S = \frac{2\sigma_H^2 - \sigma_A^2 - \sigma_A \ \sigma_H}{2\varepsilon_{HR}\ \sigma_H - \varepsilon_{AR}\ \sigma_A - \varepsilon_{AR}\ \sigma_H}$$

$$\nu = \frac{\sigma_H\ \varepsilon_{AR} - \sigma_A\ \varepsilon_{HR}}{\sigma_A\ \varepsilon_{AR} + \sigma_H\ \varepsilon_{AR} - 2\ \sigma_H\ \varepsilon_{HR}}$$

$$G = \frac{S}{2(1 + \nu)}$$

where,

S = stiffness modulus (using the Van der Poel notation for a modulus which is a function of time and temperature)

ν = Poisson's ratio from recoverable deformation

G = shear modulus from recoverable deformation

σ_H = horizontal stress

σ_A = axial stress

ε_{HR} = recoverable or elastic strain in horizontal direction

ε_{AR} = recoverable strain in the axial direction

Table 3 contains a summary of the stiffness characteristics determined by means of these relationships and the data are plotted in Fig. 33. Stiffness values have also been computed by the Shell procedure (21, 22, 23) and are shown in Fig. 34 for the three temperatures. While the measured values are larger than the computed values, the difference is less than the factor of two attributed to the nomograph estimation procedure. Interestingly, the shape of the estimated relationship provides a means

ClibPDF - www.fastio.com

TABLE 3 - STIFFNESS CHARACTERISTICS

Specimen No.	Time of Loading sec.	Recoverable Axial Strain, ε_{AR} 10^{-6} in. per in.	Recoverable Radial Strain, ε_{HR} 10^{-6} in. per in.	Stiffness Modulus, S 10^3 psi	Shear Modulus, G 10^3psi	Poisson's Ratio ν
			Test Temperature: 67°F			
7	0.12	83	-115	530	203	0.25
8	0.04	40	- 74	810	335	0.20
17	0.04	54	- 90	730	292	0.23
18	0.27	153	-143	375	135	0.36
12	0.13	98	- 27	520	210	0.24
13	0.29	180	- 55	265	102	0.32
14	0.08	67	- 18	805	330	0.25
15	0.98	76	- 20	670	290	0.22
16	0.08	76	- 17	670	275	0.21
64	0.12	- 95	25	580	230	0.24
65	0.22	-140	70	400	143	0.37
68	0.42	-140	53	290	110	0.33
			Test Temperature: 85°F			
23	0.08	200	-150	215	76	0.39
24	0.05	142	- 96	345	127	0.43
26		130	-130	280	100	0.38
27	0.13	275	-220	165	56	0.41
56	0.29	260	-105	70	26.5	0.36
59	0.24	220	- 80	92	34.5	0.34
60	0.14	214	- 80	106	40.	0.34
61	0.14	167	- 60	130	48.	0.33
62	0.14	230	- 80	118	44.	0.34
63	0.14	245	- 90	106	40.	0.35
51	0.08	-112	30	220	88	0.29
52	0.10	-170	46	202	80	0.26
53	0.13	-185	38	140	57	0.22
54	0.27	-175	63	138	51	0.39
			Test Temperature: 100°F			
42	0.08	400	-225	65.	22.5	0.48
43	0.08	100	- 90	115.	42.0	0.34
44	0.126	175	-106	77.	26.5	0.45
45	0.08	132	- 94	92.	32.5	0.40
47	0.20	330	-170	49.5	16.3	0.48
32	0.075	125	- 50	82.	31.2	0.26
33	0.075	140	- 43	77.	29.5	0.16
34	0.15	226	- 75	44.	20.0	0.20
35	0.15	200	- 80	51.5	19.0	0.31
36	0.25	260	- 85	38.5	17.0	0.15
37	0.25	260	- 85	36.5	16.0	0.17
40	0.15	380	-135	45.	16.0	0.26
41	0.15	335	-120	41.0	18.8	0.24
46	0.11	-230	80	84.	31.	0.40
48	0.11	-140	61	102.	36.	0.44
49	0.23	-245	85	65.	23.	0.36
50	0.09	-155	53	99.	36.	0.36

NOTE: 1. (-) sign denotes compression.
2. Values determined at n = 1,000 repetitions.

ClibPDF - www.fastio.com

for extending the data over a wide time scale (also noted in earlier reports).

The Poisson's ratio data, also shown in Table 3, indicate some dependence on both temperature and time of loading.

Volume Change Characeristics Permanent volume change was computed from measured values of permanent deformation. Each specimen was assumed to remain cylindrical in shape over the portion in which the deformations were measured and volume strain was computed from:

$$\varepsilon_{vol.} = \frac{\Delta V}{V} \qquad (4)$$

where:

ΔV = change in volume at a specific number of load repetitions

V = initial volume of central portion of specimen

Fig. 35 illustrates computed volume strain as a function of the algebraic difference between axial and radial permanent strain (permanent shear strain). In the majority of the tests, a volume increase at large strains was observed although in the tension tests some compression volume change was evident.

Maximum values of volume strain were of the order of 5000×10^{-6}. This is equivalent to a change in bulk specific gravity of the order of 0.01, an amount which would be difficult to detect by standard methods for specific gravity determination.

In the next section all of the axial and radial permanent strain data have been adjusted for volume change as follows:

$$\varepsilon^{p}_{adj.} = \varepsilon^{p}_{meas} - 1/3\ (\Delta\ V/V) \qquad (5)$$

Permanent Deformation Characteristics. Figs. 36, 37, and 38 illustrate permanent strain vs stress repetition data for a range in test conditions

ClibPDF - www.fastio.com

and test temperatures. On each figure is stated the particular test type. In thick asphalt-bound layers, the stress states shown in these figures can be considered representative of the following locations:

(1) Extension - near the surface (Fig. 36)

(2) Compression - center of layer (Fig. 37)

(3) Tension - near the lower boundary. (Fig. 38)

While a number of analyses* are available to permit development of relationships from the data to assist, in turn, in the estimation of rutting of the material in a pavement structure, only one technique has been used thus far. This procedure consists of fitting a third order polynominal of the form:

$$\log \varepsilon^p = C_0 + C_1 (\log N) + C_2 (\log N)^2 + C_3 (\log N)^3 \qquad (6)$$

where:

ε^p = plastic strain (corrected for volume change)

N = number of stress applications

to the data like that shown in Figs. 36 through 38 using a least squares procedure. The influences of stress state, time of loading, and temperature are reflected in the coefficients C_0, C_1, C_2, C_3. Table 4 contains a summary of these coefficients for all of the tests completed to date.

In developing the least square relationships it was found that the polynominals were very sensitive to the initial and final data points. To reduce the sensitivity, the first data point (N=1) was eliminated;

---

* e.g. -- Theory of rate dependent plasticity (14).

ClibPDF - www.fastio.com

TABLE 4 - REGRESSION COEFFICIENTS OF EQUATION (6) FOR ALL TEST DATA

Specimen No.	Regression Coefficients								Std. Error of Estimate	
	Axial Strain				Radial Strain					
	C_0	C_1	C_2	C_3	C_0	C_1	C_2	C_3	Axial	Radial
Temperature - 67°F										
64	-4.58	0.83	-0.12	0.0086	-4.88	0.83	-0.12	0.0096	.017	.017
65	-4.44	0.89	-0.13	0.011	-4.74	0.89	-0.13	0.011	.011	.011
68	-4.22	0.85	-0.14	0.012	-4.52	0.85	-0.14	0.012	.015	.015
7	-4.23	0.76	-0.059	0.0034	-4.54	0.76	-0.059	0.0033	.012	.012
8	-4.28	0.68	-0.047	0.0029	-4.58	0.68	-0.047	0.0028	.015	.015
17	-4.35	0.77	-0.084	0.0071	-4.65	0.77	-0.086	0.0070	.015	.015
18	-4.03	0.83	-0.1	0.0094	-4.33	0.82	-0.099	0.0090	.007	.007
13	-4.13	0.79	-0.060	0.0056	-4.43	0.78	-0.057	0.0050	.009	.009
14	-4.71	0.62	-0.035	0.0027	-5.01	0.62	-0.035	0.0026	.008	.008
15	-4.50	0.74	-0.037	0.0017	-4.80	0.74	-0.039	0.0017	.017	.017
16	-4.76	1.01	-0.17	0.015	-5.06	1.02	-0.17	0.015	.011	.011
Temperature - 85°F										
23	-3.88	0.82	-0.14	0.014	-4.18	0.82	-0.14	0.014	.007	.007
24	-3.90	0.92	-0.20	0.019	-4.29	0.91	-0.20	0.019	.020	.020
26	-4.12	1.08	-0.21	0.019	-4.42	1.08	-0.21	0.019	.014	.014
27	-3.90	1.00	-0.17	0.015	-4.20	1.00	-0.17	0.015	.016	.016
56	-3.78	0.68	-0.10	0.010	-4.08	0.68	-0.099	0.010	.026	.026
59	-4.30	0.77	-0.081	0.0051	-4.60	0.77	-0.081	0.0051	.014	.014
60	-4.38	0.67	-0.083	0.0065	-4.68	0.67	-0.083	0.0065	.010	.010
61	-4.33	0.71	-0.11	0.0083	-4.62	0.72	-0.11	0.0083	.014	.014
62	-4.36	0.76	-0.11	0.0098	-4.66	0.76	-0.11	0.0098	.014	.014
63	-4.30	0.80	-0.15	0.014	-4.60	0.80	-0.15	0.014	.013	.013
51	-4.64	0.90	-0.14	0.011	-4.94	0.90	-0.14	0.011	.015	.015
52	-4.22	0.87	-0.16	0.014	-4.52	0.87	-0.16	0.014	.012	.012
53	-4.25	0.96	-0.18	0.017	-4.55	0.96	-0.18	0.017	.003	.003
54	-4.08	0.79	-0.12	0.0099	-4.38	0.79	-0.12	0.0099	.022	.022
60,61*	-4.35	0.70	-0.095	0.0071	-4.65	0.70	-0.095	0.0071	.01	.01
62,63*	-4.32	0.75	-0.11	0.0095	-4.62	0.75	-0.11	0.0095	.011	.011
Temperature - 100°F										
32	-4.12	1.23	-0.33	0.032	-4.42	1.23	-0.33	0.032	.020	.020
33	-4.49	0.88	-0.19	0.019	-4.79	0.88	-0.19	0.019	.011	.011
34	-4.30	0.86	-0.13	0.012	-4.60	0.86	-0.13	0.011	.013	.013
35	-4.02	0.95	-0.22	0.021	-4.32	0.95	-0.22	0.021	.015	.015
36	-3.90	0.93	-0.16	0.015	-4.20	0.93	-0.16	0.015	.011	.011
37	-3.83	1.04	-0.23	0.020	-4.13	1.04	-0.22	0.020	.016	.016
40	-4.31	0.94	-0.14	0.011	-4.61	0.93	-0.14	0.011	.016	.016
41	-4.28	0.92	-0.15	0.012	-4.58	0.92	-0.15	0.012	.021	.021
43	-4.12	0.86	-0.15	0.013	-4.42	0.86	-0.15	0.013	.007	.007
44	-4.17	0.91	-0.17	0.014	-4.46	0.91	-0.17	0.014	.019	.019
47	-3.85	0.78	-0.11	0.0092	-4.15	0.78	-0.11	0.0090	.009	.009
46	-3.93	0.83	-0.11	0.010	-4.23	0.83	-0.11	0.010	.012	.012
48	-3.98	0.78	-0.13	0.012	-4.28	0.79	-0.13	0.012	.010	.010
49	-3.89	0.80	-0.13	0.012	-4.19	0.80	-0.13	0.012	.013	.013
50	-4.28	0.89	-0.13	0.010	-4.58	0.88	-0.13	0.010	.013	.013
32,33*	-4.28	1.18	-0.32	0.033	-4.58	1.18	-0.32	0.033	.018	.018
34,35*	-4.13	0.88	-0.17	0.016	-4.43	0.88	-0.17	0.016	.010	.010
36,37*	-3.86	0.98	-0.19	0.017	-4.16	0.98	-0.19	0.017	.012	.012
40,41*	-4.29	0.92	-0.14	0.011	-4.59	0.92	-0.14	0.011	.016	.016

ClibPDF - www.fastio.com

this was considered to be reasonable since seating errors tend to influence the initial readings. Because the majority of tests were stopped at less than 10,000 repetitions, the data were linearly extrapolated to $N = 10^5$ to control the fit at large numbers of repetitions; this must be considered an expedient technique until additional data become available.

Data from the repeated load tests can also be examined in other ways. To illustrate the variations in total, elastic, and permanent strain with load applications, data for the specimens whose permanent strain characteristics are shown in Fig. 36 through 38 are plotted in Figs. 39, 40 and 41. The permanent strain per load application relationships shown in these figures were obtained by differentiating the curves expressed by equation (6) which had been developed by least squares procedures from the data of Figs. 36 through 38. In Figs. 39 through 41 it will be noted that after about 100 stress repetitions, the permanent strain per cycle is small.

The regression coefficients C_1, C_2 and C_3 of equation (6) have been plotted versus elastic strain in Fig. 42. Analysis of the data do not indicate any apparent trends with temperature, stress level, stress direction, or elastic strain for the coefficients C_1, C_2, and C_3 for this particular mix. Unfortunately, however, no analyses were performed to define the independence of the coefficients of each other or their interpdendence. The results of the analysis are:

Coefficient	Mean	Standard Deviation
C_1	0.85	0.14
C_2	0.013	0.006
C_3	-0.14	0.06

ClibPDF - www.fastio.com

The coefficient C_0 (in this case the logarithm of permanent deformation resulting from the initial load application) appears to be dependent on a number of factors including stress, strain, and temperature. In an attempt to combine the influence of stress and strain on C_0 at a particular temperature, the following relationship was developed:

$$\varepsilon_1^p = K(\sigma_d \cdot \varepsilon_e)^n \qquad (7)$$

where:

$\varepsilon_1^p = 10^{C_0}$ (permanent strain at first load repetition)

$\sigma_d = \sigma_A - \sigma_R$, stress difference in triaxial compression

ε_e = elastic strain

K, n = experimentally determined coefficients

Fig. 43 contains the data and the regression lines conforming to equation (7)* for axial and radial deformations and includes both extension and compression results. While there may be alternative relationships, this form lends itself, as will be seen subsequently, to be used to permit an estimate to be made of permanent deformation in a pavement structure resulting from an applied load at the surface.

It is also of interest to briefly examine the range in stiffnesses which can be expected to occur in situ and to relate these to the laboratory loading times and temperatures required to measure permanent deformation properties.

---

* Correlation coefficients for the regressions were approximately 0.80 indicating that the product of stress and strain may not be the most suitable parameter.

ClibPDF - www.fastio.com

Fig. 44, obtained from TE 71-8, illustrates the variation in stiffness modulus with traffic applications for a 12 in. thick asphalt concrete layer for a wide range in environmental conditions (in this case as measured by average monthly temperatures). For the location with the warmest temperature conditions (Phoenix) only a small amount of truck traffic is applied when the asphalt concrete stiffness is less than 50,000 psi. Lower stiffness values may occur during temperature extremes, when traffic operates at lower speeds, or when mixtures are improperly designed or inadequately compacted.

To relate the conditions of Fig. 44 to laboratory test conditions, a simple time-temperature superposition procedure demonstrated in Fig. 45 was derived from the laboratory test data using nomograph values as a guide. Times of loading in the range 0.1 to 0.4 seconds were considered to be a convenient laboratory range, while times of loading of 0.01 to 0.04 were considered appropriate for highway traffic. As shown on Fig. 45 at times of loading of 0.1 to 0.4 seconds, laboratory test temperatures of 100°F are adequate to cover a service temperature range up to 135°F at times of loading corresponding to moving highway traffic. Pavement temperatures higher than these values occur only infrequently even under severe climatic conditions. Proportionally longer loading times or higher laboratory test temperatures would be required to evaluate material stiffness for lower speed traffic or for severe climatic conditions.

Creep Test Data

Volume Change Characteristics. Volume change was estimated by the same procedure as used for the repeated load tests, i.e. from the axial and radial strains together with equation (5). Fig. 46 illustrates volume strain as a function of shear strain for both compression and extension.

ClibPDF - www.fastio.com

These data are essentially the same as obtained in the repeated load tests although the observed values are less than those measured in repeated loading.

Creep Compliance. Creep compliances were estimated from the following equations (13).

$$\psi_E(t) = \frac{\varepsilon_A(t)}{\sigma_A - \sigma_R} \tag{8}$$

$$\psi_G(t) = \frac{2[\varepsilon_A(t) - \varepsilon_R(t)]}{\sigma_A - \sigma_R} \tag{9}$$

$$\nu(t) = \frac{\varepsilon_R(t)\ \sigma_A - \varepsilon_A(t)\ \sigma_R}{2\varepsilon_R\sigma_R - \varepsilon_A(t)\sigma_A - \sigma_A - \varepsilon_A(t)\ \sigma_R} \tag{10}$$

where:

$\psi_E(t)$ = axial creep compliance

$\psi_G(t)$ = shear compliance

$\nu(t)$ = Poisson's ratio

$\varepsilon_A(t)$, $\varepsilon_R(t)$ = axial and radial strains respectively

σ_A, σ_R = axial and radial stresses, respectively.

Shear compliances are shown in Fig. 47 for a range in temperatures. Differences in compliances measured in extension and compression are apparent at all temperatures. This figure also illustrates the repeatability of the creep test used in this investigation. In Fig. 47 the degree of linearity is also indicated, in this instance to times of about 10 sec. and strains of the order of 400 x 10^{-6} in per in. This observation compares quite well with the value 270 x 10^{-6} in per in reported by Nair et al (15).

ClibPDF - www.fastio.com

Shear moduli estimated from the creep tests* are compared with those determined from repeated loading in Table 5. In general the agreement is considered reasonable.

Axial creep compliance data are presented in Fig. 48. Other than for the compression tests at 67°F, some non-linearity is observed.

Poisson's ratio data are shown in Fig. 49. Generally the values determined from the creep tests compare favorably with these estimated from repeated loading.

TABLE 5

Temperature °F	Shear Modulus - 10^3 psi			
	Repetitive Loading		Creep	
	t = 0.1 sec	t = 1.0 sec	t = 0.1 sec	t = 1.0 sec
67	240	67	294	77
85	65	18	84	28
100	30	8	27	10

ANALYSIS OF PAVEMENT STRUCTURES

To estimate permanent deformation in pavement structures from repetitive traffic loading, Heukelom and Klomp (16), Barksdale (10) and Romain (17), have suggested the use of elastic layer theory to compute stresses and strains and to utilize these values in estimating permanent deformations from appropriate constitutive relationships.

---

* In this instance simply defined as the reciprocal of the compliance.

ClibPDF - www.fastio.com

Alternatively, viscoelastic layer theory together with creep data incorporated in an analysis like that developed by Elliott et al (18) and included in the FHWA program VESYS II (12) may also be utilized to estimate permanent deformation. In this section both methodologies will be examined.

Elastic Analysis

In this procedure the elastic layer program termed CHEV 5L has been used together with the relationships represented by equations (6) and (7).

For simplicity the computations have been done for a two-layer system (asphalt concrete directly on subgrade) and for a load applied to a single circular area.

Following the procedure suggested by Barksdale (10) wherein the particular layer under consideration is subdivided into a series of layers, computations were performed at intervals of one inch throughout the depth of the upper layer (asphalt concrete) and at the boundaries -- all on the axis of the loaded area. The upper layer was also assumed to have a constant stiffness modulus.

To permit the use of equations (6) and (7) it was first necessary to compute σ_d and ε_e of equation (7). These were determined with the aid of the computer program by assuming (Fig. 50):

$$\sigma_d = \sigma_V - \sigma_H \tag{11}$$

and

$$\varepsilon_e = \varepsilon_V$$

where:

σ_V = vertical stress

σ_H = horizontal stress (note radial and tangential stresses are equal for the condition analyzed)

ε_V = vertical strain

ClibPDF - www.fastio.com

These values were then used, for a particular number of load repetitions, to compute permanent strains which in turn permit permanent deformation in the layer to be obtained from the relation:

$$\delta^p = \sum_{i=1}^{n} (\varepsilon_i^p \Delta z_i) \qquad (12)$$

where:

δ^p = rut depth or permanent deformation in the upper (asphalt-bound) layer

ε_i^p = permanent strain in subdivided layer (Fig. 50)

A series of pavement systems have been studied by this procedure to ascertain the influence of a number of parameters on the accumulation of permanent deformation.

To insure that the procedure under investigation would pass "the test of reasonableness", rut depth vs number of load repetitoons obtained under controlled conditions by Hofstra and Klomp (19) have been included for comparison. Their data were obtained by subjecting a 20 cm (8 in.) layer of asphalt concrete resting directly on a subgrade to a 1500 lb wheel load with a contact pressure of 70 psi in a laboratory test track. About 200,000 load repetitions were applied at a temperature of 30°C (86°F). Rut depth vs. number of load repetitions is shown in Fig. 51.

Computations were made using the procedure described above with the same asphalt concrete stiffness as that reported by Hofstra and Klomp*, 155,000 psi and the same subgrade modulus, 28,000 psi.

---

* It should be noted that the mix tested by Hofstra and Klomp contained a 40-50 penetration asphalt cement and would be considered an overasphalted mix with less than 2 percent air voids. The mix whose data was reported in the previous section, by comparison, contained an 85-100 penetration asphalt cement and had a void content in the range of 4 to 6 percent. At the 86°F temperature and time of loading reported by Hofstra and Klomp this mix exhibited a stiffness of 2.5×10^5 psi. Accordingly, it should be kept in mind when comparing the results that the form of the load-deformation relationship is more important than the absolute magnitude of the deformations.

ClibPDF - www.fastio.com

Table 6 contains the parameters used in the computations and, as noted in the table, five cases were examined. Results of these computations are shown in Fig. 51 for purposes of comparison with the Hofstra and Klomp data. Fig. 52 illustrates the distribution of elastic stresses and strains and permanent strains with depth for condition one of Table 6 (at N = 5,000 stress applications for permanent strain).

While the mixtures are different (as noted in the footnote) the shapes of the curves are similar, indicating the potential of such a procedure.

TABLE 6

DATA USED FOR SENSITIVITY STUDIES
OF PERMANENT DEFORMATION ESTIMATION PROCEDURE

Condition	Coefficients:				
	Equation (4)		Equation (3)		
	K	n	C_1	C_2	C_3
1. mean	0.37	0.66	0.85	-0.14	0.013
2. K_{mean} + 10%	0.41	0.66	0.85	-0.14	0.013
3. K_{mean} + 10%	0.37	0.73	0.85	-0.14	0.013
4. max. of range	0.37	0.66	1.23	-0.33	0.032
5. min. of range	0.37	0.66	0.62	-0.035	0.0027

In Fig. 52 the distribution of permanent strain is similar in shape to the distributions of stress difference and elastic vertical strain. Hofstra and Klomp observed that the distribution of permanent strain was approximately uniformly distributed in the layers of each section of the laboratory test track pavements. A number of factors might contribute to

ClibPDF - www.fastio.com

this difference. For example, time of loading has been assumed constant with depth (constant stiffness modulus). Barksdale's (10) analysis and that contained in Appendix C indicate an increase in loading time with depth which would in turn reduce the stiffness. As will be seen subsequently this could influence the distribution of permanent strain. Other considerations await the results of additional studies.

To examine the influence of material characteristics, temperature, and pavement thickness, a series of solutions were developed using this procedure. Two subgrade stiffnesses, 5000 psi and 10,000 psi were utilized; the stiffness vs temperature relationship of Fig. 53 was used for the asphalt concrete layer (time of loading of 0.011 sec.)*; and the other factors are shown in Table 7. Mean values for the coefficients C_1, C_2 and C_3 (Table 6) were utilized. Computations were made for a 4500 lb wheel load with a contact pressure of 80 psi.

Influence of the stiffness of the asphalt concrete on rut depth is illustrated in Fig. 54. Reducing the stiffness by a factor of two increases the permanent deformation more than proportionally, indicating, at least from the calculations presented, that the procedure recommended for stiffness estimation using the characteristics of the asphalt in the mix (21, 22, 23) (considered accurate within a factor of two) requires careful evaluation for use in this part of the design process.

---

* The time of loading of 0.011 sec. corresponds to that associated with the vertical stress at mid depth in a 12 in. layer for a vehicle speed of 60 mph (20).

ClibPDF - www.fastio.com

TABLE 7 - FACTORS USED IN DEFORMATION ANALYSIS

T °F	E_1 psi x 10^6	E_1 MN/m^2	ν_1 [a]	Coefficients of Equation (4) [b] K	n
72	1.0	6900	0.21	0.22	0.62
85	0.51	3450	0.28	0.32	0.66
100	0.225	1550	0.36	0.44	0.70
114	0.1	690	0.43	0.56	0.73
126	0.05	345	0.50	0.63	0.76

a. Reference (15), among others, indicates ν to be a function of mixture stiffness and/or temperature.

b. Dependent on temperature (see Fig. 43).

Fig. 55 illustrates, at least for this set of circumstances (h_1=12 in) that the subgrade stiffness has practically no effect on the accumulation of permanent deformation in the asphalt concrete layer. It must be recognized, however, that subgrade stiffness will influence the total permanent deformation at the pavement surface (factor not considered in this analysis), and for a given thickness, h_1, total deformation will increase as the stiffness is reduced.

The influence of layer thickness on permanent deformation within the asphalt-bound layer is shown in Fig. 56 to be minimal*. This same result was reported by Hofstra and Klomp in their laboratory test track study.

---

* At least for the thicknesses examined in this study.

ClibPDF - www.fastio.com

To ascertain the influence of the parameters of equations (6) and (7) on permanent deformation in the pavement structure, a few sensitivity analyses were performed. Fig. 57 illustrates the influence of the coefficients K and n of equation (7) on rut depth. Change in the parameter K has only a small influence whereas only a 10 percent change in n results in a 100 percent change in permanent deformation. Thus, while the use of equations (6) and (7) has provided an expedient technique for estimation of rut depth with available methodology it is desirable to develop an improved methodology to account for the initial permanent strain. The influence of changes in the coefficients C_1, C_2 and C_3 are shown in Fig. 58. At larger numbers of repetitions the influence of variations in these parameters is also apparent.

The influence of Poisson's ratio of the asphalt bound layer, ν_1, on permanent deformation is shown in Fig. 59, with a change in ν_1 from 0.5 to 0.35 resulting in a 15 percent increase in permanent deformation. It should be noted, however, that while the change in total deformation is comparatively small, Poisson's ratio does have an influence on the distribution of stress and strain with depth.

Generally these comparisons, it is believed, indicate that the use of elastic theory to estimate stress and strain distributions together with a constitutive relationship determined from laboratory repeated load tests have the potential to assist in the estimate of permanent deformation accumulation in thick asphalt-bound layers. It should be noted, however, that the method presented in this section, in all probability, would tend to oversestimate the amount of rutting.

Viscoelastic Analysis

In this section the procedure using the program termed VESYS II will

ClibPDF - www.fastio.com

be used to examine the accumulation of permanent deformation in the same structure discussed in the previous section.

This approach utilizes a creep compliance determined from laboratory tests. Two conditions have been used for compliance determination: (1) compression and (2) extension. Table 8 contains a summary of measured compliance values together with those determined from equations which had been developed using a least squares procedure. The two test techniques result in different compliance values which in turn will influence rut depth prediction.

TABLE 8 - AXIAL CREEP COMPLIANCE VALUES FOR TEST DATA AND FITTED CURVES

Time, sec.	Axial Creep Compliance, 10^{-6} in/in/psi							
	Compression				Extension			
	85°F		100°F		85°F		100°F	
	Data	Fitted	Data	Fitted	Data	Fitted	Data	Fitted
0.1	4.1	7.1	13.5	16.6	4.1	5.2	13.5	17.1
0.5		11.0		22.9		9.4		28.6
1.0	15.5	15.1	32.5	29.1	13.0	13.7	43.5	40.9
5.0		29.2		49.8		31.2		99.9
10	34.5	34.0	55.0	55.3	39.0	40.3	141.0	141.0
50		45.3		66.0		70.1		270.0
100	48.8	49.2	69.5	69.3	85.0	84.3	315.0	310.0
500		59.1		77.5		124.0		389.0
1000	65.0	63.5	82.0	81.1	140.0	136.0	405.0	407.0
5000		78.3		93.5		183.0		444.0
10000	86.0	86.5	101.0	101.0	222.0	223.0	470.0	469.0
50000		109.0		123.0		341.0		539.0
100000		112.0		126.0		358.0		549.0

Results of the first part of the program termed "Curve Fit" are shown in Table 9 and from the basis for the subsequent calculations. Deflections computed from the data are shown in Fig. 61 as a function of time for a 4500 lb single wheel load with a contact pressure of 80 psi.

ClibPDF - www.fastio.com

In this system the thickness of the asphalt layer (h_1) was taken as 12 in. and the subgrade modulus was assumed to be 5,000 psi.

In the portion of the VESYS II program to estimate the accumulation of permanent deformation ("Repeated Load") the time of loading (load assumed to vary with time as a Haversine function), t, and the total length of time before the next load is applied, T, are variables. Two conditions for these variables have been utilized:

(1) t = 0.25 sec, T = 2.5 sec; Fig. 61

(2) t = 0.50 sec, T = 1.0 sec; Fig. 62

In both Figs. 61 and 62 it will be noted that the permanent deformations which have been estimated are substantially less than those computed earlier for essentially the same conditions. Moreover, the accumulation of permanent deformation with number of load applications by this procedure does not exhibit the same shape as observed in the studies of Hofstra and Klomp.

The reasons for these differences are not clear at this time.

TABLE 9 - AXIAL CREEP COMPLIANCE DATA, COEFFICIENTS FOR DIRICHLET SERIES*

δ_i 1/sec	$G_i \times 10^{-6}$			
	Compression		Extension	
	85°F	100°F	85°F	100°F
50	1.9	-14.8	-4.1	-13.8
5.0	-21.0	-33.8	-19.3	-41.4
0.05	-16.5	-15.8	-35.1	-201.0
0.005	-12.4	-10.6	-61.5	-135.0
0.0005	-14.3	-10.1	-14.6	-24.0
0.00005	-41.8	-40.7	-225.0	-134.0
0	112.0	126.0	360.0	550.0

$$* \; J(t) = \sum_{i=1}^{n} G_i \exp \delta_i t$$

ClibPDF - www.fastio.com

SUMMARY

In this report progress is reported on the development of a procedure whereby the accumulation of permanent deformation in a pavement structure resulting from repeated loading can be estimated.

Test data have been developed permitting estimation of the contribution of the subgrade to the total permanent deformation occurring at the pavement surface by means of elastic theory and constitutive equations of the form developed herein. These relationships are:

$$\varepsilon^p = AN^b \tag{1}$$

and

$$\Delta\sigma_a = \frac{\varepsilon^p}{\ell + m\varepsilon_a^p} \tag{2}$$

the first relating permanent strain to number of stress applications and the second relating applied stress and permanent strain.

The coefficients of equations (1) and (2) must be determined experimentally since no general guidelines are available as yet.

To consider the effects of cumulative loading it would seem possible only to bound the subgrade contribution to permanent deformation since the influence of stress history is not well defined. The time-hardening and strain-hardening procedures described herein which make use of permanent strain vs number of stress applications data at single stress levels have the potential to provide these bounds.

An extensive study of the response of asphalt concrete to repetitive loading indicates that permanent strain can be related to stress state, time of loading, temperature, and numbers of stress applications by the relationships:

ClibPDF - www.fastio.com

$$\log \varepsilon^p = C_0 + C_1 \log N + C_2 (\log N)^2 + C_3 (\log N)^3 \quad (6)$$

and

$$\varepsilon_1^p = 10^{C_0} = k (\sigma_d \cdot \varepsilon_e)^n \quad (7)$$

As in earlier investigations the results of creep tests indicate that asphalt concrete can be approximated as a linear viscoelastic material so long as the deformations are small (<400 x 10^{-6} in per in).

Methodology is also presented whereby permanent deformation in asphalt bound layers can be estimated from the results of the laboratory tests, one procedure using the repeated load tests together with elastic theory and the other using static creep tests and viscoelastic theory.

While there are little field data available which demonstrate the development of rutting with load repetitions under controlled conditions, Hofstra and Klomp have presented a few results from studies with a laboratory test track. The use of the repeated load test data together with elastic theory provides the same form of relationship of rut depth vs load applications measured by Hofstra and Klomp suggesting that the procedure has potential to examine this facet of the design problem.

When used to study the influence of a number of parameters on pavement response this approach produced the following results:

(1) Subgrade stiffness appears to have little influence on the accumulation of permanent deformation in the asphalt-bound layer -- at least for the range in stiffnesses examined.

(2) Asphalt concrete stiffness exerts a significant influence on rutting in the asphalt-bound layer.

(3) Like the measurements of Hofstra and Klomp, the calculation procedure indicated that rut depth in the asphalt layer was independent of layer thickness for the range examined.

ClibPDF - www.fastio.com

The procedure in which the creep test was used to estimate rutting provided estimates of rutting which were very small. Moreover the shape of the rut depth vs application relationship determined using this methodology did not resemble the form reported by Hofstra and Klomp. These observations require that a careful evaluation be made of this procedure to ascertain the reasons for these apparent discrepancies.

Finally, it should be noted that neither of the methods discussed herein can be considered, in the judgment of the authors, implementable for design at present.

ACKNOWLEDGMENTS

The authors wish to acknowledge support provided this project by the Institute of Transportation and Traffic Engineering of the University of California in the form of shop, office, and research facilities.

The contributions of Dr. Charles Freeme on leave from the National Institute of Road Research, South Africa are also gratefully acknowledged.

The investigation was supported in part by the Transportation Laboratory of the State of California, Department of Transportation, Division of Highways and the Federal Highway Administration.

The contents of this report reflect the views of the authors who are responsible for the facts and the accuracy of the data presented herein. The contents do not necessarily reflect the official views or policies of the State or the Federal Highway Administration. This report does not constitute a standard, specification, or regulation.

ClibPDF - www.fastio.com

REFERENCES

1. Monismith, C. L., J. A. Epps, D. A. Kasianchuk, and D. B. McLean, Asphalt Mixture Behavior in Repeated Flexure, Report No. TE 70-5, University of California, Berkeley, Dec. 1970, 303 pp.

2. Monismith, C. L. and D. B. McLean, Design Considerations for Asphalt Pavements, Report No. TE 71-8, University of California, Berkeley, Dec. 1971.

3. Seed, H. B., F. G. Mitry, C. L. Monismith, and C. K. Chan, Prediction of Flexible Pavement Deflections from Laboratory Repeated-Load Tests. Highway Research Board, NCHRP Report 35, Wash., D. C.: 1967.

4. Monismith, C. L., D. B. McLean, and R.Yuce, Design Considerations for Asphalt Pavements, Report No. 72-4, University of California, Berkeley, Dec. 1972.

5. Barksdale, R., "Compressive Stress Pulse Times in Flexible Pavements For Use in Dynamic Testing", Highway Research Record No. 345, Highway Research Board, 1971.

6. Seed, H. B., and C. K. Chan, "Effect of Stress History and Frequency of Stress Application on Deformation of Clay Subgrades Under Repeated Loading," Proceedings, Highway Research Board, Vol. 37, 1958.

7. Seed, H. B., R. L. McNeill and J. DeGuenin, "Increased Resistance to Deformation of Clay Caused by Repeated Loading," Transactions, ASCE, Vol. 125, Part I, 1960, p. 141.

8. Kondner, R. L., "Hyperbolic Stress-Strain Response; Cohesive Soils" Journal of the Soil Mechanics and Foundations Division, ASCE, Vol. 89, No. SM1, 1963, pp 115-143.

9. Duncan, J. M. and C. Y. Chang, "Non-Linear Analysis of Stress-Strain in Soils" Journal of the Soil Mechanics and Foundations Division, ASCE, Vol. 96, No. SM5, 1970, pp. 1929-1953.

10. Barksdale, R. D., "Laboratory Evaluation of Rutting in Base Course Materials," Proceedings, Third International Conference on the Structural Design of Asphalt Pavements, University of Michigan, 1972.

11. Dehlen, G. L., "The Effect of Non-Linear Material Response in the Behavior of Pavements Subjected to Traffic Loads, Ph.D. Dissertation, University of California, 1969.

12. Kenis, W. J. and T. F. McMahon, "Advance Notice of FHWA Pavement Design System and a Design Check Procedure", Prepared for Presentation at AASHO Design Committee Meeting, October 1972.

13. Nair, K. and C. Y. Chang, "Translating AASHO Road Test Findings: Basic Properties of Pavement Components - Materials Characterization", NCHRP Projects 1-10 and 1-10/1; Highway Research Board, Dec. 1970.

ClibPDF - www.fastio.com

14. Mendelson, A., PLasticity: Theory and Application, MacMillan Company, New York, 1968.

15. Nair, K., W. S. Smith, and C. Y. Chang, "Applicability of a Linear Viscoelastic Characterization for Asphalt Concrete", Proceedings Third International Conference on the Structural Design of Asphalt Pavements, University of Michigan, 1972.

16. Heukelom, W. and A. J. G. Klomp, "Consideration of Calculated Strains at Various Depths in Connection with the Stability of Asphalt Pavements", Proceedings, Second International Conference on the Structural Design of Asphalt Pavements, University of Michigan, 1967.

17. Romain, J. E., "Rut Depth Prediction in Asphalt Pavements," Proceedings Third International Conference on the Structural Design of Asphalt Pavements, University of Michigan, 1972.

18. Elliott, J. F., and Moavenzadeh, F., and H. Findakly, "Moving Load on Viscoelastic Layered Systems Phase II - Addendum." Research Report R70-20, Department of Civil Engineering, M.I.T., Cambridge, Mass., April 1970.

19. Hofstra, A., and A. J. G. Klomp, "Permanent Deformation of Flexible Pavements Under Simulated Road Traffic Conditions," Proceedings, Third International Conference on the Structural Design of Asphalt Pavements, University of Michigan, 1972.

20. McLean, D. B., Permanent Deformation Characteristics of Asphalt Concrete, Ph.D. Dissertation, University of California, Berkeley, November, 1974.

21. van der Poel, C., "A General System Describing the Viscoelastic Properties of Bitumens and Its Relation to Routine Test Data," Journal of Applied Chemistry, v. 4, pt. 5, May 4, 1954, pp. 221-236.

22. Heukelom, W. and A. J. G. Klomp, "Road Design and Dynamic Loadings." Proceedings, Association of Asphalt Paving Technologists, Vol. 33, 1964, pp. 92-125.

23. Van Dratt, W. E. F., and P. Sommer, "Ein Gerat xur Bestimmung der dynamischen Elastizitatsmoduln von Asphalt." Strasse und Autobahn, Vol. 35, 1966.

ClibPDF - www.fastio.com

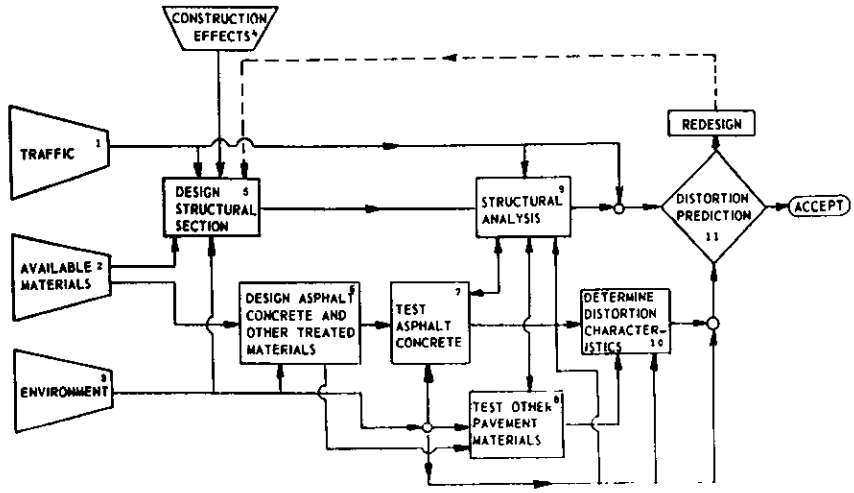

Fig. 1 — Block diagram of a distortion subsystem.

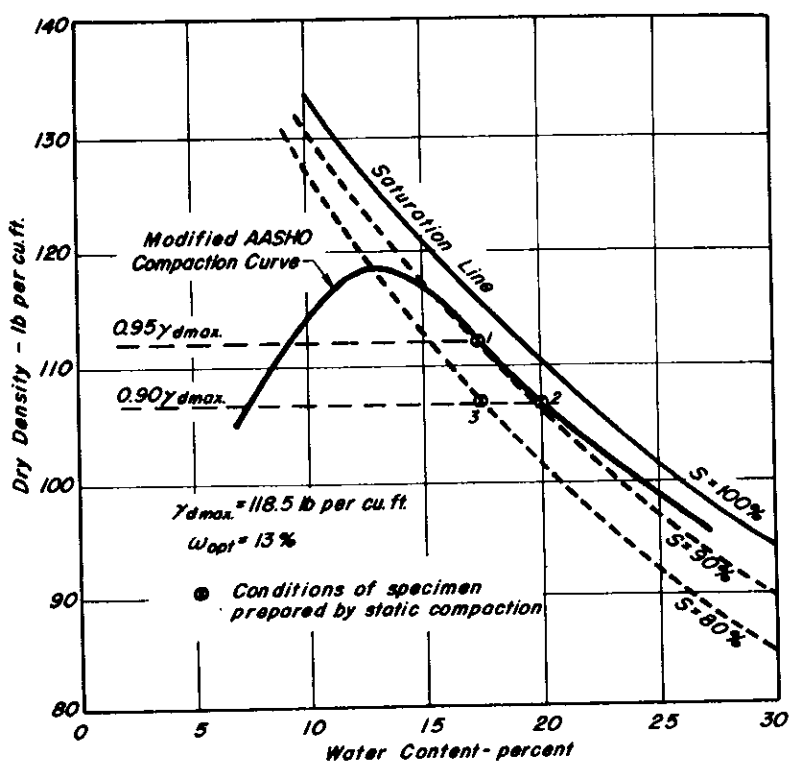

Fig. 2 — Density vs. water content relationship for Ygnacio Valley subgrade soil.

ClibPDF - www.fastio.com

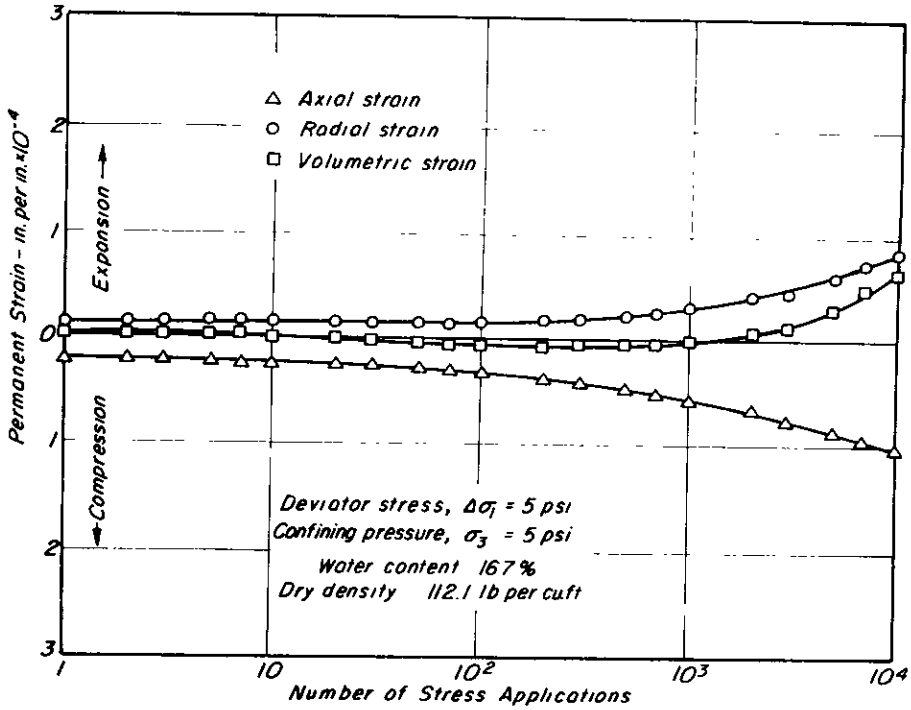

Fig. 3 – Axial, radial, and volumetric permanent strain vs. number of stress applications, deviator stress = 5 psi (soil condition 1, Fig. 2).

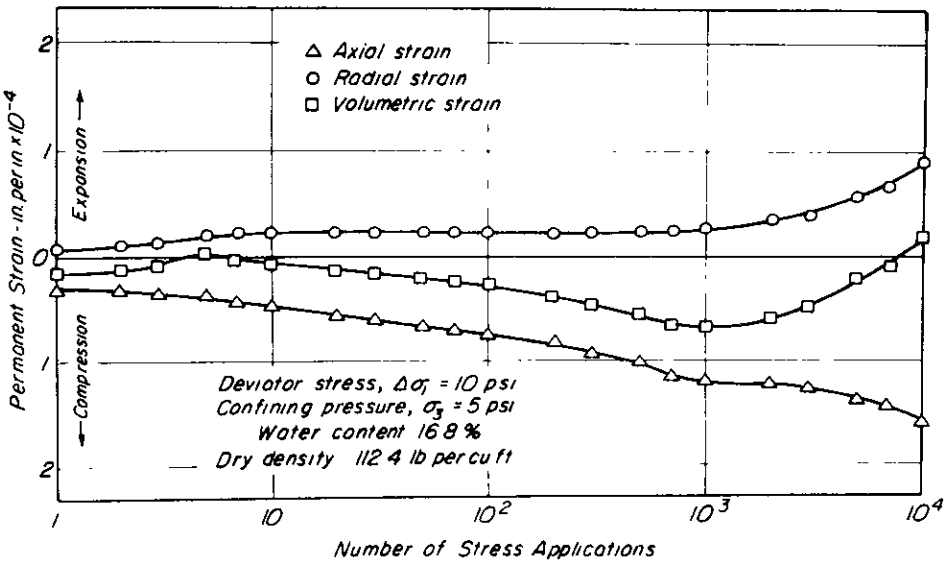

Fig. 4 – Permanent strain vs. number of stress applications relationship.

ClibPDF - www.fastio.com

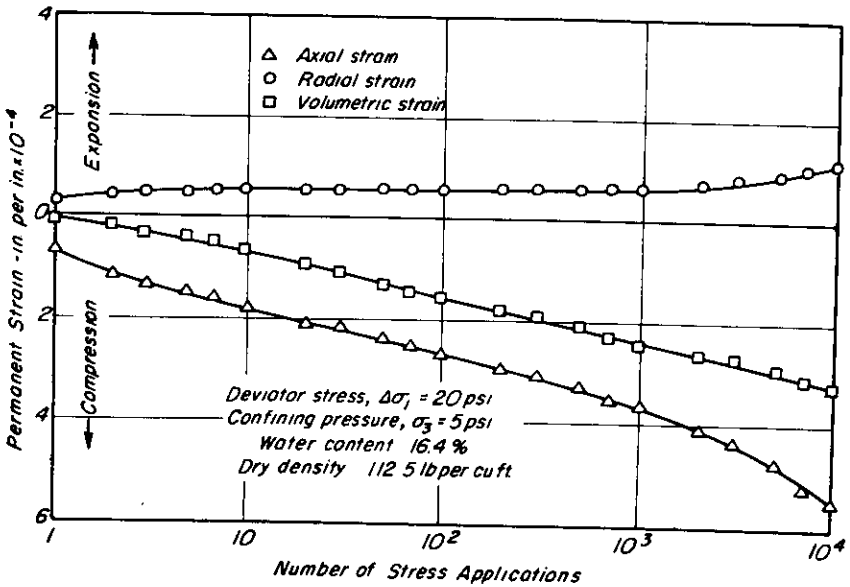

Fig. 5 – Axial, radial, and volumetric permanent strain vs. number of stress applications, deviator stress = 20 psi (soil condition 1, Fig. 2).

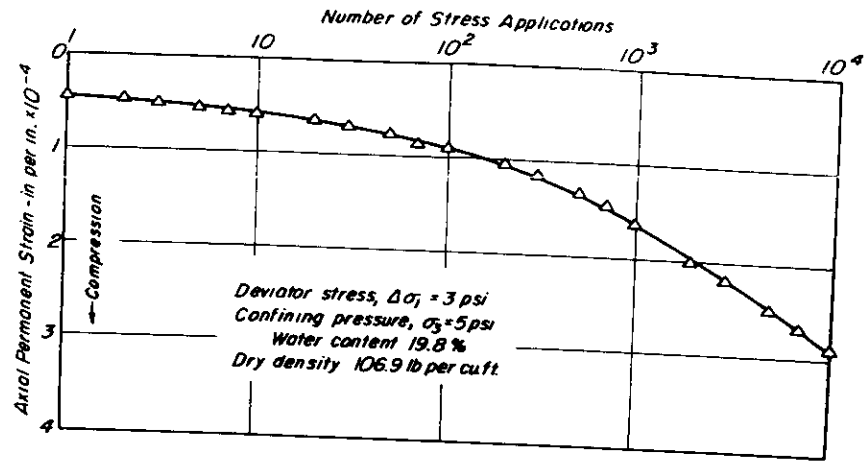

Fig. 6 – Permanent strain vs. number of stress applications relationship.

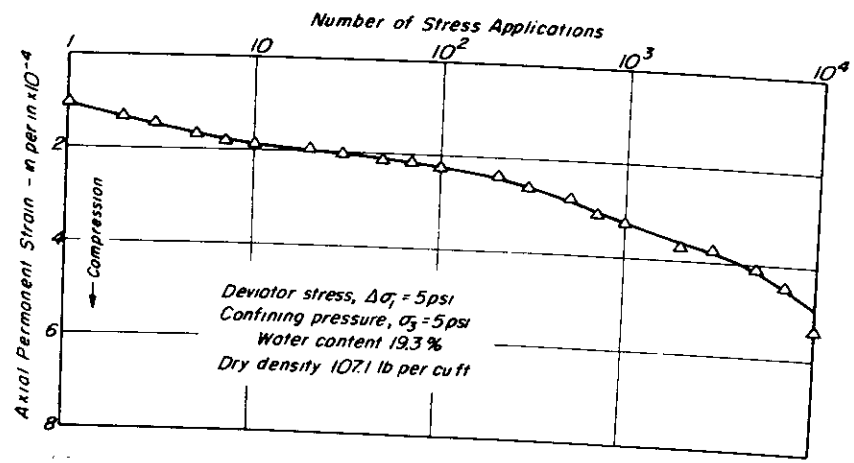

Fig. 7 – Permanent strain vs. number of stress applications relationship.

ClibPDF - www.fastio.com

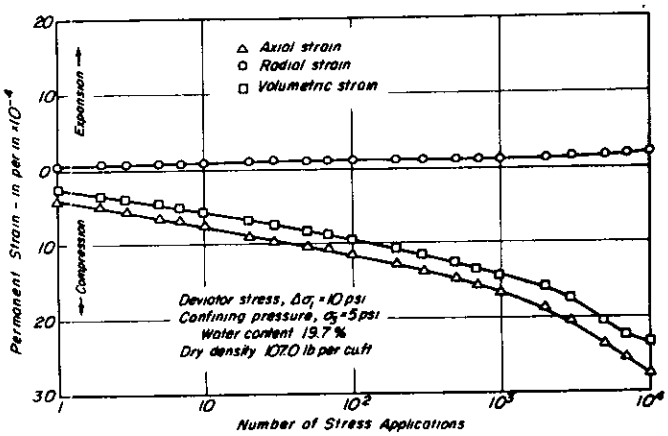

Fig. 8 – Permanent strain vs. number of stress applications relationship.

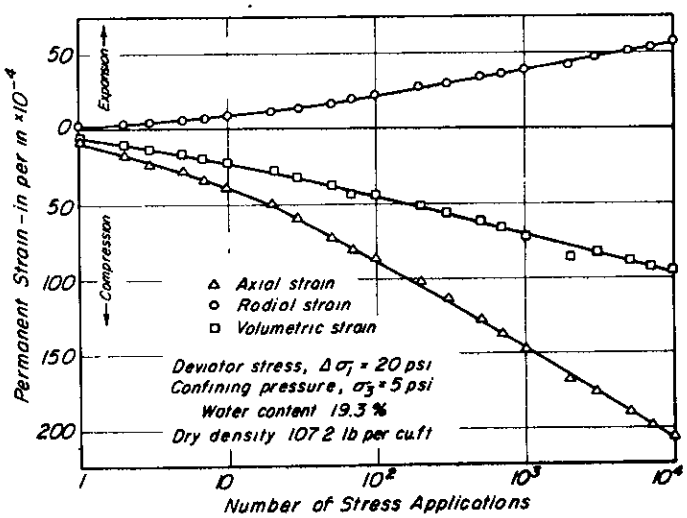

Fig. 9 – Axial, radial, and volumetric permanent strain vs. number of stress applications, deviator stress = 20 psi (soil condition 2, Fig. 2).

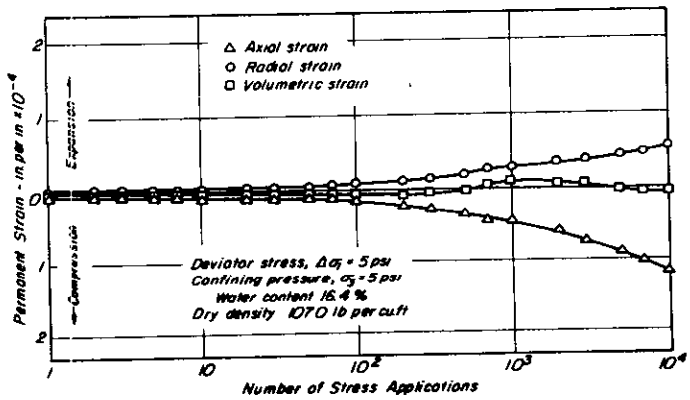

Fig. 10 – Permanent strain vs. number of stress applications relationship.

ClibPDF - www.fastio.com

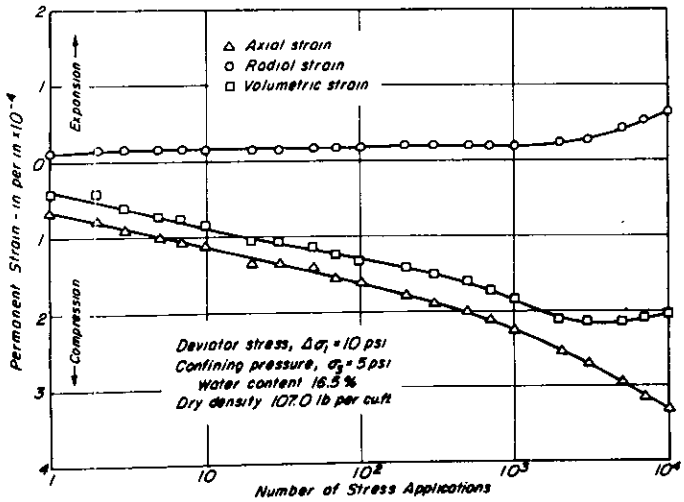

Fig. 11 — Permanent strain vs. number of stress applications relationship.

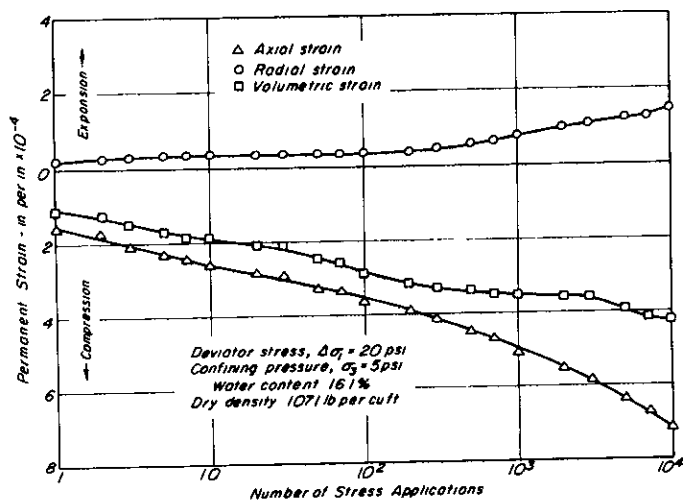

Fig. 12 — Permanent strain vs. number of stress applications relationship.

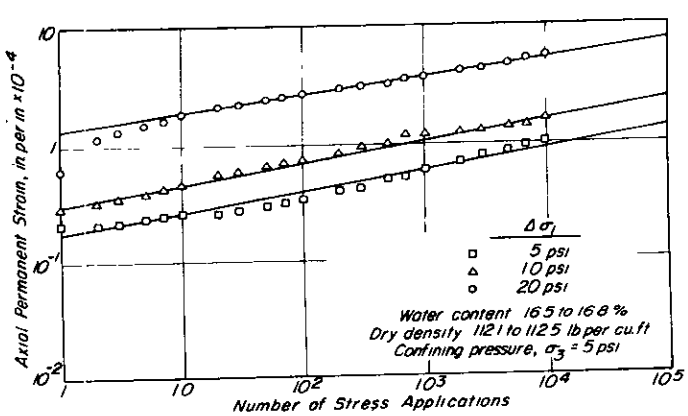

Fig. 13 — Relationship between axial permanent strain and number of stress applications (soil condition 1, Fig. 2).

ClibPDF - www.fastio.com

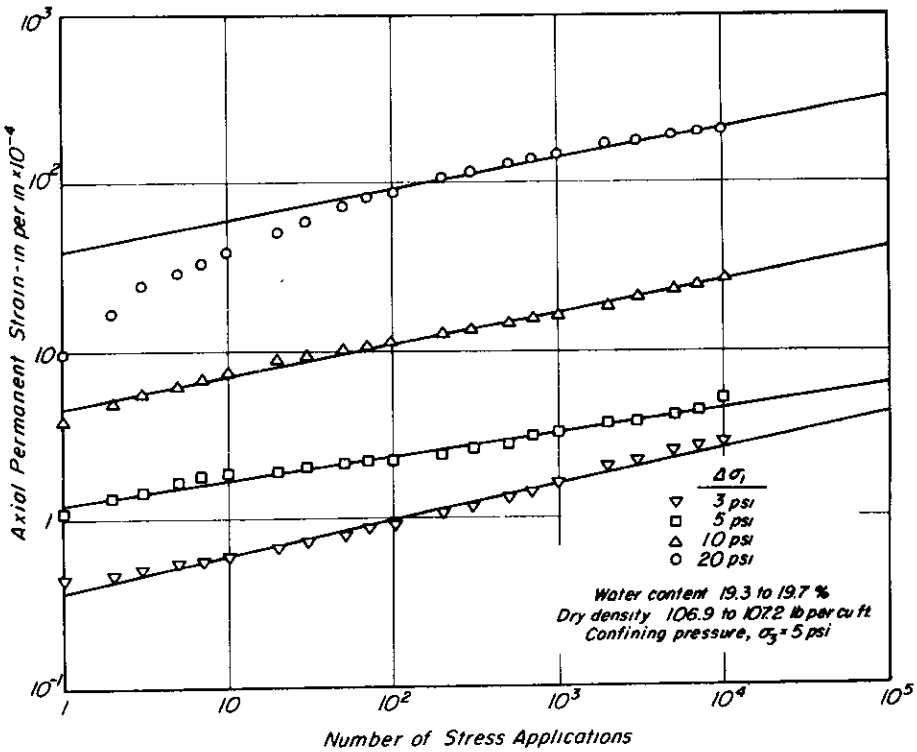

Fig. 14 – Relationship between axial permanent strain and number of stress applications (soil condition 2 , Fig. 2).

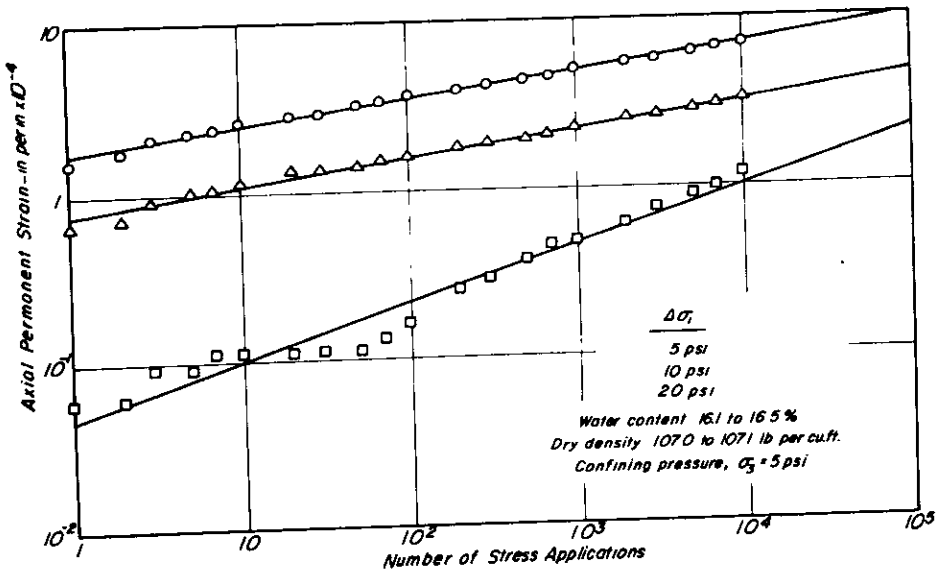

Fig. 15 – Relationship between axial permanent strain and number of stress applications (soil condition 3 , Fig. 2).

ClibPDF - www.fastio.com

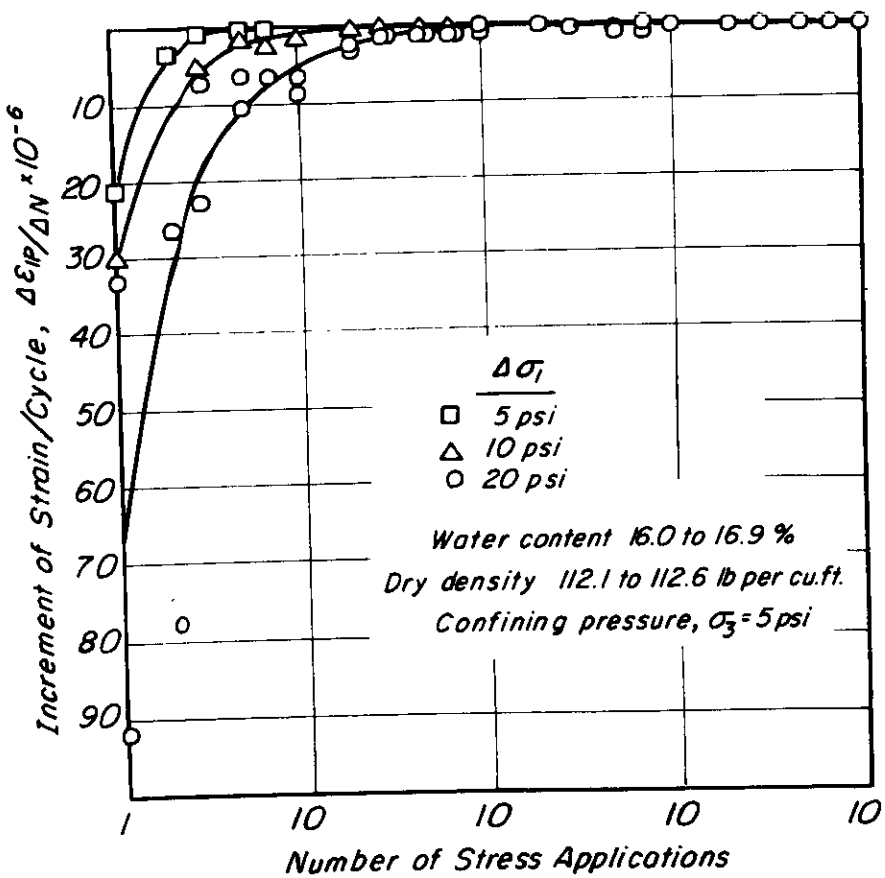

Fig. 16 - Strain increment vs. number of stress applications (soil condition 1 , Fig. 2).

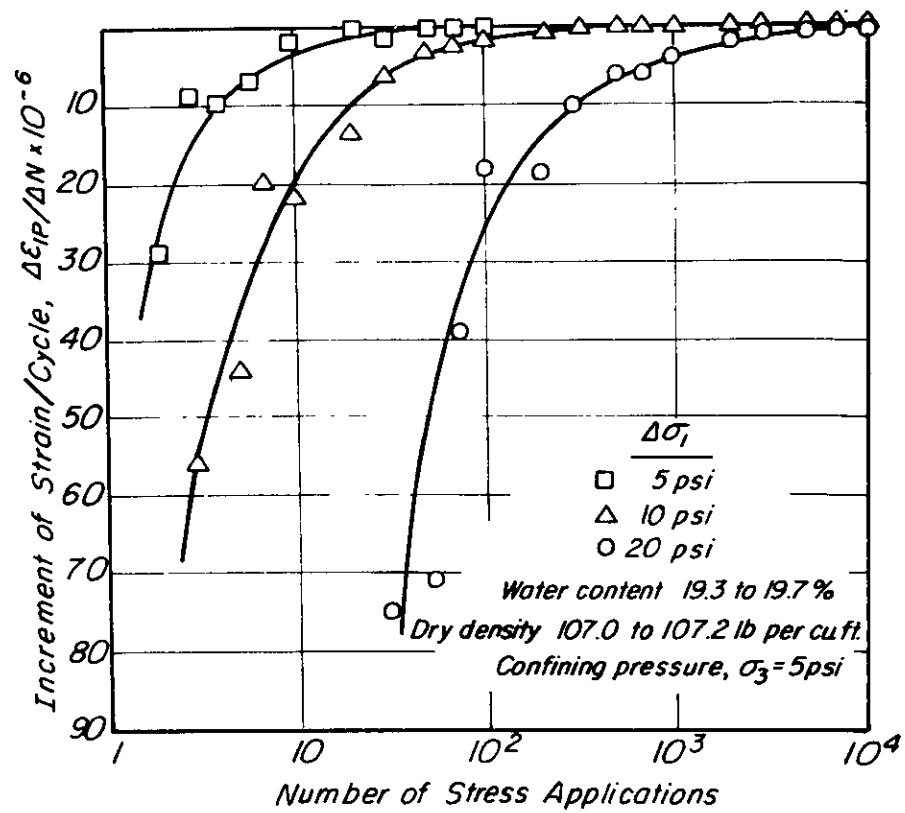

Fig. 17 - Strain increment vs. number of stress applications (soil condition 2 , Fig. 2).

ClibPDF - www.fastio.com

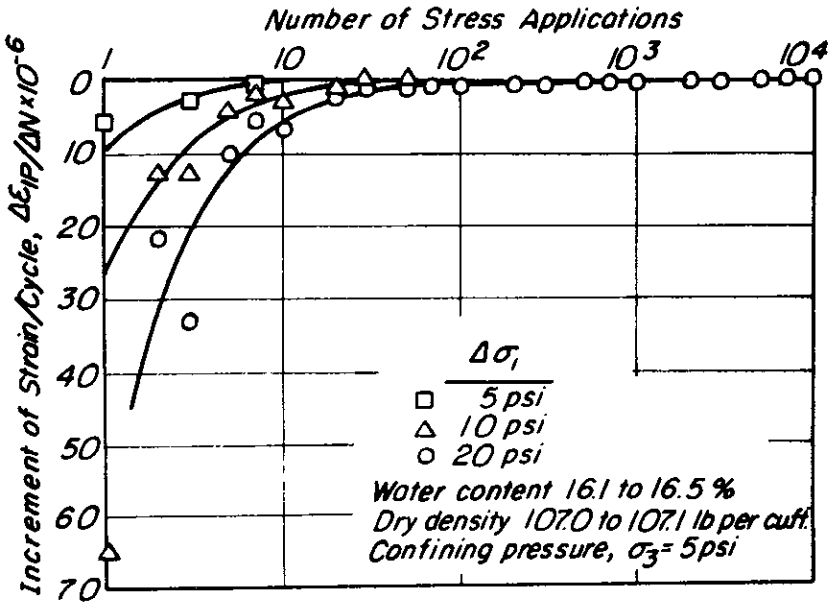

Fig. 18 – Strain increment vs. number of stress applications relationship.

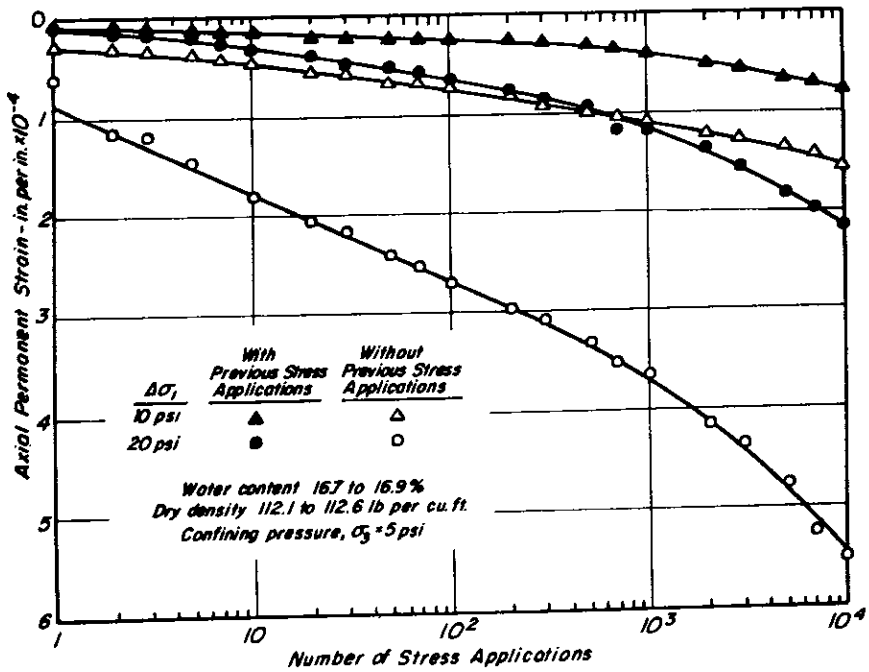

Fig. 19 – Influence of stress history on permanent strain accumulation (soil condition 1, Fig. 2).

ClibPDF - www.fastio.com

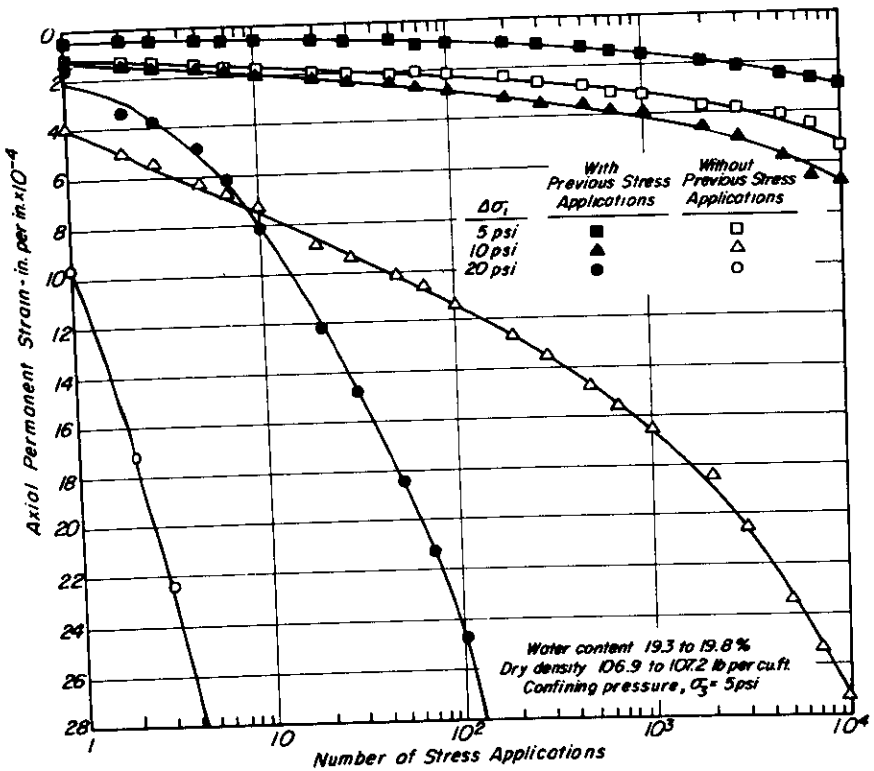

Fig. 20 – Influence of stress history on permanent strain accumulation (soil condition 2, Fig. 2).

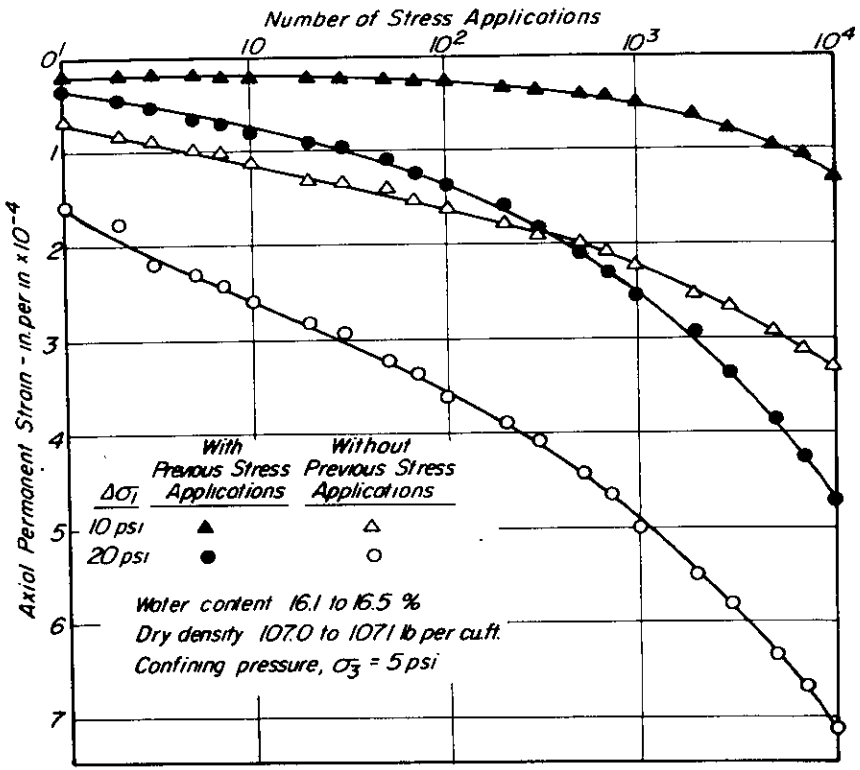

Fig. 21 – Effect of stress history on permanent strain.

ClibPDF - www.fastio.com

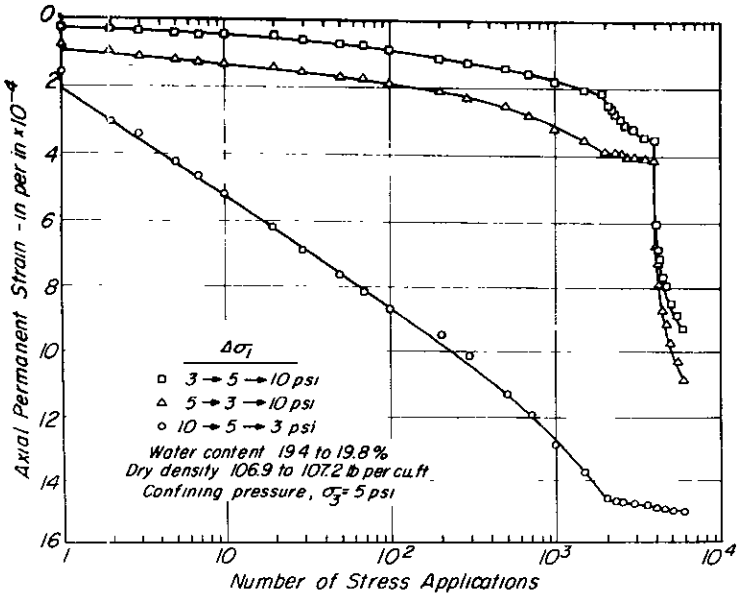

Fig. 22 – Influence of stress sequences on accumulation of permanent strain.

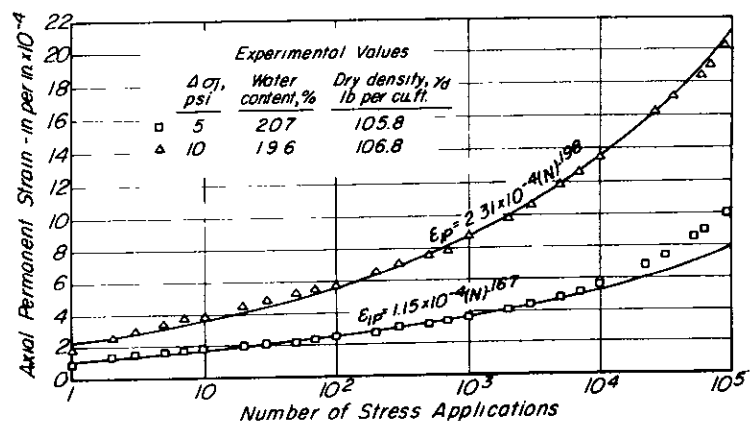

Fig. 23 – Comparisons of predicted and measured permanent strains vs. stress applications to 100,000 stress applications.

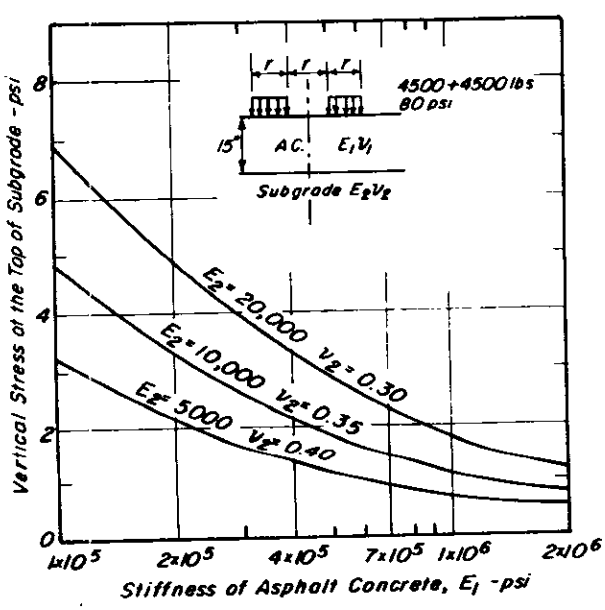

Fig. 24 – Influence of asphalt concrete and subgrade stiffnesses on vertical compressive stress at the subgrade surface.

ClibPDF - www.fastio.com

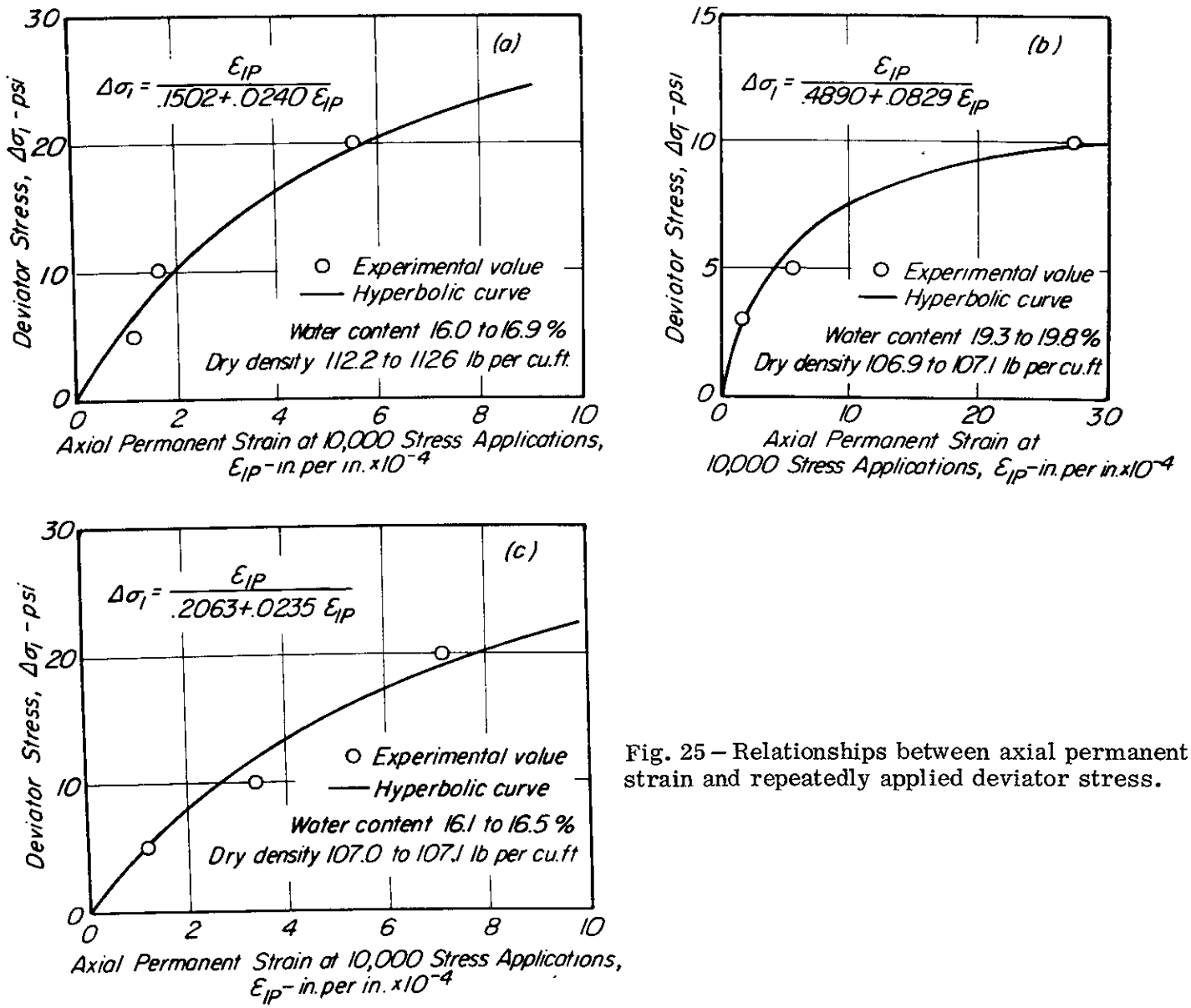

Fig. 25 – Relationships between axial permanent strain and repeatedly applied deviator stress.

ClibPDF - www.fastio.com

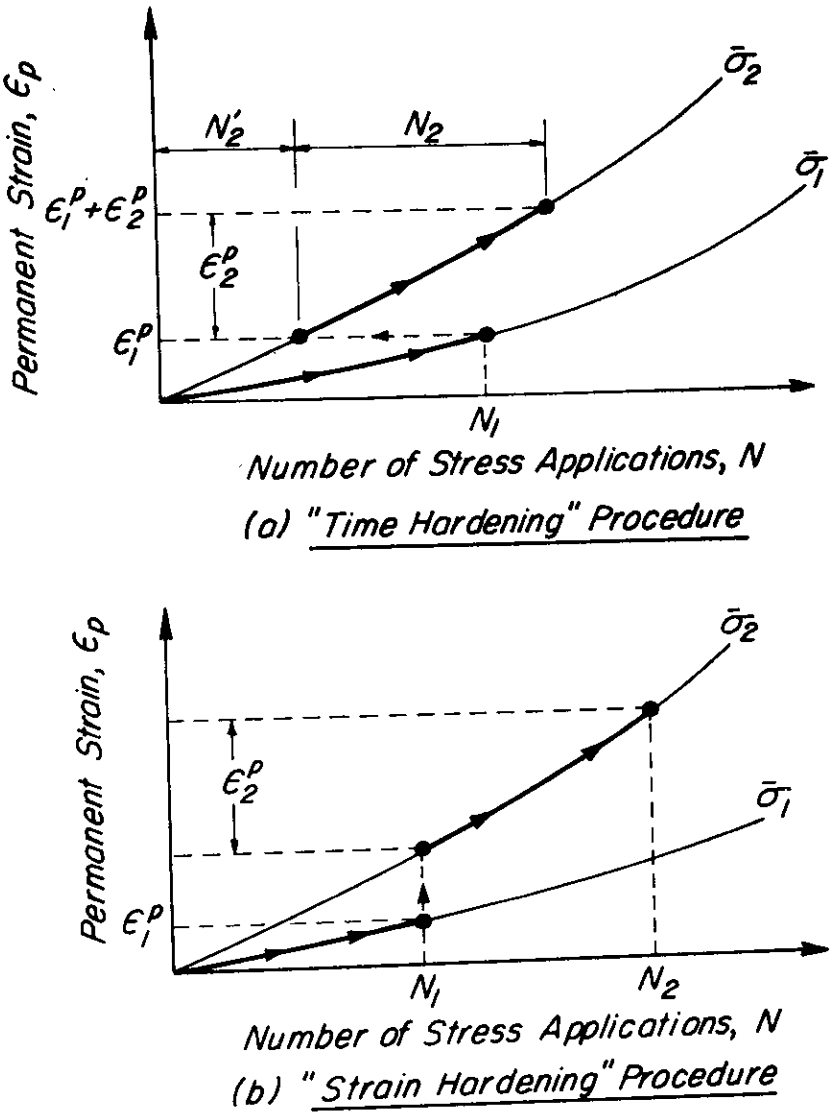

Fig. 26 – Procedures to predict cumulative loading from the results of simple loading tests.

ClibPDF - www.fastio.com

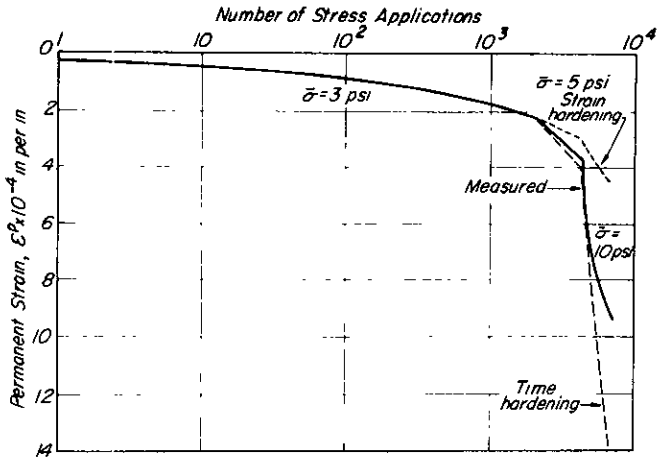

Fig. 27 — Comparison of predicted and measured cumulative permanent strain; 3-5-10 psi sequence; 2000 applications at each stress level.

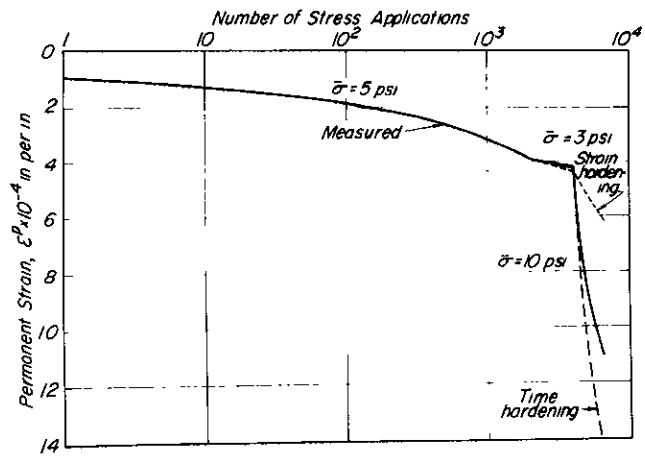

Fig. 28 – Comparision of predicted and measured cumulative permanent strain; 5-3-10 psi sequence; 2000 applications at each stress level.

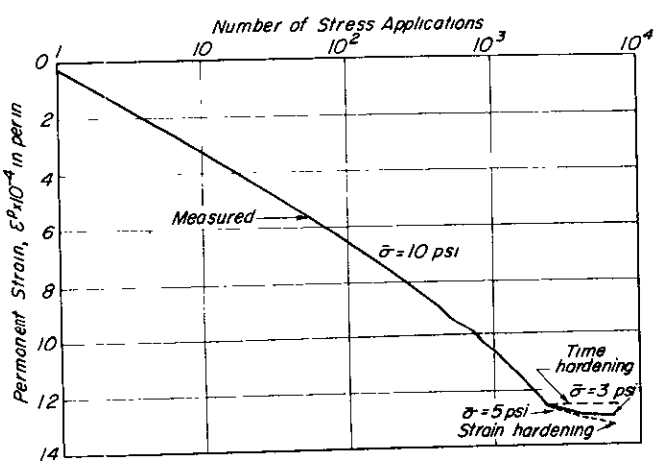

Fig. 29 – Comparison of predicted and measured cumulative permanent strain; 10-5-3 psi sequence; 2000 applications at each stress level.

ClibPDF - www.fastio.com

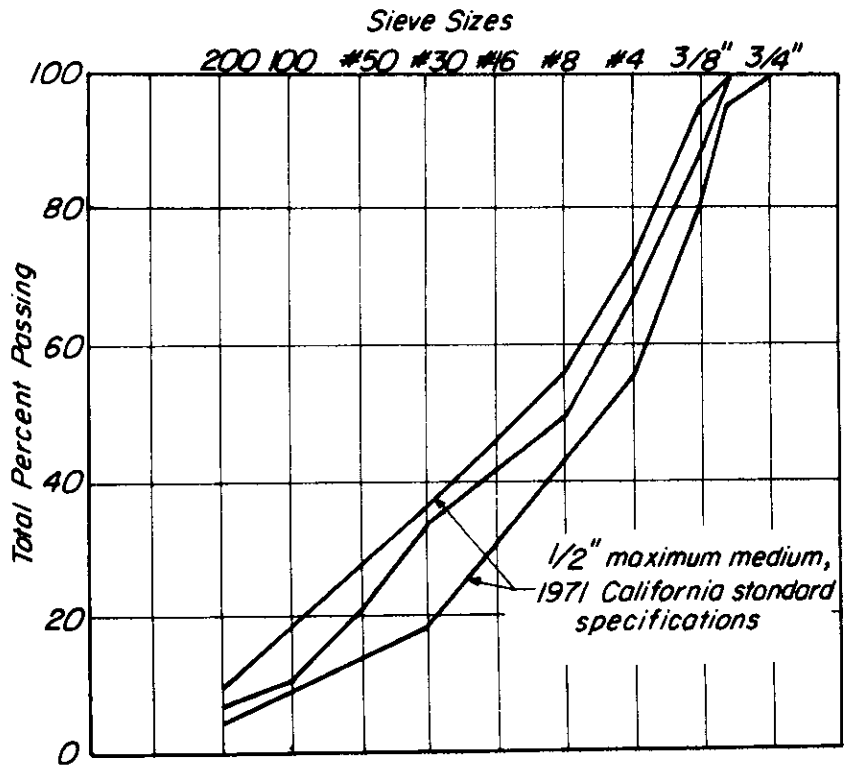

Fig. 30 – Aggregate grading curve, Watsonville granite (average of six test results).

ClibPDF - www.fastio.com

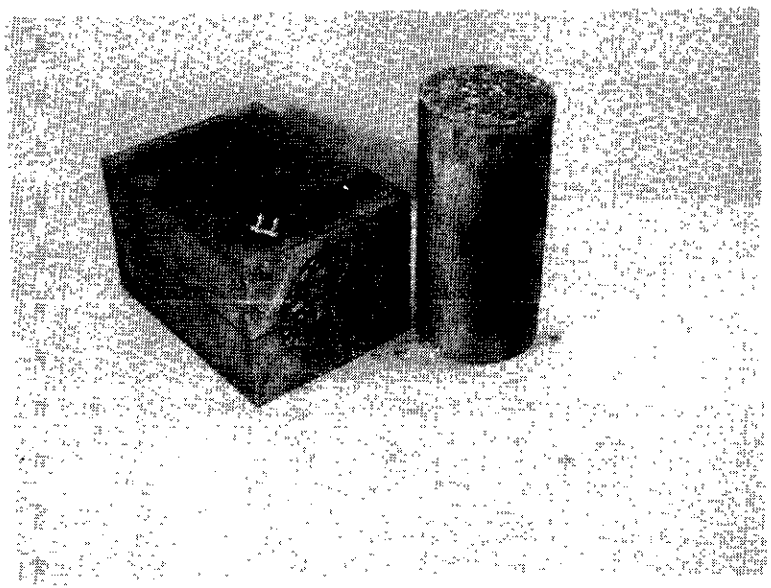

Fig. 31 – Jig used for trimming and drilling asphalt concrete specimens.

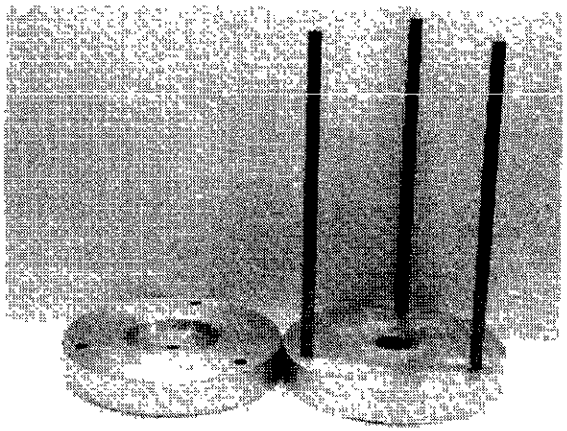

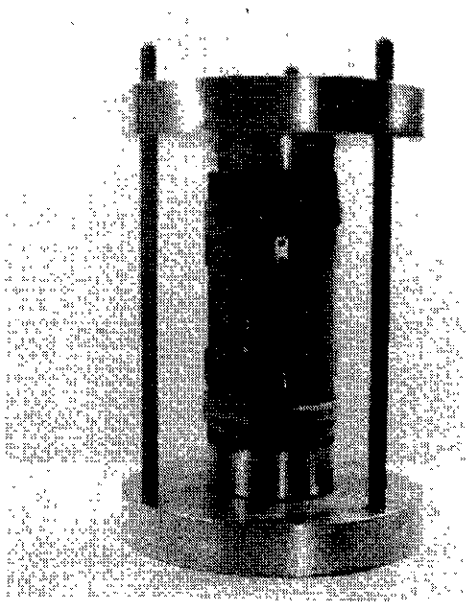

Fig. 32 – Devise used to align end caps.

LClibPDF - www.fastio.com

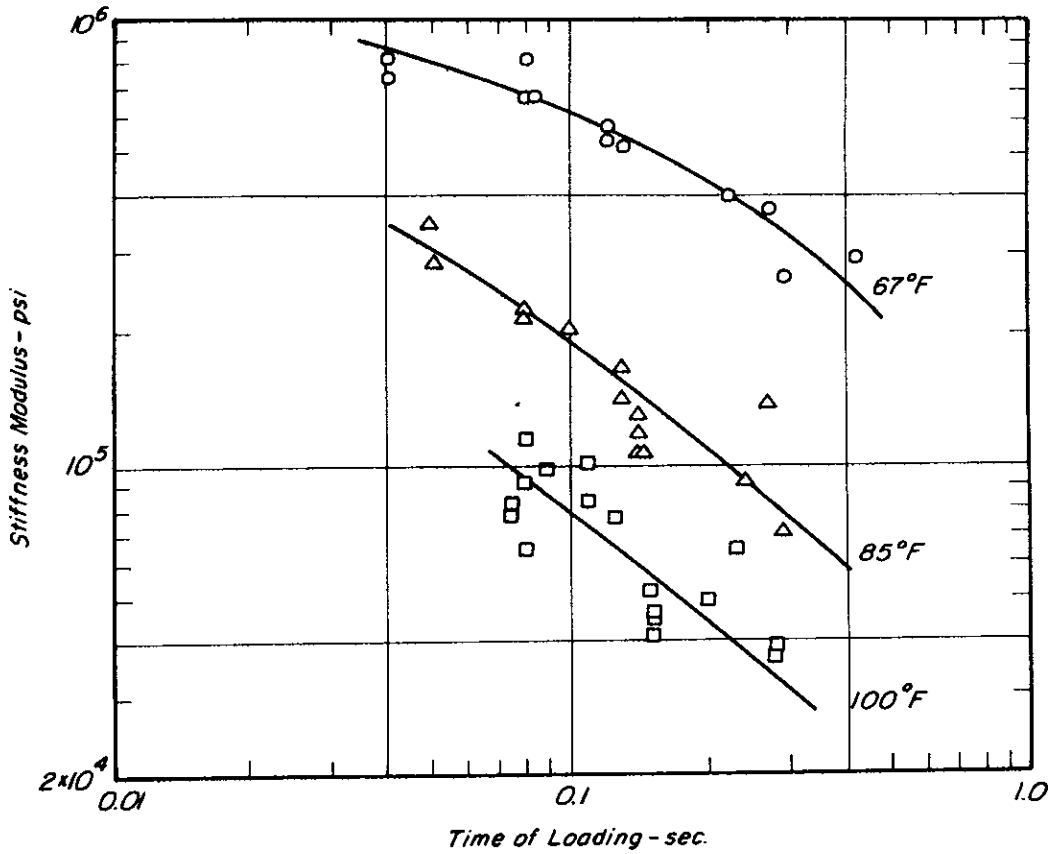

Fig. 33 — Stiffness vs. time of loading data for asphalt concrete specimens.

ClibPDF - www.fastio.com

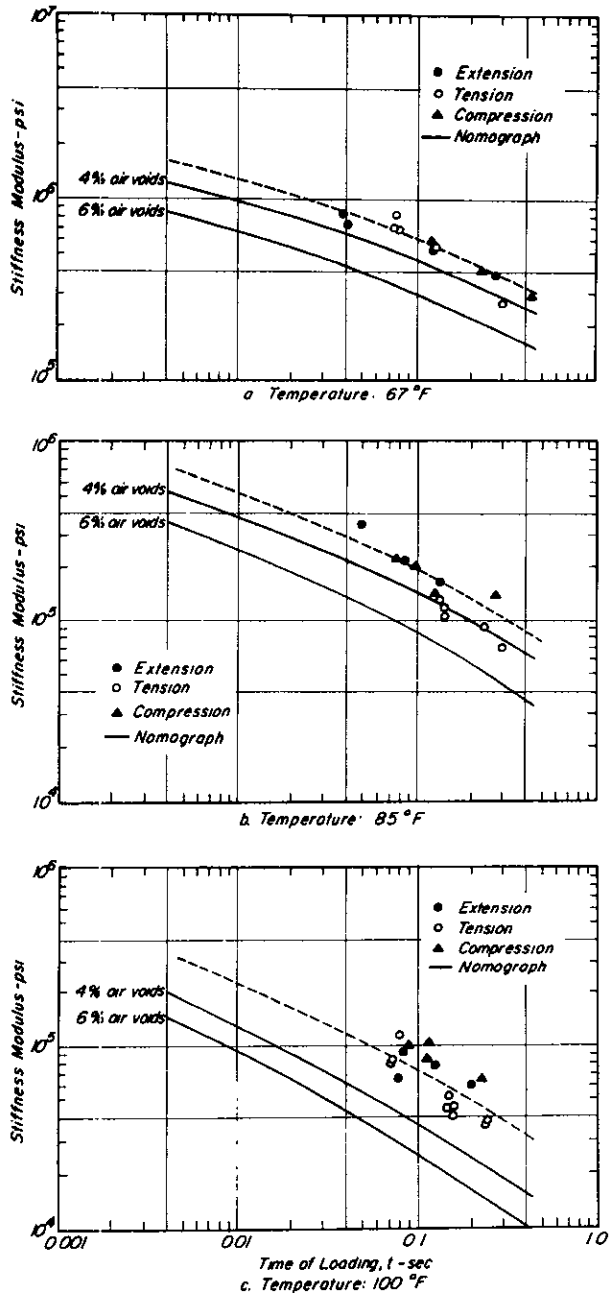

Fig. 34 – Comparisons between measured stiffnesses and estimated stiffnesses by the Shell procedure over a range in times of loading and temperature.

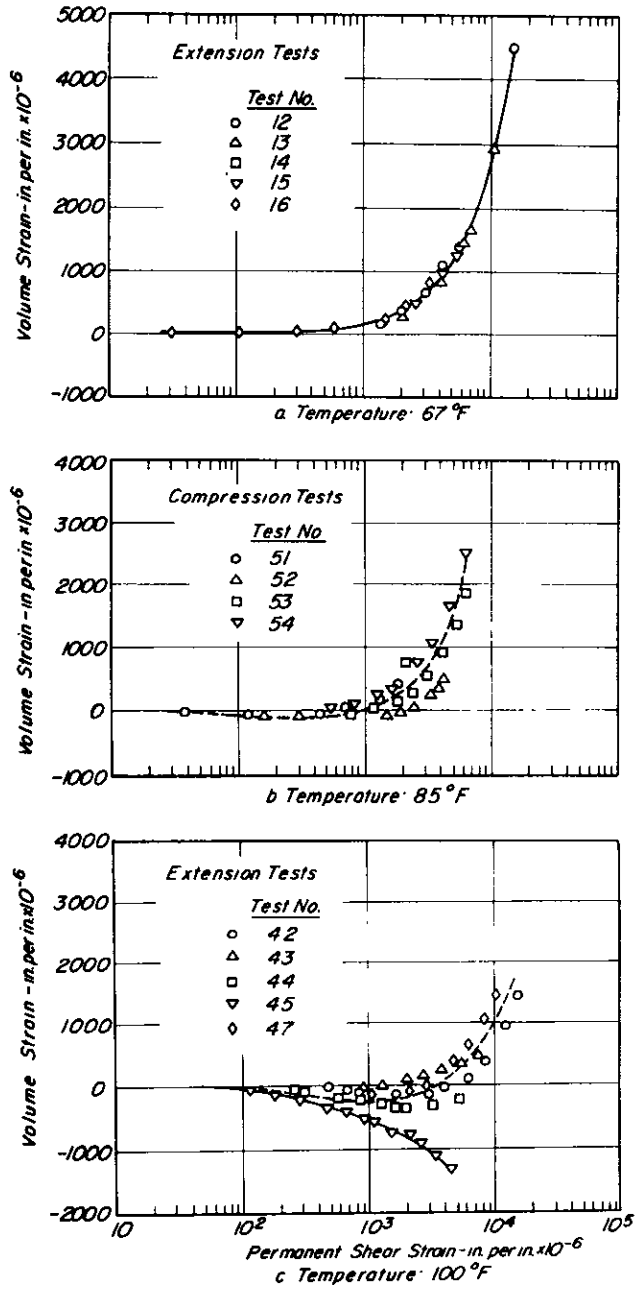

Fig. 35 — Volume strain vs. permanent shear strain relationships – repeated loading.

ClibPDF - www.fastio.com

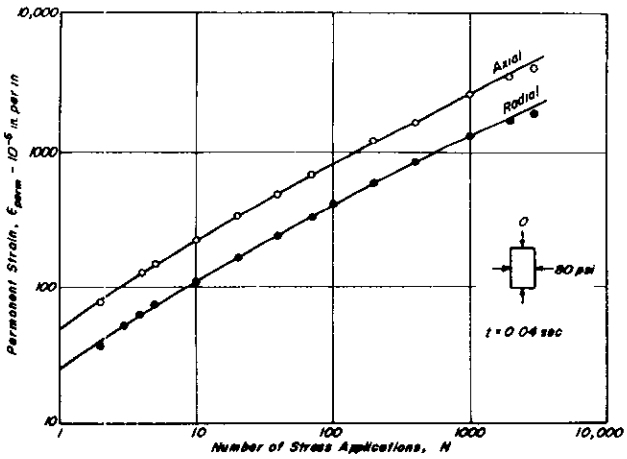

Fig. 36 — Relationships between permanent strain and stress applications, extension test - 67° F.

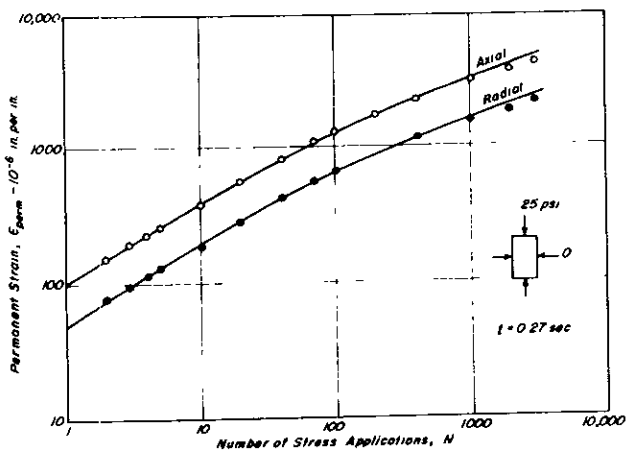

Fig. 37 – Relationships between permanent strain and stress applications, compression test - 85° F.

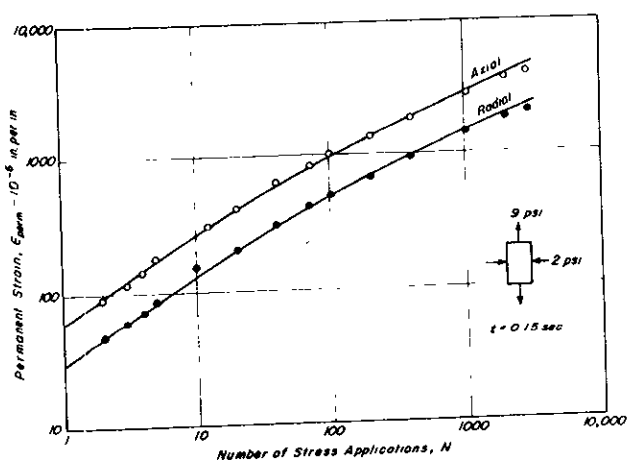

Fig. 38 – Relationships between permanent strain and stress applications, tension test - 100° F.

ClibPDF - www.fastio.com

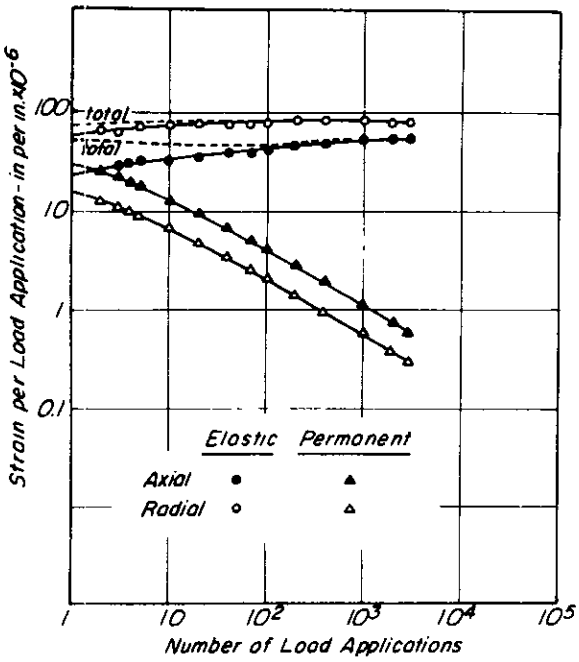

Fig. 39 – Typical strain per load application, data from extension tests, T = 67° F.

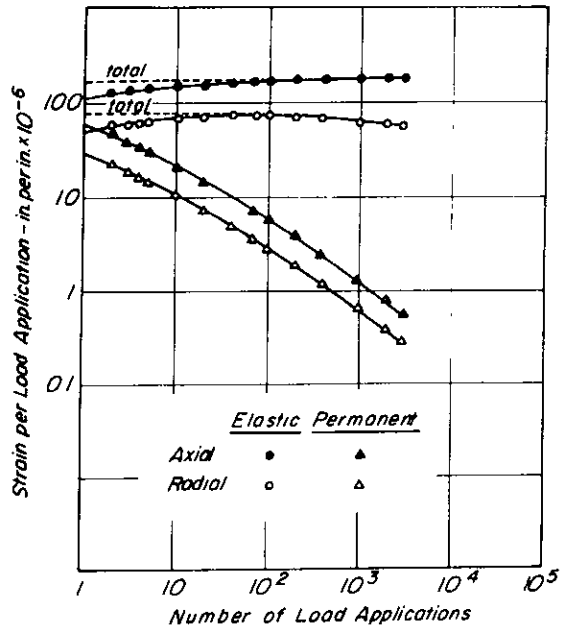

Fig. 40 – Typical strain per load application, data from compression tests, T = 85° F.

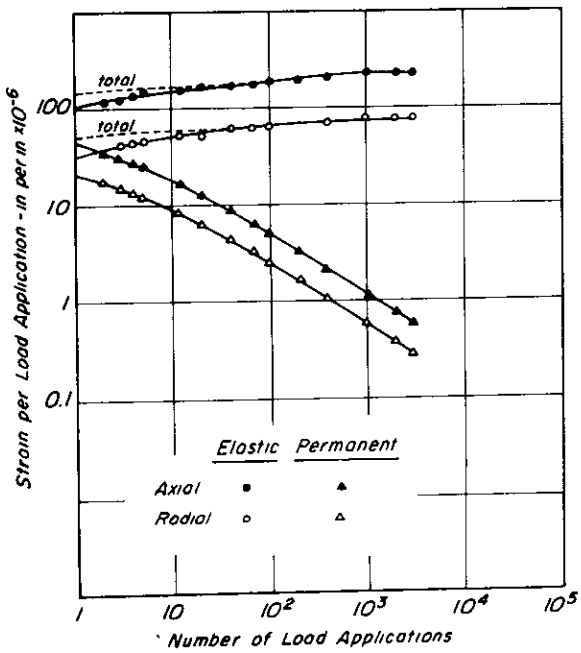

Fig. 41 – Typical strain per load application, data from tension tests, T = 100° F.

ClibPDF - www.fastio.com

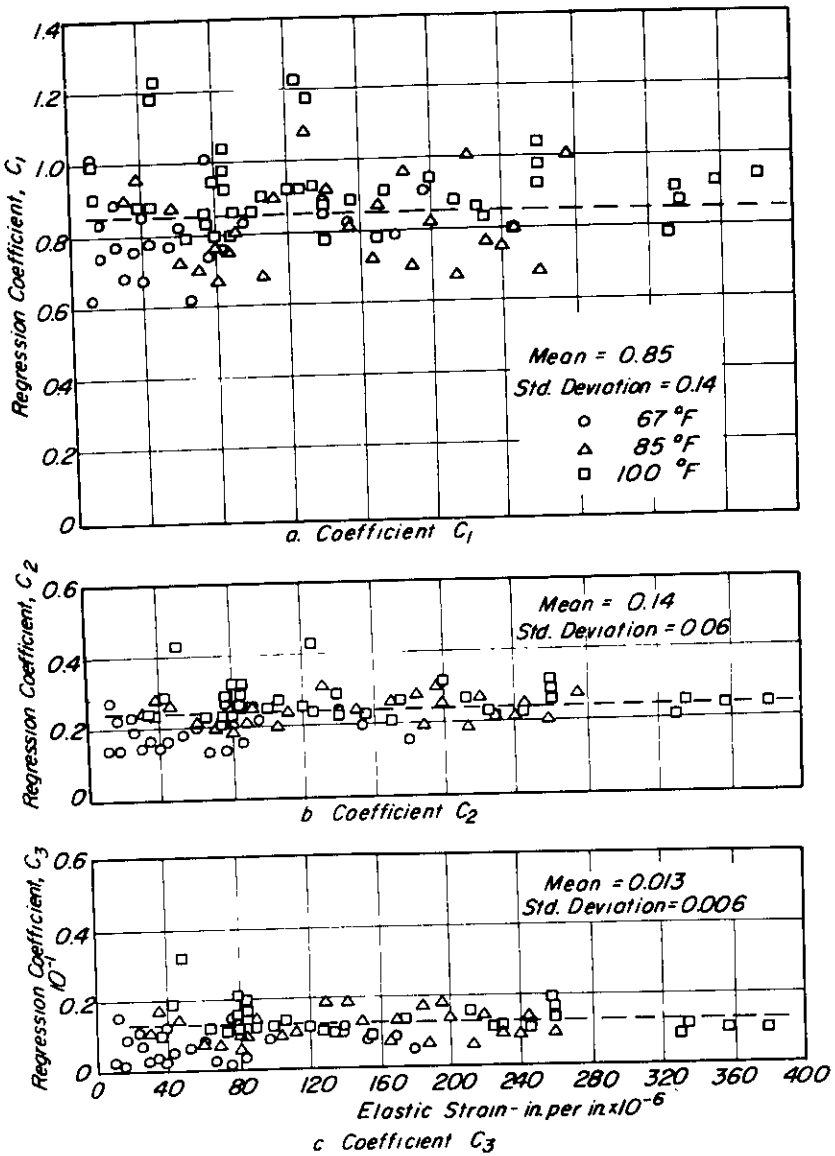

Fig. 42 – Regression coefficients C_1, C_2, C_3 as a function of elastic strain.

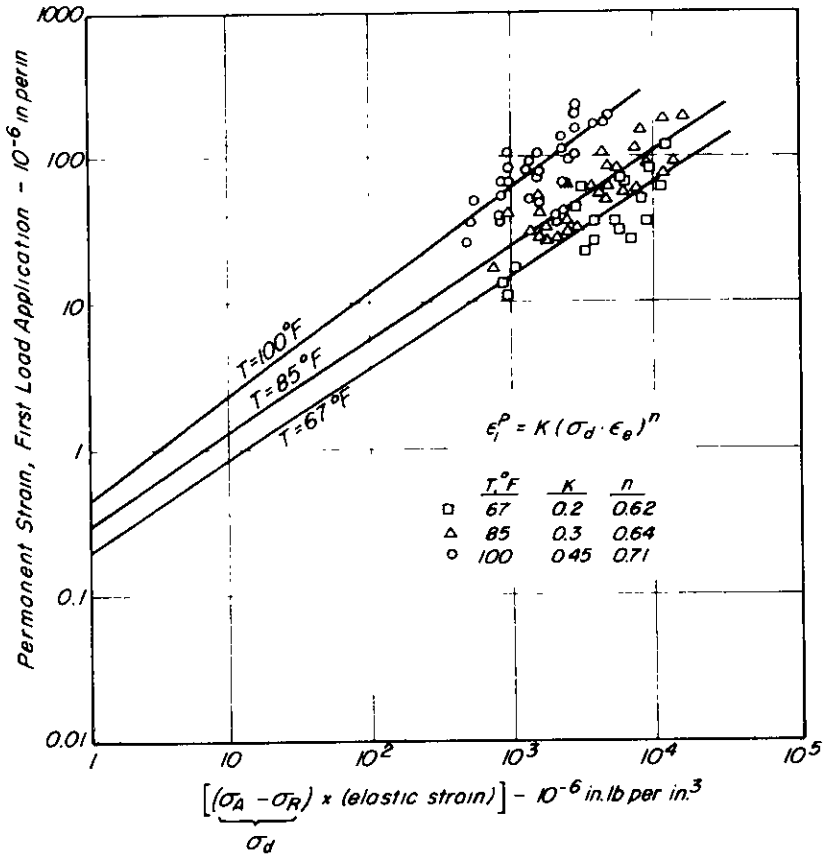

Fig. 43 – Relationship between the product of elastic strain and stress difference and permanent strain at first load application, repeated load triaxial compression tests.

ClibPDF - www.fastio.com

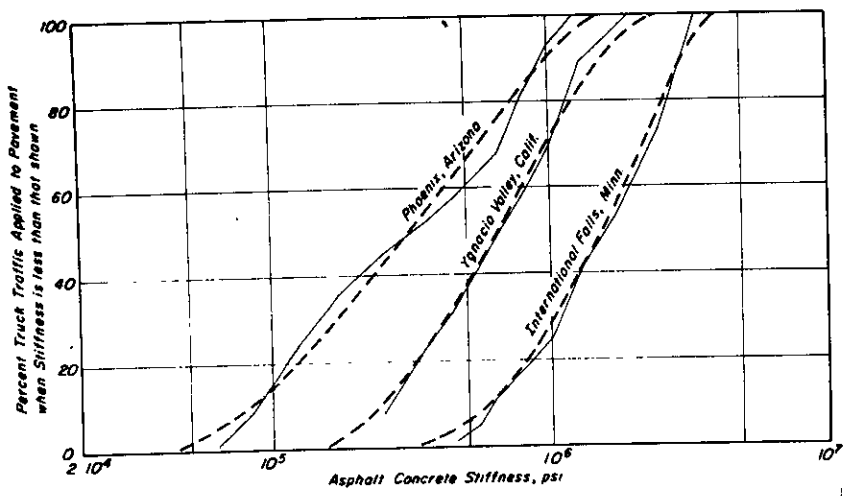

Fig. 44 – Stiffness variations with traffic applications – 12-in. thick asphalt concrete layer.

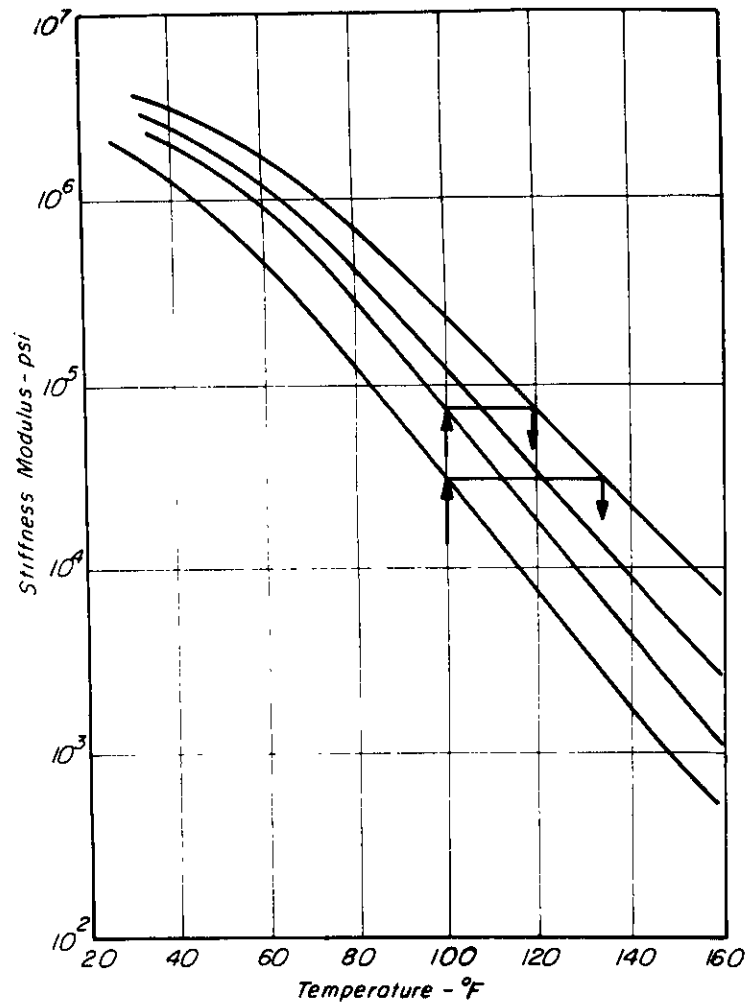

Fig. 45 – Time of loading and temperature relationships showing time - temperature super-position at constant stiffness.

Clib.PDF - www.fastie.com

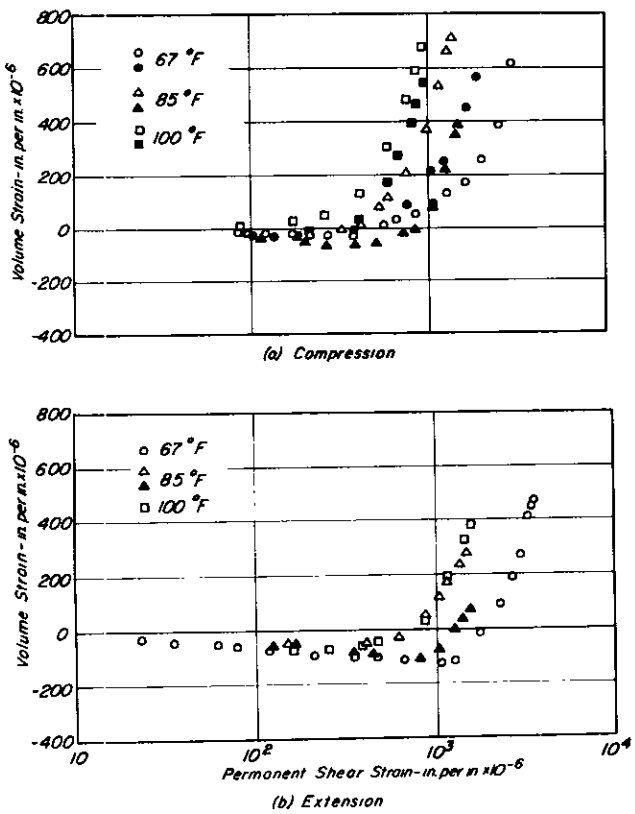

Fig. 46 – Volume strain vs. permanent shear strain relationships - creep.

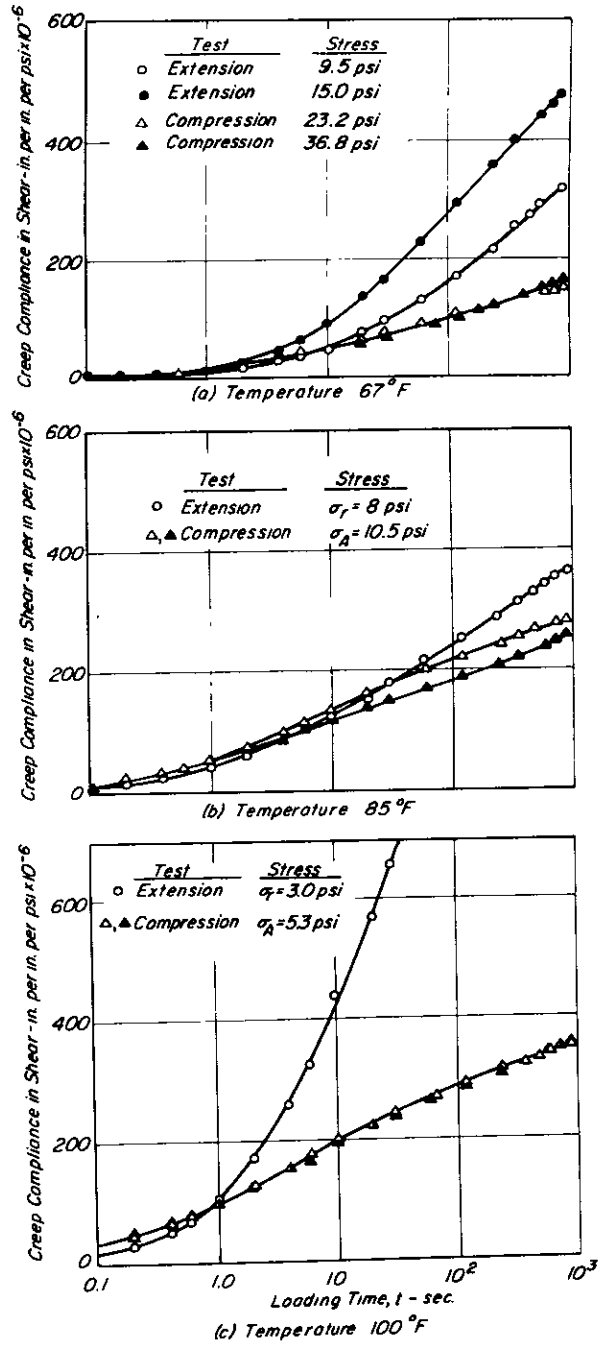

Fig. 47 – Shear compliance data – compression and axial extension.

ClibPDF - www.fastio.com

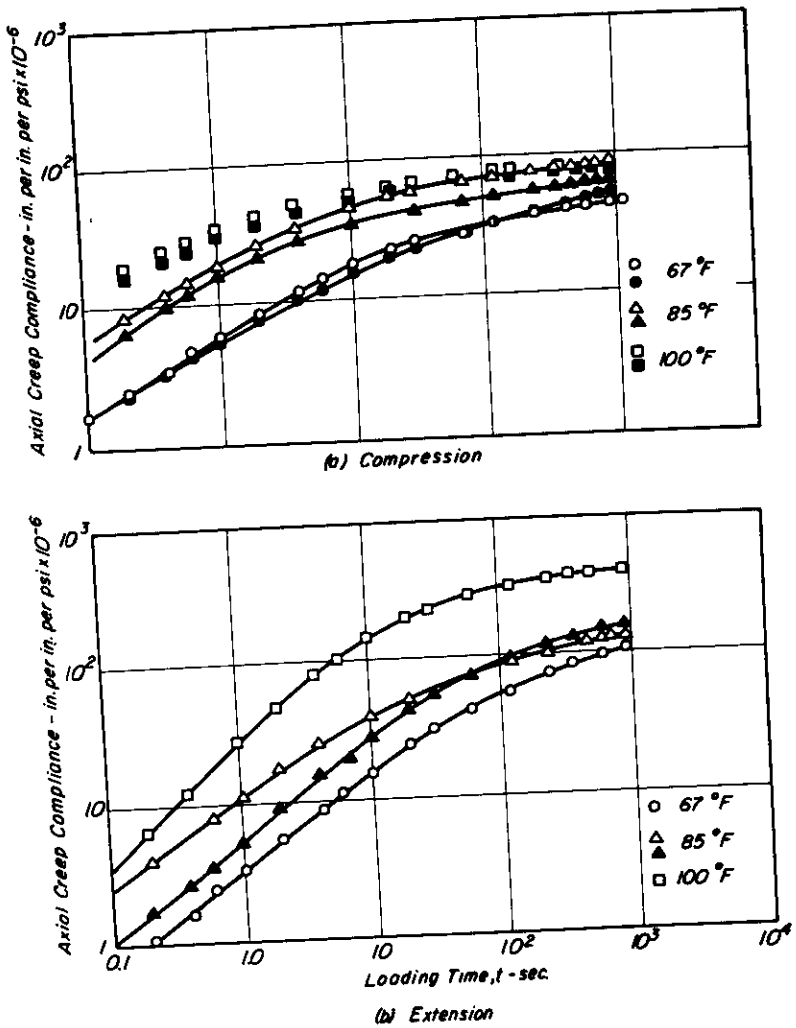

Fig. 48 — Axial compliance in compression and extension.

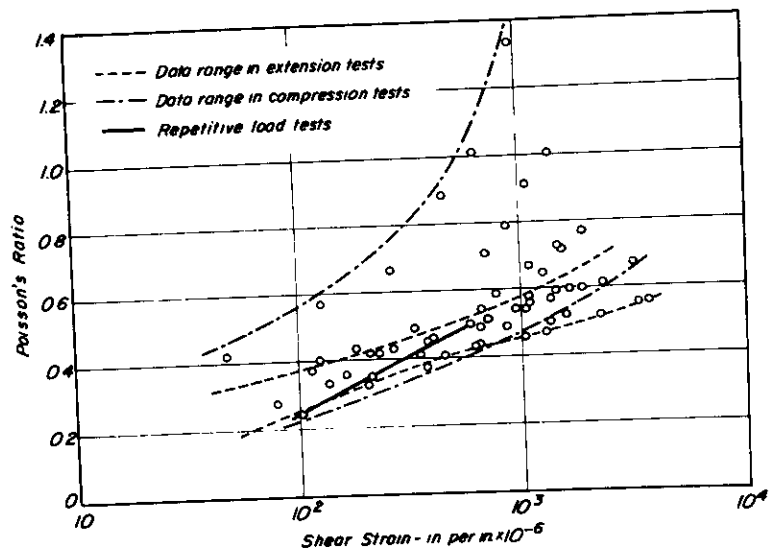

Fig. 49 – Poisson's ratio - shear strain data for creep tests, T = 67°, 85°, and 100° F.

ClibPDF - www.fastio.com

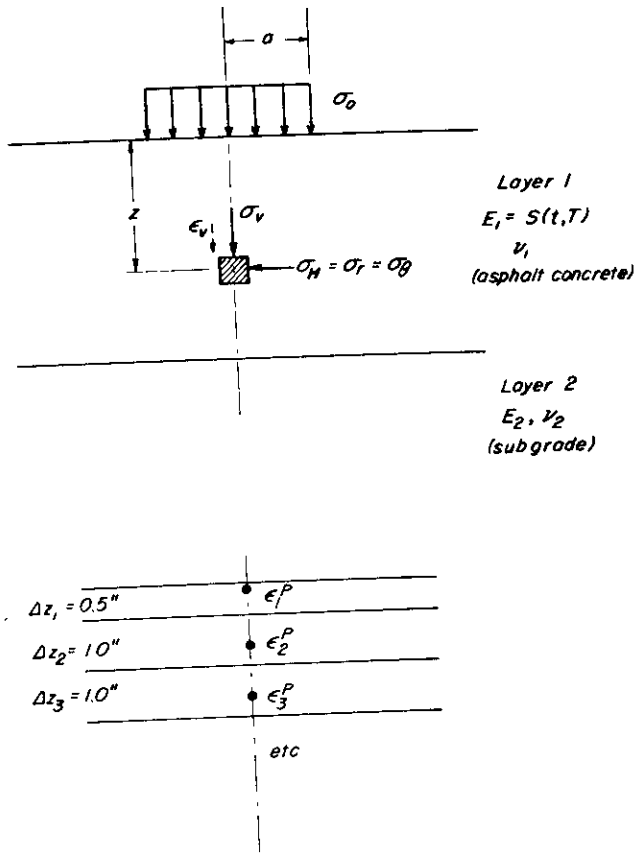

Fig. 50 – Schematic representation of pavement system used to estimate permanent deformation.

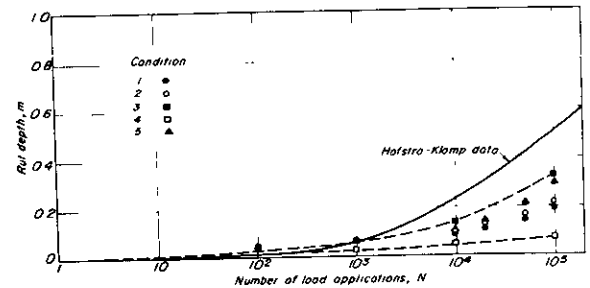

Fig. 51 – Comparison of computed rut depths with those measured by Hofstra and Klomp.

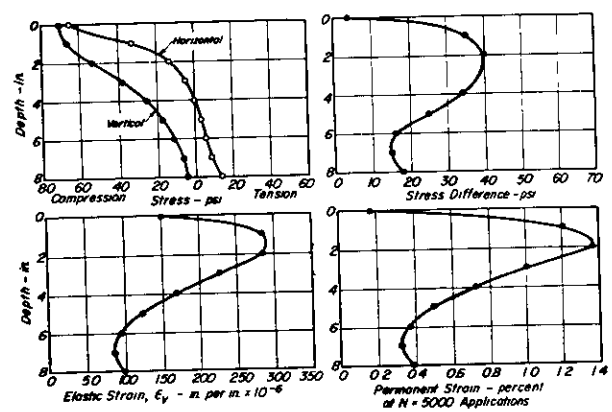

Fig. 52 – Stress and strain distributions in 8-in. thick asphalt concrete pavement subjected to 1500 lb. wheel load with 70 psi contact pressure.

ClibPDF - www.fastio.com

Clib.PDF - www.fastio.com

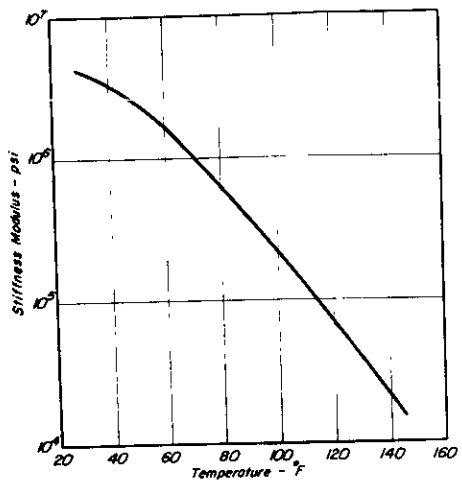

Fig. 53 – Stiffness vs. temperature relationship based on test data for asphalt concrete; t = 0.011 sec.

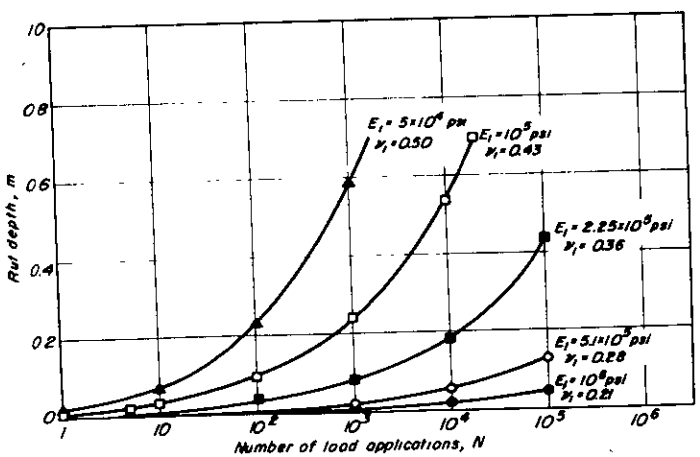

Fig. 54 – Influence of stiffness modulus of asphalt concrete on permanent deformation; $E_2 = 10,000$ psi; $\nu_2 = 0.45$.

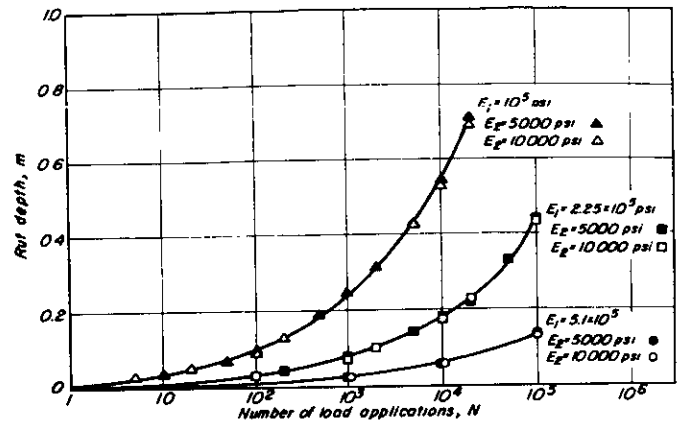

Fig. 55 – Influence of subgrade stiffness on permanent deformation.

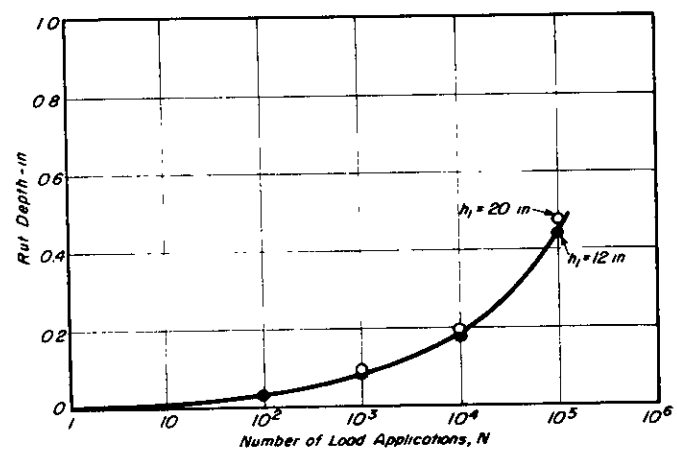

Fig. 56 – Influence of pavement thickness on permanent deformation $E_1 = 2.25 \times 10^5$ psi; $E_2 = 10,000$ psi.

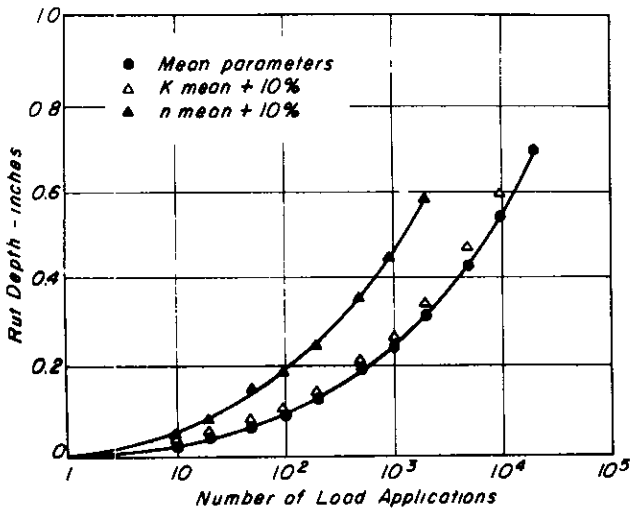

Fig. 57 – Sensitivity of computed deformations to regression coefficients K and n; 12-in. layer, $E_1 = 10^5$ psi, $E_2 = 10^4$ psi, $\nu_1 = 0.43$, $\nu_2 = 0.45$.

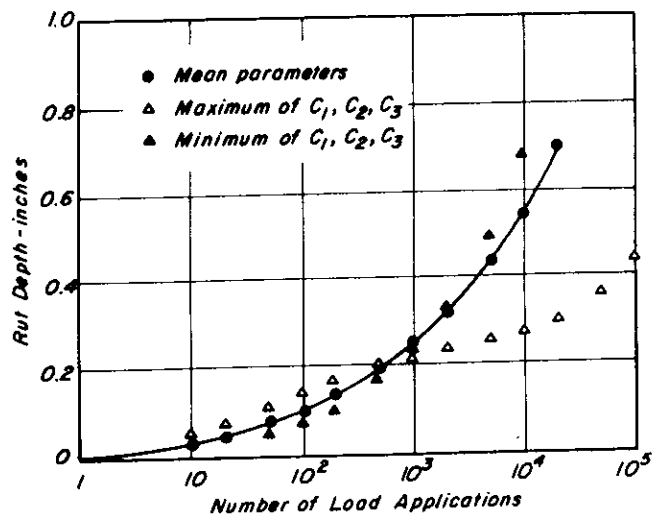

Fig. 58 – Sensitivity of computed deformations to regression coefficients C_1, C_2, C_3 in 12-in. layer, $E_1 = 10^5$ psi, $E_2 = 10^4$ psi, $\nu_1 = 0.43$, $\nu_2 = 0.45$.

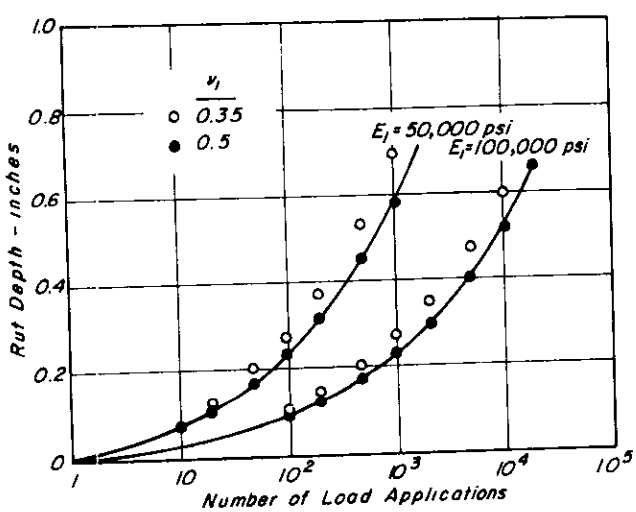

Fig. 59 – Sensitivity of computed deformations to Poisson's ratio of layer 1, $h_1 = 12$ in., $E_2 = 10^4$ psi.

ClibPDF - www.fastio.com

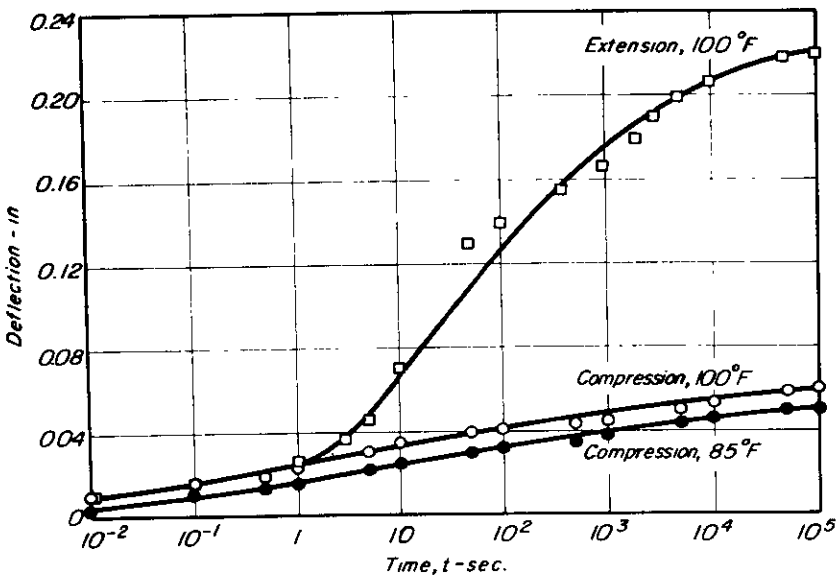

Fig. 60 – Computed deflection vs. time relationships.

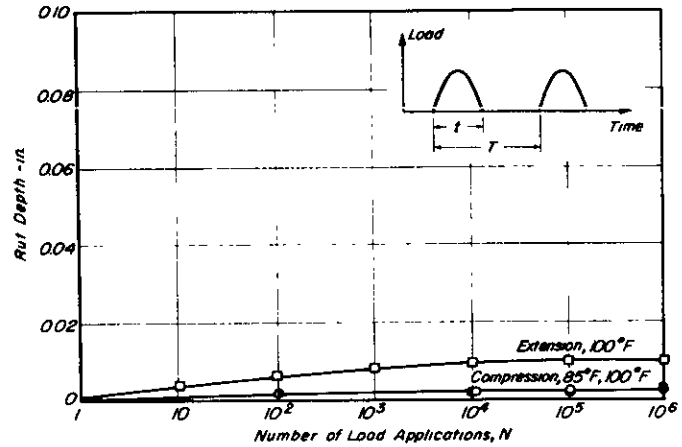

Fig. 61 – Computed permanent deformation vs. number of load applications using VESYS II; t = 0.25 sec., T = 2.5 sec.

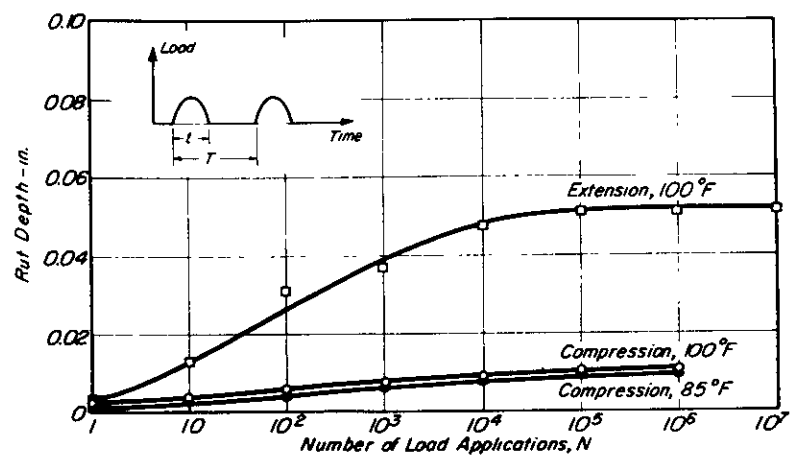

Fig. 62 – Computed permanent deformation vs. number of load applications using VESYS II; t = 0.5 sec., T = 1.0 sec.

ClibPDF - www.fastio.com

APPENDIX A

TEST DATA SUMMARY FOR REPEATED LOAD TESTS ON YGNACIO VALLEY SUBGRADE SOIL

Specimen No.	Water Content percent	Dry Density lb per cu ft	Confining Pressure psi	Repeated Deviator Stress psi
1	16.7	112	5	5
2	16.8	112	5	10
3	16.0	113	5	20
4	16.7	112	5	5, 10*
5	16.7	112	5	5, 10, 20*
6	19.3	107	5	5
7	19.7	107	5	10
8	19.3	107	5	20
9	19.3	107	5	5, 10*
10	19.3	107	5	5, 10, 20*
11	16.4	107	5	5
12	16.5	107	5	10
13	16.1	107	5	20
14	16.4	107	5	10
15	16.4	107	5	5, 10, 20*
16	19.8	107	5	3
17	19.8	107	5	3, 5*
18	19.8	107	5	3, 5, 10*
19	19.3	107	5	10
20	19.6	107	5	10
21	19.6	107	5	10
22	20.7	106	5	5
23	19.4	107	5	3, 5, 10**
24	19.8	107	5	5, 3, 10**
25	19.8	107	5	10, 5, 3**
31	19.5	107	5	5
32	19.4	107	5	3
33	19.4	107	5	10
34	16.1	107	5	20
35	16.2	107	5	10
36	16.2	107	5	5
37	16.4	113	5	5
38	15.8	113	5	10
39	16.4	113	5	20

* 10,000 applications of each stress
** 2,000 applications of each stress

ClibPDF - www.fastio.com

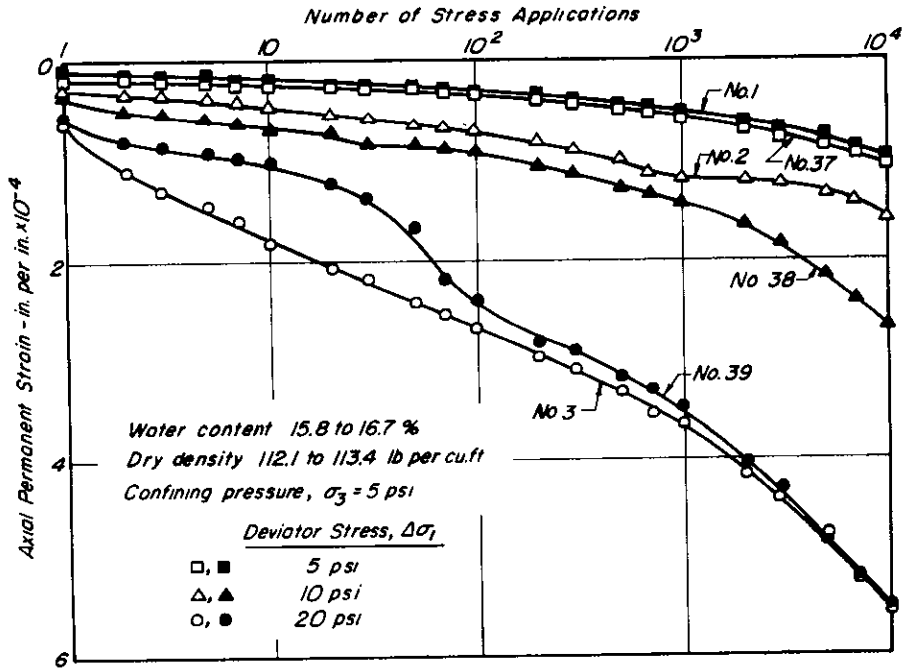

Fig. A1 — Axial permanent strain vs. number of stress application relationships (soil condition 1, Fig. 2).

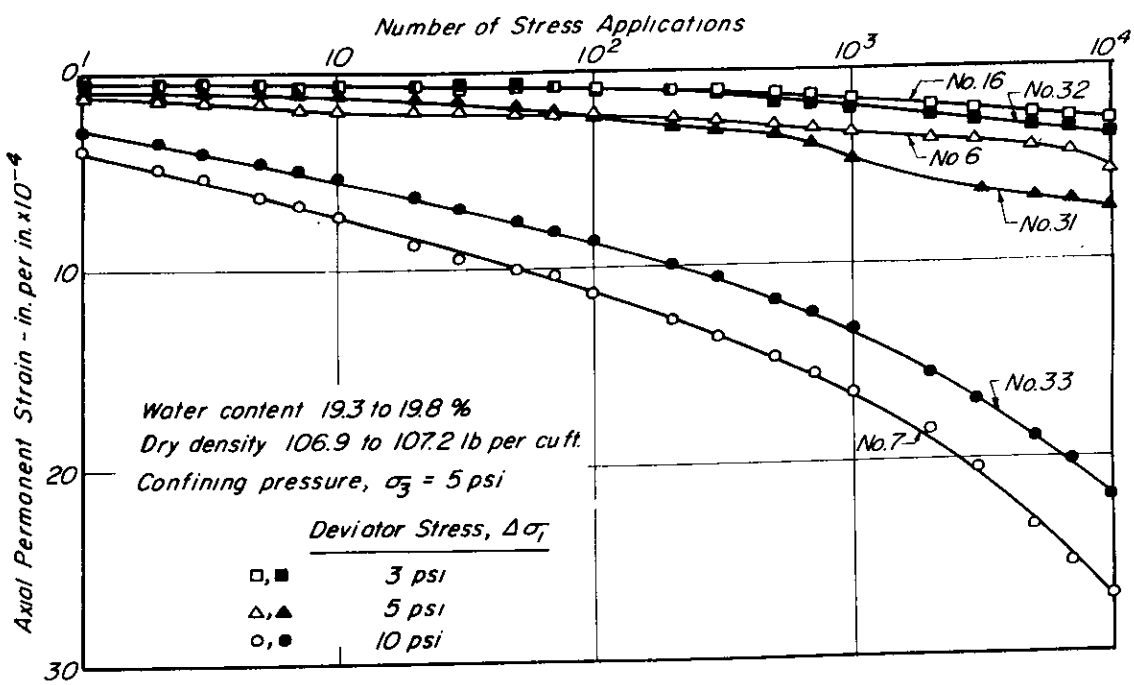

Fig. A2 — Axial permanent strain vs. number of stress application relationships (soil condition 2, Fig. 2).

ClibPDF - www.fastio.com

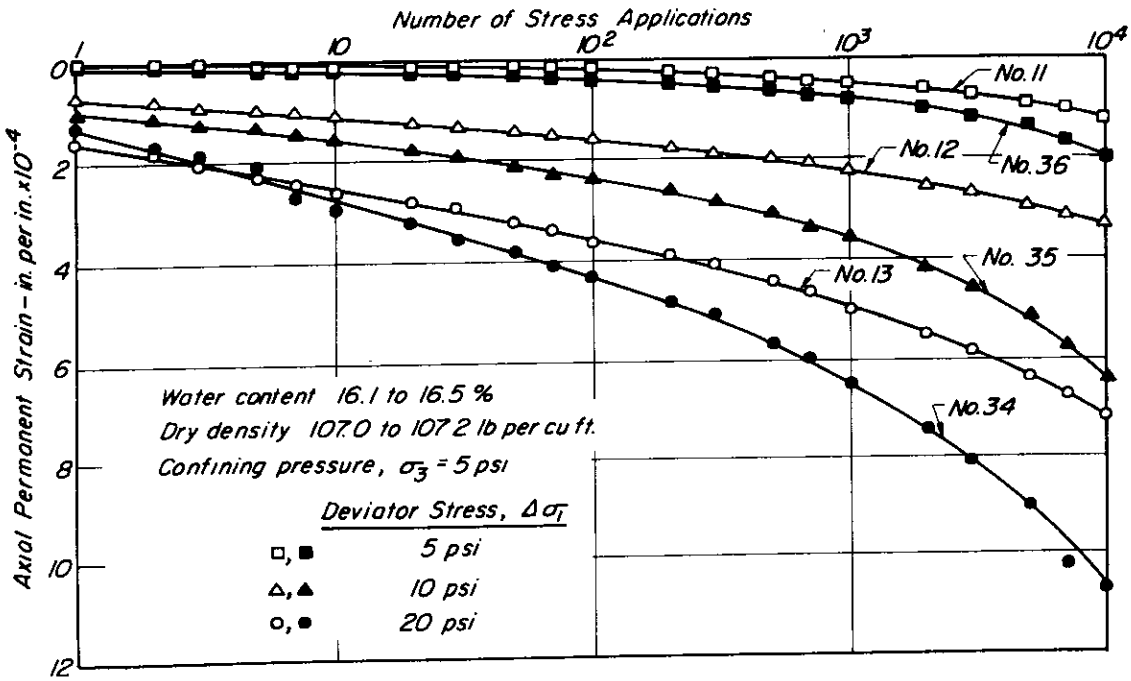

Fig. A3 – Axial permanent strain vs. number of stress application relationships (soil condition 3, Fig. 2).

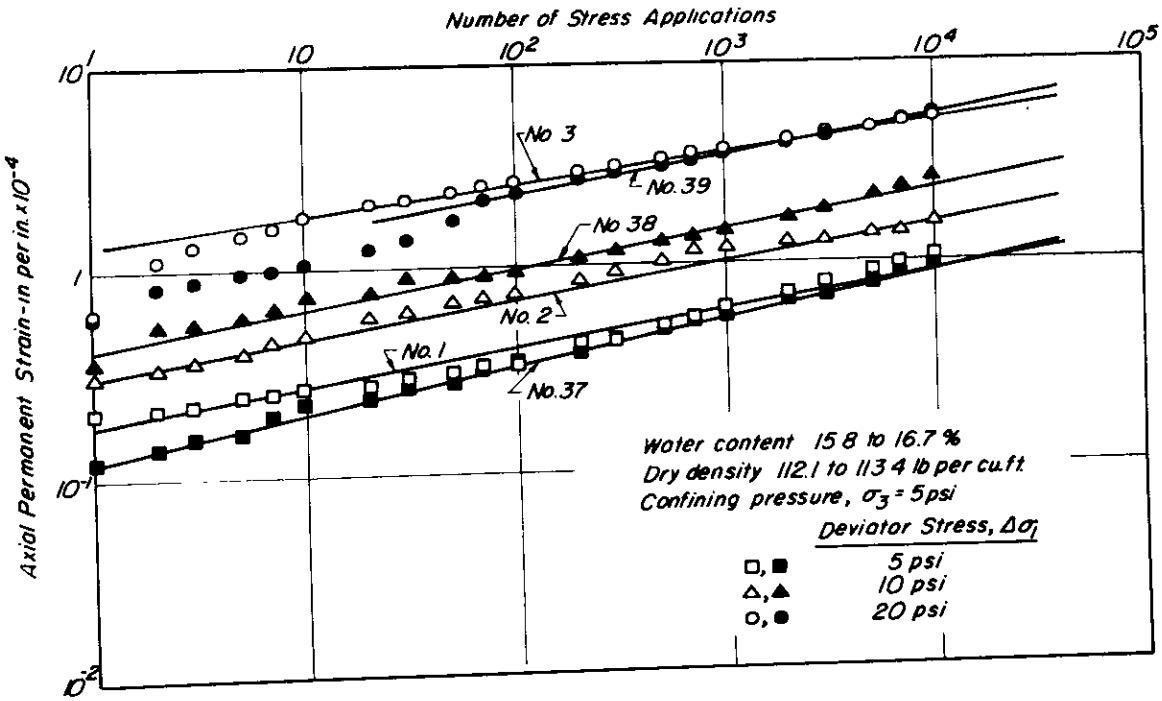

Fig. A4 – Axial permanent strain vs. number of stress application relationships (soil condition 1, Fig. 2).

ClibPDF - www.fastio.com

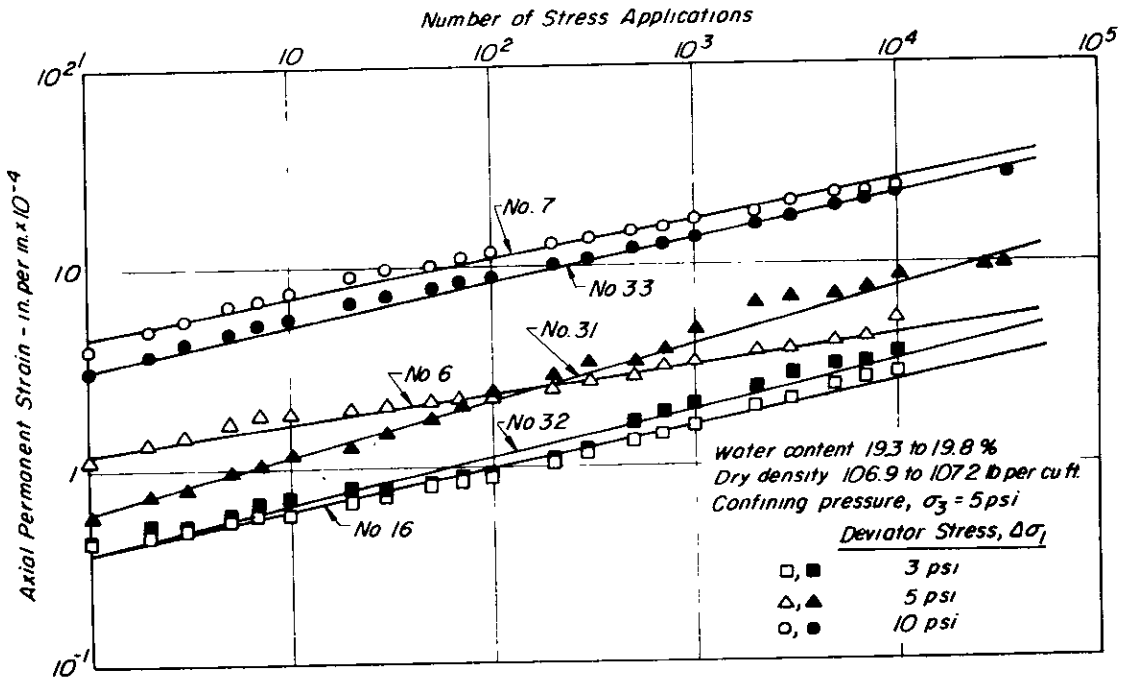

Fig. A5 – Axial permanent strain vs. number of stress application relationships (soil condition 2, Fig. 2).

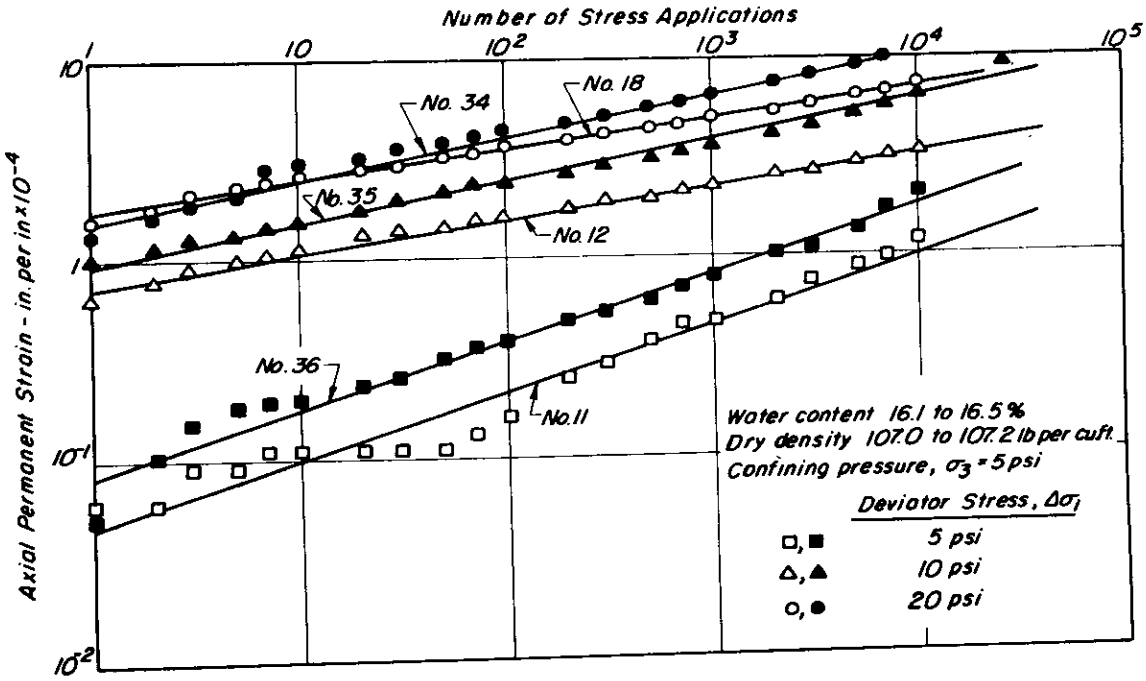

Fig. A6 – Axial permanent strain vs. number of stress application relationships (soil condition 3, Fig. 2).

ClibPDF - www.fastio.com

APPENDIX B

RELATIONSHIPS BETWEEN PERMANENT STRAIN AND APPLIED STRESS

The figures in this Appendix represent relationships between permanent strain at 10,000 stress repetitions and applied deviator stress for all of the data obtained in the investigation to date.

ClibPDF - www.fastio.com

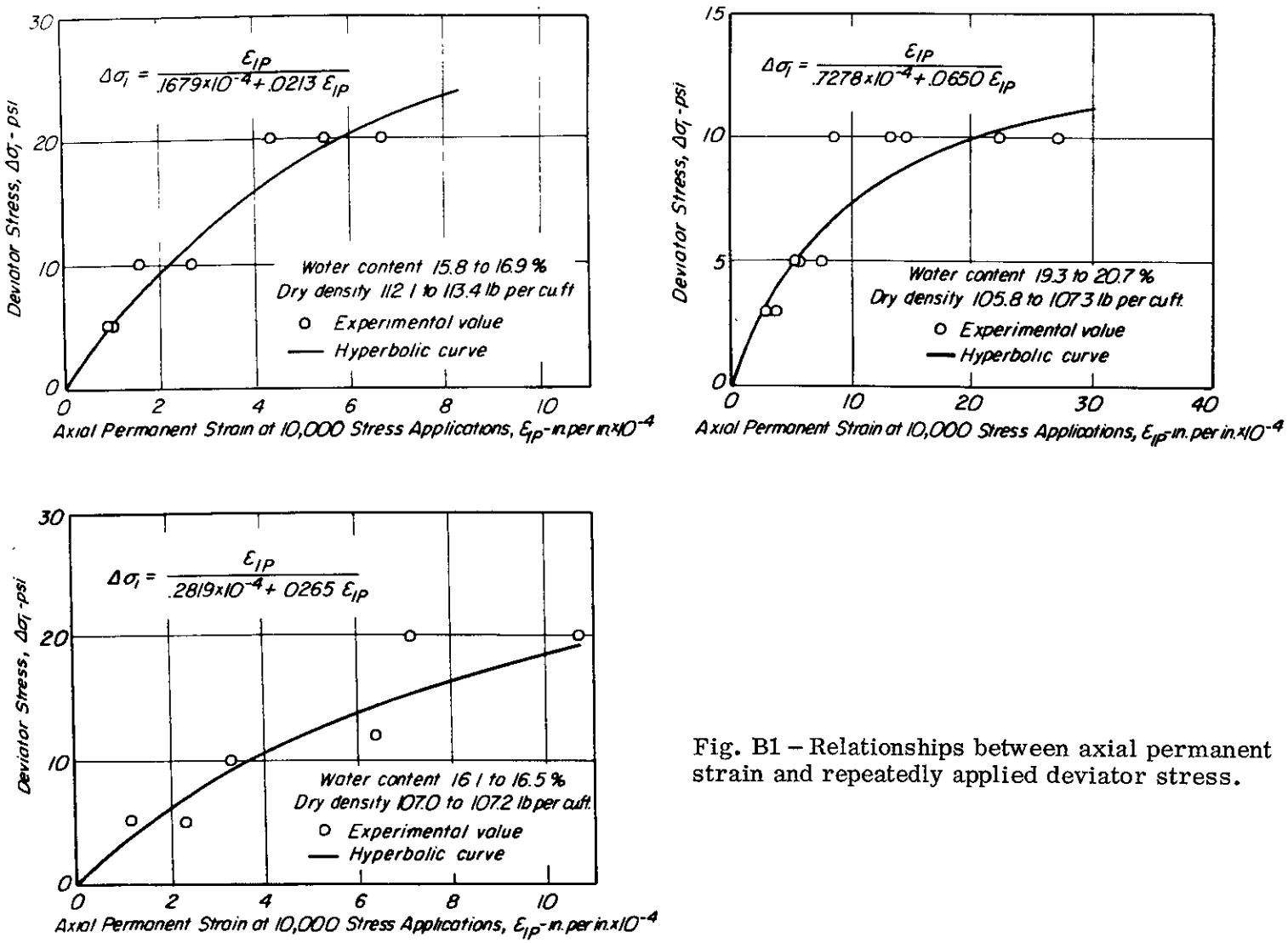

Fig. B1 – Relationships between axial permanent strain and repeatedly applied deviator stress.

ClibPDF - www.fastio.com

APPENDIX C
STRESS-TIME RELATIONSHIPS IN LAYERED SYSTEMS

Introduction

Stress paths generated in a pavement by the passage of a wheel are a complex array in three dimensions and time. If the deformation properties of a material are to be studied in the laboratory, a reasonable first step is of to establish an understanding of pavement stress conditions. Determination of real stress states are beyond present analytical capability. Therefore an approximate equivalent system which can be evaluated must be substituted. Options include linear and non-linear elastic systems and a linear visco-elastic system.

At the time that this study was undertaken, the visco-elastic system had not been fully evaluated. Available knowledge of input parameters was also limited. Therefore, the visco-elastic layered system was not considered to be suitable for the present investigation. However, it is recognized that this system may offer an alternate approach to the use of elastic layer theory when dealing with pavements containing thick asphalt-bound layers.

Numerous studies (summarized in TE 70-5(1)) have shown that linear and non-linear elastic models provide a reasonable estimate of transient pavement response. Barksdale (5) estimated vertical compressive stress pulse times using both non-linear and linear elastic models and has found that results from the two systems are not significantly different.

Much of the analysis presented in this appendix is based on the assumption that the pavement can be represented as a linear elastic model. Stress relationships obtained from the linear model are compared to values obtained from a non-linear model. Further, much of the analysis is based on a two layer system. Comparison with values obtained for a five layer system demonstrate this to be a reasonable approximation. The two layer system geometry and loading configuration utilized in this study are shown in Fig. C1.

ClibPDF - www.fastio.com

An example of stress-time relationships at selected points in layer one of the system of Fig. C1, are shown in Fig. C2. This distribution differs from actual pavement conditions because of the necessity to introduce a simple eleastic model as described previously. Further simplification imposed by laboratory testing capability must also be introduced.

Of the six independent stresses which may be considered, principal stresses change orientation as a load passes a given point. Such a condition is beyond current laboratory testing technology. It should be noted that the magnitude and orientation of the principal stresses do not differ greatly from those of the normal stresses at the point of maximum values. As shown in Fig. C2, the six stresses in the XYZ planes may be reduced to essentially four by observing that shear stresses on the XY and YZ planes are small (observed to seldom exceed 5 psi for the loading conditions imposed). Therefore, a desirable minimum for laboratory simulation would be to impose three independent normal stresses plus the one shear stress of significant magnitude.

Testing equipment of the type developed by Lade* for sands could perhaps be adapted to other materials. This would permit independent control of three normal stresses or control of one normal stress plus a shear stress (torsion). Such a system is limited to compressive stresses and to static or slowly varying stresses.

Equipment of the type used herein permits independent control of two normal stresses and is suitable for either tension or compression in the axial direction while the radial stress must be compression. This system, coupled with a suitable controller would then permit independent control

---

* Lade, P., "The Stress-Strain and Strength Characteristics of Cohesionless Soils", Ph.D. Dissertation, University of California, August 1972.

ClibPDF - www.fastio.com

of two stress magnitudes and times of loading.

The triaxial system selected for use in the present study was considered the best currently available without extensive development. Since only two normal stresses can be simulated by this system, one of S_{xx} or S_{yy} must be disregarded, as must the shear stress on the XZ plane. No justification can be provided for disregarding the shear stress other than that it is not currently feasible to consider such a system in laboratory testing units. With respect to the XX and YY stresses, it was observed that S_{xx} was subjected to frequent reversal of directions, particularly in thin pavement sections. This condition is not reproducible with triaxial equipment when horizontal stresses are applied by a chamber fluid pressure. It was also noted that the maximum values of S_{xx} and S_{yy} do not differ greatly. Therefore, stress differences (S_{zz} and S_{yy} or $S_{zz} - S_{yy}$) would not be greatly different. Stress S_{yy} was noted to generally be of longer time duration (start of loading to maximum) than S_{xx}, therefore S_{yy} generally represents a more severe loading condition in time than does S_{xx}. For the forgoing reasons, stresses S_{zz} and S_{yy} were selected for modeling in the laboratory testing program.

With regard to the preceding discussion, it should be noted that the decision to neglect stress reversal may impose a significant restriction on the general applicability of test results. It is conceivable that, in the thinner pavement sections where stress reversals are most apparent, these reversal effects sould be more significant in determining deformation characteristics than are the maximum stress values.

To conduct laboratory tests to simulate pavement loading conditions using a triaxial loading system requires that the following information is available:

ClibPDF - www.fastio.com

1. The maximum stress to be applied

2. The time duration of this stress

The remainder of this appendix describes analyses performed to establish this information.

Stress States

Stresses near layer interface. Stresses in the vicinity of the interface between layers 1 and 2 were calculated using the Chevron program. In this program, computations are performed in a cylindrical coordinate system. Rectangular coordinate system stresses on the Y-axis of Fig. C.1 can be established by simple linear superposition.

Graphic comparisons of boundary stresses in layered elastic systems have frequently made use of the ratio of moduli of elasticity (E_1/E_2), Poisson's ratio in the layers being held constant. Recent investigations have shown that the Poisson ratios of pavement materials vary with stress state and that deformations may be similarly affected. Accordingly a ratio of shear moduli (G_1/G_2) for two layer systems (more generally $G_i + 1$ for a multi-layered system) was found to provide a useful ratio for comparison of boundary stresses; Table C1 contains a tabulation of the values used together with corresponding values for Young's Modulus (E) and Poisson's ratio (ν).

Comparative values of stresses for a 5 layered system were obtained from computations performed for the layered system and loading geometry shown in Fig. C3. These computations were performed using program PSAD2, stress modulus iteration in the Chevron 5 layer program.

Vertical compressive stresses at the base of the upper layer of a two layered system are shown in Fig. C4. Values shown are the maximum occurring beneath the loading configuration, that is beneath the axis of one load where the thickness of layer one is five inches or less and midway between

ClibPDF - www.fastio.com

TABLE C1

MODULAR RATIOS OF TWO LAYER ELASTIC SYSTEMS
TO EVALUATE BOUNDARY STRESS CONDITIONS

	Modular Ratios G_1/G_2				
	E_2	2000	5000	10000	20000
	ν_1	0.50	0.50	0.45	0.40
E_1	ν_1				
50000	0.45	25.8	10.3	5.0	2.4
100000	0.43	52.4	21.0	10.1	4.9
200000	0.41	106.4	42.6	20.6	9.9
600000	0.39	322.6	129.9	62.6	30.2
1000000	0.36	555.6	222.2	106.7	51.5

the loaded areas for a greater thickness of the layer. Also shown are vertical compressive stresses at the lower boundary of layer one of the five layer system. As shown in Fig. C4, stresses obtained from the multi-layered configuration compare closely with those obtained using the two layered analysis.

Horizontal compressive stresses at the center of one loaded area and at the surface of layer one are shown in Fig. C5. Data points converge to the contact pressure for the homogenous layer case. Dashed lines have been extended to modular ratios less than one, cases which would occur when stiffness increases with depth as in asphalt concrete layers with temperature gradients. The condition is examined in more detail later in the appendix.

Comparative values for the same loading conditions in the five layer system are also shown in Fig. C5. As before, values obtained from the five

ClibPDF - www.fastio.com

layer analysis compare favorably with the two layer data.

Maximum horizontal compressive stresses at the surface of layer one, midway between the loaded areas are shown in Fig. C6. Stresses obtained from the five layer analysis are shown and compare quite reasonably. Convergence to the homogenous case (zero stress) is apparent, though somewhat distorted by the logarithmic scales.

Maximum horizontal tensile stresses at the base of layer one are shown in Fig. C7 along with comparative values derived from the five layer cases. Maximum stress values in this layer were found to occur beneath one loaded area for depths of eight inches and less, and midway between the loaded areas for greater depths.

The ratio of the maximum horizontal tensile stress at the base of layer one to the maximum vertical compressive stress at the same point is shown in Fig. C8. The data are contained within a narrow band, and may be considered practically independent of the thickness of layer one. This relationship was found to be quite useful in selecting values for compressive stresses associated with axial tension.

Analysis of interface stresses in two layer elastic systems have been shown to provide a reasonable measure of the corresponding stress conditions in layer one of multi-layer systems. It is believed that the two layer system can therefore be used to bound laboratory test conditions. To develop a reasonable complete pattern of stresses those within the layers must also be examined.

Stresses within a particular layer. Stress distributions were established using the ELSYM5 computer program. This program determines the complete state of stress, six principal stresses and the three normal and three

ClibPDF - www.fastio.com

shear stresses on the X-Y-Z planes at any point in a layered linear elastic system. One to ten identical vertical loads can be applied to the surface. Stresses and deformations are output in a rectangular coordinate system. The loading and structural configuration was as shown in Fig. C1. Only the three normal stresses were considered for stress distribution purposes for reasons stated previously.

Vertical compressive stresses in layer one at points beneath the center of one loaded area are shown in Fig. C9. Corresponding values at points midway between the loaded areas are shown in Fig. C10. The effect of layer one thickness and of the modular ratio is demonstrated. Stress magnitudes are shown to closely approximate the homogeneous elastic layer condition for the upper one-half of the layer.

Horizontal stresses in a 12-inch layer, directly beneath one loaded area are shown in Fig. C11. A similar diagram for horizontal stresses at points midway between the loaded areas is shown in Fig. C12. The stress distribution is generally 'S' shaped with the bottom tensile stresses of lower magnitude than the surface compressive stresses, most notably at lower modular ratios. Stresses in the Y-Y direction of Fig. C12 follow a somewhat different distribution in that maximum compressive stresses occur at a shallow depth below the surface rather than at the surface as in other cases. In all cases a zero or near zero horizontal stress condition occurs very near mid depth of the layer. Similar diagrams for thicknesses of layer one of 5 and 20 inches are contained at the end of this appendix.

Representative stress states

At the outset, reference was made to the use of a triaxial test

ClibPDF - www.fastio.com

system. The range of possible stress combinations which can be obtained in the triaxial test can be depicted graphically as shown in Fig. C13. In this figure the positive and negative x-directions represent axial compression and tension stresses, respectively. Since only compressive stresses can be obtained in the radial direction, these can be represented on the positive Y-axis. The range of triaxial stress states shown in Fig. C13 probably exceeds that which will occur in a pavement. To exclude unrepresentative stress combinations, and therefore to concentrate experimental efforts, stress combinations described in preceding sections can be used to prepare diagrams similar to Fig. C13 representing the range of stress states likely to occur in pavements.

Probable stress states for two cases are shown in Fig. C14 and C15. Stress combinations have been expressed as proportions of the surface contact pressure. Many such diagrams are required to define stress states for all conditions. The range of values is dependent on both depth and modular ratio G_1/G_2 .

Time of Loading

A variety of techniques have been developed or proposed for use in expressing the time of loading for asphalt concrete. Some of the techniques used to define time of loading in research reported to the Third International Conference on the Structural Design of Asphalt Pavements are included in Table C2. Of those summarized, relationships used by Thrower, et al, and by Hofstra and Valkering involve measurements of time elements and will be referred to further.

For laboratory testing, the shape of the load time trace commonly is

ClibPDF - www.fastio.com

one of three forms: sine, square or triangular. Barksdale (5) developed data for vertical compressive stresses in layered elastic systems and related these to both triangular and sine forms, suggesting that these two forms could be used to approximate the elastic layer forms. Fatigue data for asphalt concrete reported in TE 70-5 were obtained using square-shaped loads. It was observed that at comparable stiffnesses $\left(S_{(t,T)} = \sigma/\varepsilon\right)$, fatigue results obtained using square waves did not differ significantly from data obtained with sine wave loading forms.

This study considered use of both triangular and square load shapes as these were the forms which could be most readily obtained with a simple time-load control system. To develop some information relative to the effects of square versus triangular loading forms, an abbreviated laboratory testing program was undertaken. A specimen of asphalt concrete 4 in. in diameter and 8 in. high was tested at 70°F. Both triangular and square load shapes of variable duration were applied. Rise times, that is, the time from zero to full load, in the square load tests was 0.003 seconds, the minimum that could be achieved using the pneumatic loading system. Stiffness of the asphalt concrete was determined for both cases. Results of the testing are shown in Fig. C16 where stiffness is plotted versus an equivalent time of loading. Equivalent time of loading was defined as the time duration of a square load having the same maximum stress magnitude and the same area as a triangular load form. As shown in Fig. C16, results from the two load shapes are comparable when time of loading is defined as described above.

As a further evaluation of the method, the relationship for time of loading suggested by Hofstra and Valkering (Table C2) was also applied.

ClibPDF - www.fastio.com

TABLE C2

SUMMARY OF TIMES OF LOADING FOR DETERMINATION OF ASPHALT CONCRETE STIFFNESS

Type of Pavement	Author(s)	Vehicle Speed	Time of Loading (or frequency)
Highway	Brown and Pell	80 kph	$t = \frac{1}{(2\pi)\ (0.4V)} = .005$ sec. for $V = 80$ kph
	Finn, et al	30-40 mph	0.015 sec.
	Hofstra and Valkering	---	$\Delta t = 0.4 \times d$ where d = width of strain signal
	Miura	4-80 kph	.04 to 1.0 sec.
	Thrower, et al	---	Length of stress pulse σ_z at top of subgrade*, $f = (1/\text{time})$
Airfields	Witczak	10-20 mph	$f = 2$ cps

*For very soft asphalt layers, Thrower suggests using the length of the stress pulse in the asphalt layer.

ClibPDF - www.fastio.com

In their method, 'd' is the time width of the strain signal at half the maximum strain value. Time of loading is defined as 0.4d. Time of loading results obtained by the Hofstra and Valkering technique are also shown on Fig. C16. Results are comparable to those previously obtained.

Results of this experimental program were used as basis for obtaining general time of loading relationships for layered elastic systems; the area beneath a load-time curve for elastic stresses was determined and then reduced to an equivalent square wave loading time having the same area and maximum stress.

Specific relationships were obtained from layered elastic system computations using the ELSYM5 program and applied to the two layer system of Fig. C1. Stress-time relationships like those shown in Fig. C2 were plotted for each stress S_{xx}, S_{yy} and S_{zz} for various depths in the system. All structural combinations shown in Table C1 were considered as were locations beneath one loaded area and midway between the loaded areas. Areas beneath the stress-time curves were determined by planimetering. Equivalent square wave time loading values were then determined. The resulting equivalent time of loading values were plotted versus modular ratio (G_1/G_2) at each depth, then cross plotted versus depth for various selected values of the modular ratio. Due to reversal, stress-time relationships could not be defined for the S_{xx} orientation.

Equivalent times of loading for vertical stress, S_{xx}, are shown in Fig. C17. The relationship was found to depend only on depth and to be nearly independent of structural effects, a result which agrees with the findings of Barksdale. Time of loading values determined from stresses directly beneath one loaded area were found to agree closely with time

ClibPDF - www.fastio.com

of loading values for stresses midway between the loaded areas. Some structural effects were found to exist near the base of the upper layer. At these points, vertical stress-time relationships were found to be the same as those for horizontal, S_{yy}, stresses.

Barksdale's data for triangular load shapes have been shown on Fig. C17 for comparison. It is noted that Barksdale's time of loading data are greater than those developed as described in the foregoing; however, the slopes are seen to be nearly identical. Differences are due to at least the following:

1. Barksdale's data are for triangular load shapes, which should account for a factor of at least two when compared to square load shapes, and,
2. Barksdale included an adjustment to his data based on comparison of the linear elastic stress-time relationships with measured relationships from the AASHO road test. These adjustments were described by Barksdale as accounting for viscous and inertial effects.

Time of loading values for the horizontal YY stress direction are shown in Fig. C18. Time of loading for these stresses were found to be dependent on both depth and the modular ratio G_1/G_2. Comparison of Figs. C17 and C18 shows that substantial differences occur between time of loading in the vertical and horizontal directions. To demonstrate the differences, the ratio of the horizontal to vertical time of loading was computed and plotted versus depth in Fig. C19. Ratios of up to 5 are shown to exist for high modular ratios and large depths. For the probable

ClibPDF - www.fastio.com

range of interest, that is for values of G_1/G_2 of 50 or less, maximum ratios of 3.5 were found.

While the computations shown above make use of an equivalent square wave, two shapes of load-time relationships were used in the investigation - square and triangular. The appropriate shape was based on the shape of the load-time relationship determined in the elastic layer analysis. Load shapes used were:

1. Square shapes for vertical stresses near the applied load.
2. Triangular shapes for all other conditions.

All times of loading in the experimental work are reported in terms of the equivalent square wave to provide a uniform basis for comparison.

An additional factor in the simulation was the observation that near the base of layer 1 differences in time of loading between vertical and horizontal stresses are largely absent. Therefore, in simulating conditions near the base of this layer, time of loading values for horizontal stresses appear to be appropriate for both horizontal and vertical stress directions.

Temperature Effects on Stress-Time Relationships

To determine the influence of temperature gradients on stress and time relationships developed in preceding sections, four structural sections having the geometry and elastic parameters shown in Fig. C20 were examined. The range of elastic parameters of the upper four layers is considered to be due to temperature gradients such as might exist in an asphalt concrete layer. Stiffness related to temperature and time of loading, for a typical condition, is shown in Fig. C21. These relationships

ClibPDF - www.fastio.com

were obtained by the Shell procedure.

If time of loading within the full 12 inch depth (layer 1 to 4) is considered constant at 0.1 sec., then from Fig. C21, the cooling condition of Fig. C20a corresponds to a temperature gradient of approximately 28°F while the heating case of Fig. C20b corresponds to a gradient of approximately 48°F. These conditions approximate typical measured gradients in southwestern United States.

Previously it has been shown that time of loading is not invariant with depth. Thus, if the times of loading for the vertical strain of Fig. C17 are used, that is, that the time of loading increases with depth, then the temperature gradient no longer follows an isoline of constant time of loading on Fig. C21. Therefore, when a variable time of loading is considered, the temperature gradient for the cooling condition (Fig. C20a) is reduced from 28°F to 22°F while that for the heating condition is increased from 48°F to 54°F, a change of 6°F in both cases. Within the limit of accuracy of current temperature prediction methods and analytical procedures, this effect is considered to be small and for most structural conditions involving asphalt concrete layer thickness less than 16 to 18 inches, is probably negligible.

Comparison of vertical compressive stresses from the temperature gradient cases to those of corresponding two layer cases are shown in Fig. C22. An average modular ratio $\left(G_{ave}/G_5\right)$ for the multi-layer cases is used for the comparison. Substantial differences between the two cases are evident. Similar comparisons for horizontal stresses are shown in Fig. C23. Again substantial differences are apparent.

Introduction of variable moduli thus result in changes in stress

ClibPDF - www.fastio.com

distributions compared to the mean conditions in a two layer system. In any analytical procedure to evaluate deformation, this can be expected to be of importance. However, for purposes of establishing a range of conditions for laboratory testing, the two layer analysis is believed to provide reasonable bounds.

Figs. C24 and C25 show comparative stress-time effects for the multiple layered cases and for two layer cases. Stress variations are again shown to be significant, but the time effects are shown to be small. It is therefore believed that derivation of time of loading information from two layered systems analyzed herein provides a reasonable representation of more complex conditions.

SUMMARY

In this Appendix, stresses in two layer linear elastic systems have been examined in considerable detail. The purpose of this study was to define stress-time relationships suitable for use in laboratory testing programs. Factors examined were:

1. The range of boundary stresses.
2. The distributions of stresses within the layer.
3. Stress-time relationships.

This analysis was found to provide a reasonable guide to stress conditions in multi-layered systems involving non-linear layers. Introduction of temperature gradients was found to have a substantial effect on time of loading. Generally, the stress magnitudes fell within bounds developed for the two layer cases as shown in Fig. C14 and C15.

Table C3 provides a summary of the range of conditions proposed for use in the laboratory testing program. Selection of the shape of the

ClibPDF - www.fastio.com

stress-time relationship was based on observation of a large number of cases and is believed to be a reasonable approximation.

Time of loading data developed for both horizontal and vertical stresses showed that for many conditions, the horizontal stress is of much longer duration than the vertical. This factor is expected to exert a substantial influence on the deformation properties of asphalt concrete.

TABLE C3

SUMMARY OF STRESS=TIME CONDITIONS

Location in Section	Stress Orientation	Approximate Stress-Time Shape	Ratio of Horizontal To Vertical Time	Ratio of Vertical to Horizontal Stress
Near Surface	Vertical	Square	Fig. C19	Range from less than 1 to 5
	Horizontal	Triangle		
Inter-mediate	Vertical	Triangle	Fig. C19	Horizontal stresses may be compressive tensile or zero
	Horizontal	Triangle		
Bottom	Vertical	Triangle	1.0	Fig. C8
	Horizontal	Triangle		

ClibPDF - www.fastio.com

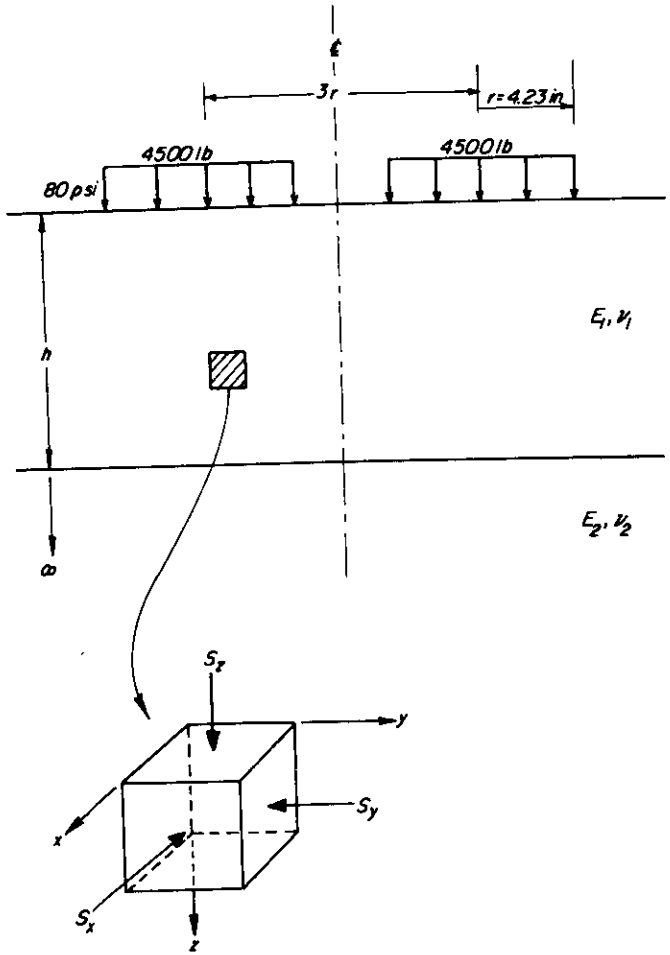

Fig. C1 – Two layer elastic system.

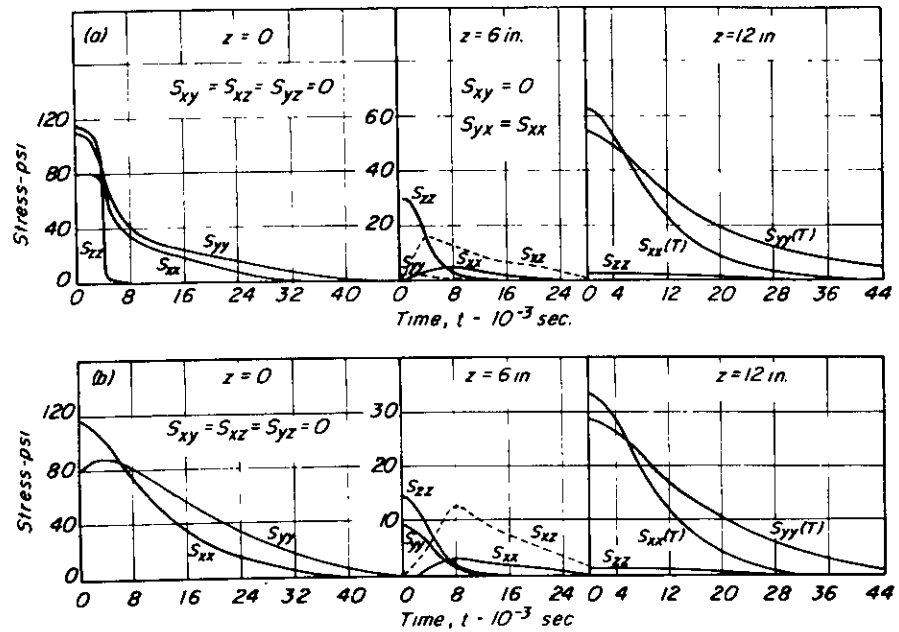

Fig. C2 – Stress-time relationships in layer 1 where $E_1 = 600{,}000$ psi, $E_2 = 10{,}000$ psi, $\nu_1 = 0.39$, $\nu_2 = 0.45$, $h_1 = 12$ in., 60 mph vehicle speed; (a) centerline of one loaded area, (b) midway between dual loaded areas. Tensile stresses are designated by (T); all others are compressive.

ClibPDF - www.fastio.com

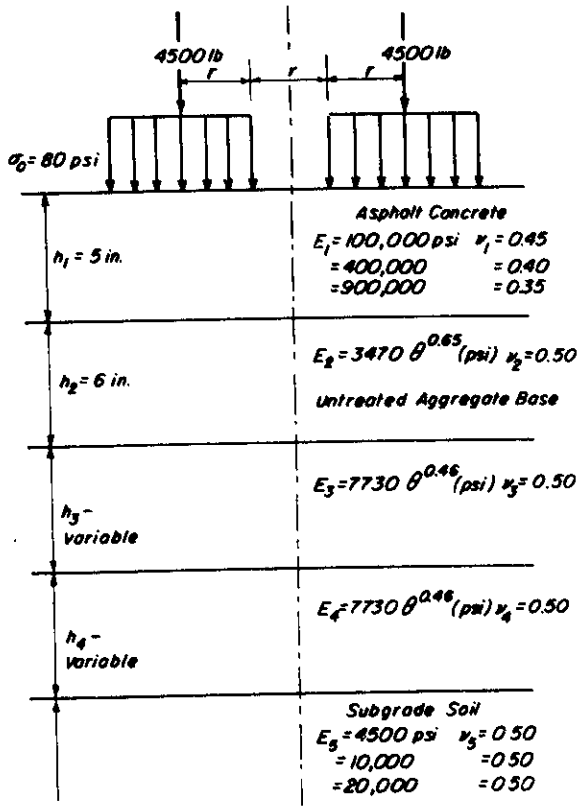

Fig. C3 – Structural pavement sections analyzed for boundary stresses in multi-layered system.

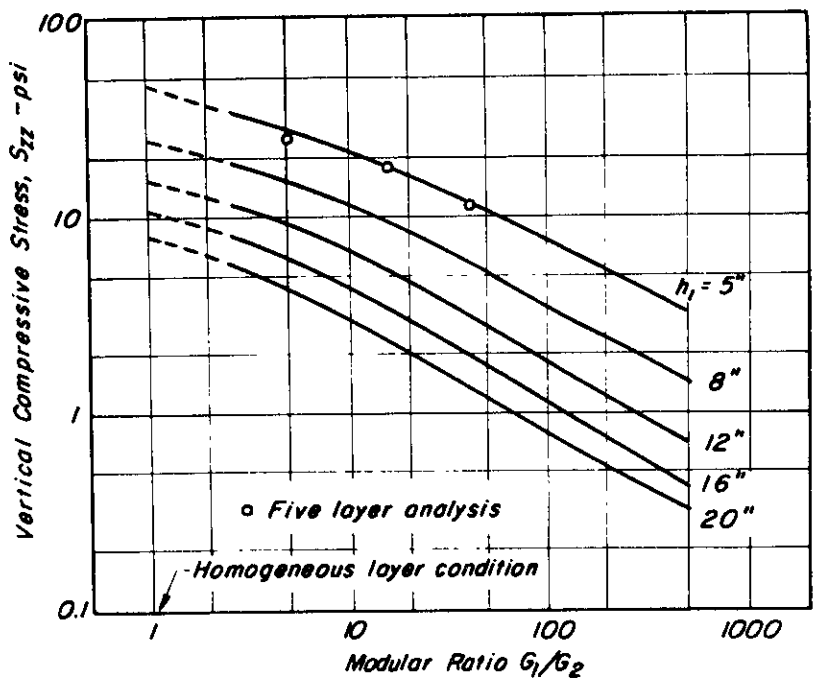

Fig. C4 – Vertical compressive stresses at the base of layer one of a two layer elastic system.

ClibPDF - www.fastio.com

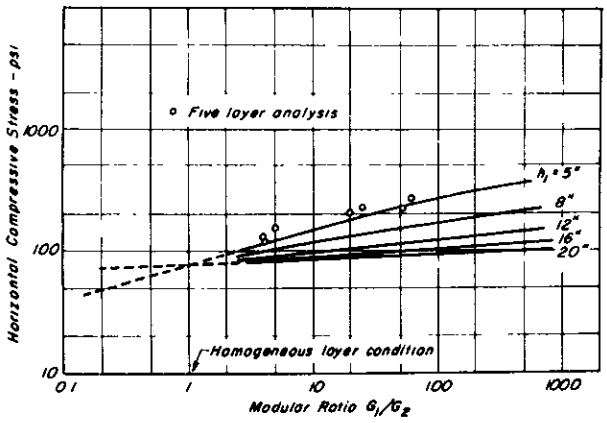

Fig. C5 – Horizontal compressive stresses at the surface of layer one of a two layer elastic system, beneath one loaded area.

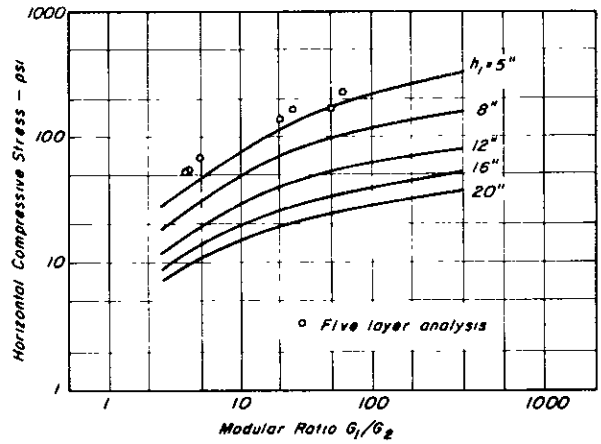

Fig. C6 – Horizontal compressive stresses at the surface of layer one of a two layer elastic system, midway between the loaded areas.

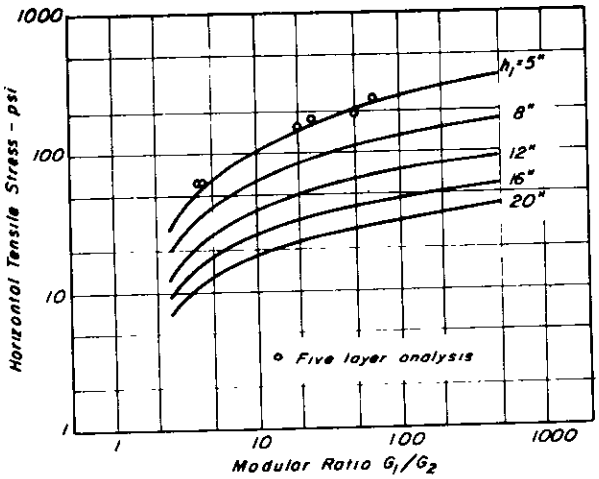

Fig. C7 – Maximum horizontal tensile stress at the base of layer one of a two layer elastic system.

ClibPDF - www.fastio.com

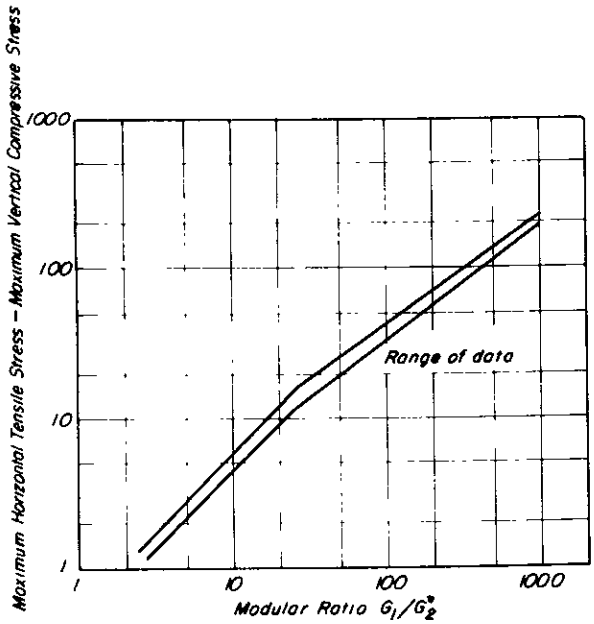

Fig. C8 – Ratio of the maximum horizontal tensile stress to the maximum vertical compressive stress at the base of layer one of a two layer system.

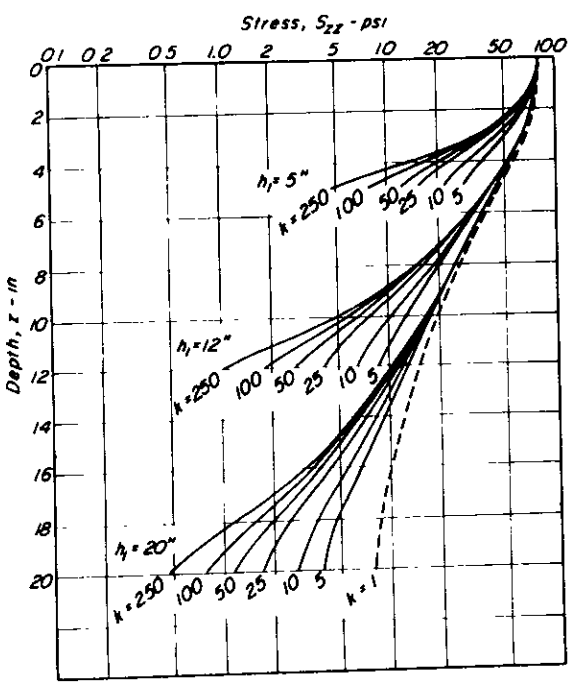

Fig. C9 – Vertical compressive stresses in layer one of a two layer elastic system, points beneath the center of one loaded area; $k = G_1/G_2$.

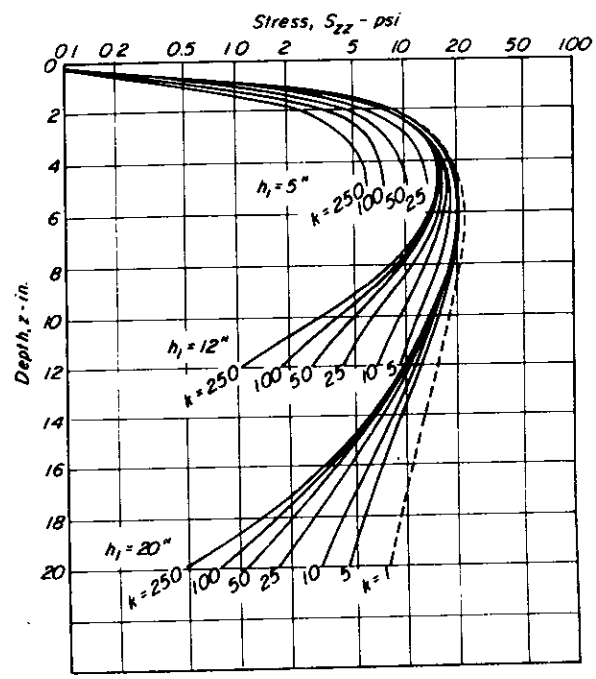

Fig. C10 – Vertical compressive stresses in layer one of a two layer elastic system, points midway between loaded areas; $k = G_1/G_2$.

ClibPDF - www.fastio.com

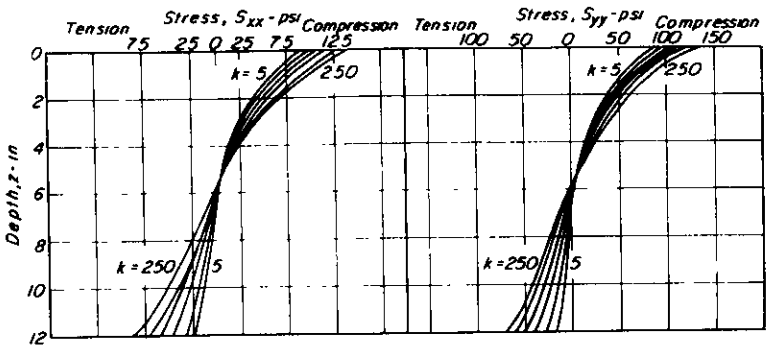

Fig. C11 – Horizontal stresses in layer one of a two layer elastic system at points directly beneath the center of one loaded area, $h_1 = 12$ in., $k = G_1/G_2$.

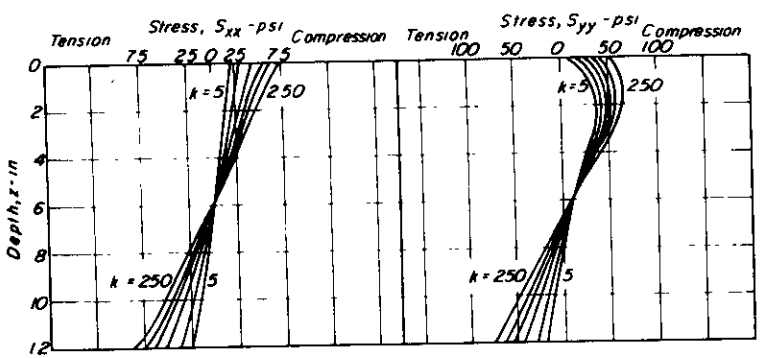

Fig. C12 – Horizontal stresses in layer one of a two layer elastic system at points midway between the loaded areas, $h_1 = 12$ in., $k = G_1/G_2$.

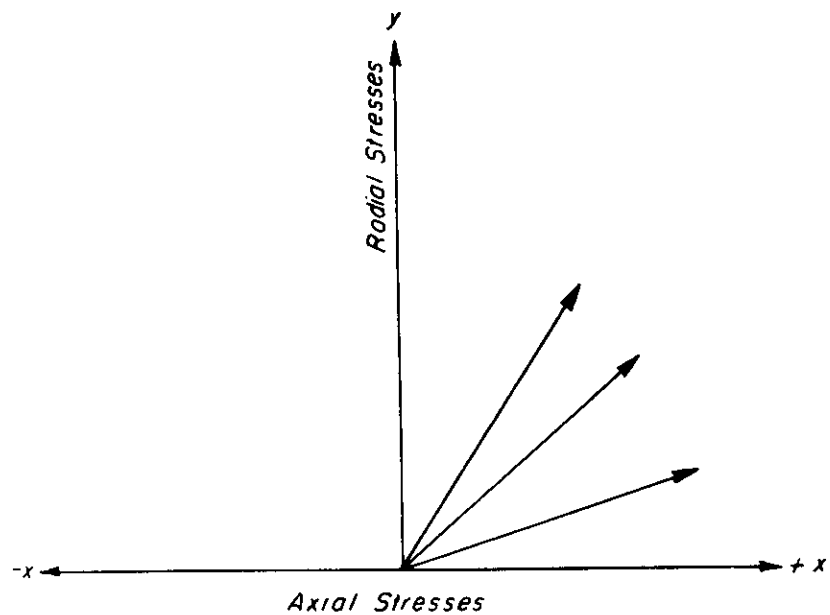

Fig. C13 – Representation of stress states in a triaxial test.

ClibPDF - www.fastio.com

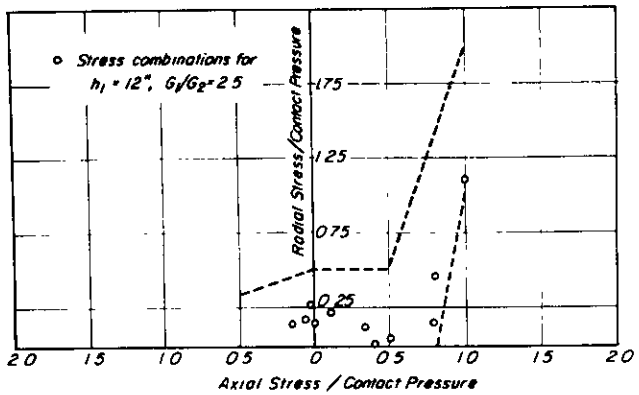

Fig. C14 – Probable range of stress combinations in layer one of a two layer elastic system.

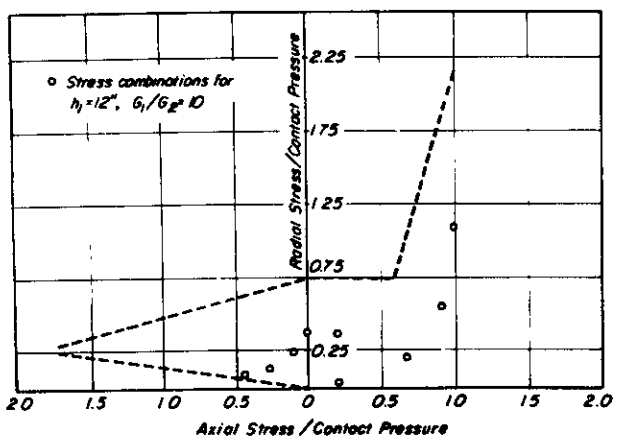

Fig. C15 – Probable range of stress combinations in layer one of a two layer elastic system.

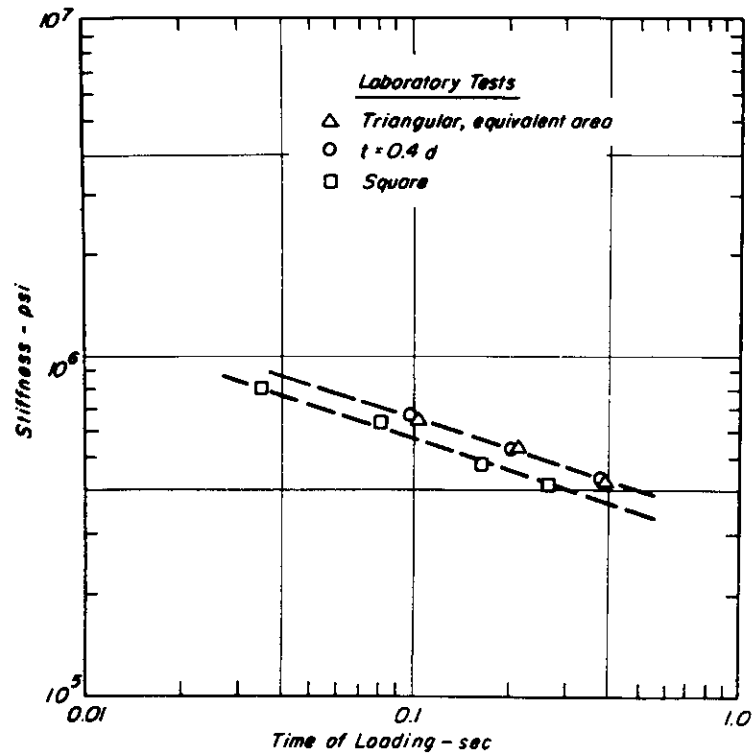

Fig. C16 –Equivalent time of loading from laboratory test data.

ClibPDF - www.fastio.com

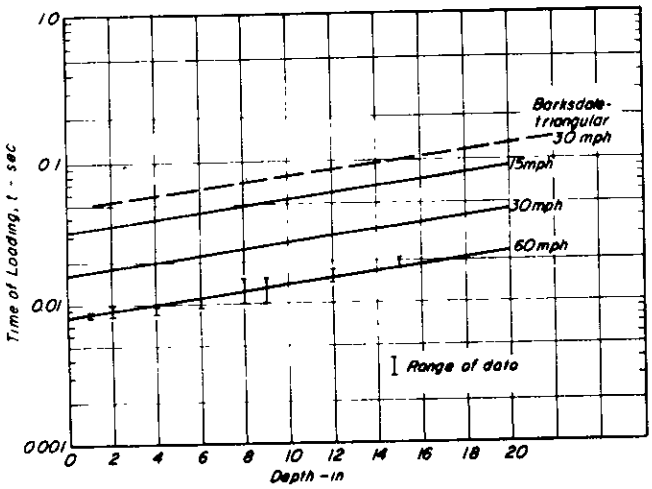

Fig. C17 – Equivalent time of loading - depth relationship for vertical compressive stresses.

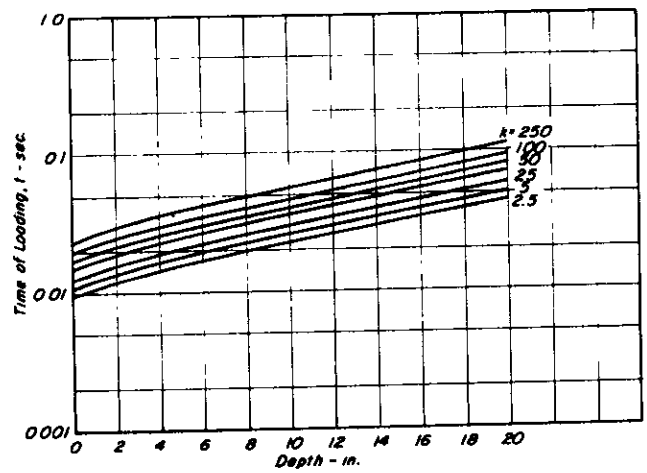

Fig. C18 – Equivalent time of loading - depth relationship for horizontal stresses, 60 mph, $k = G_1/G_2$.

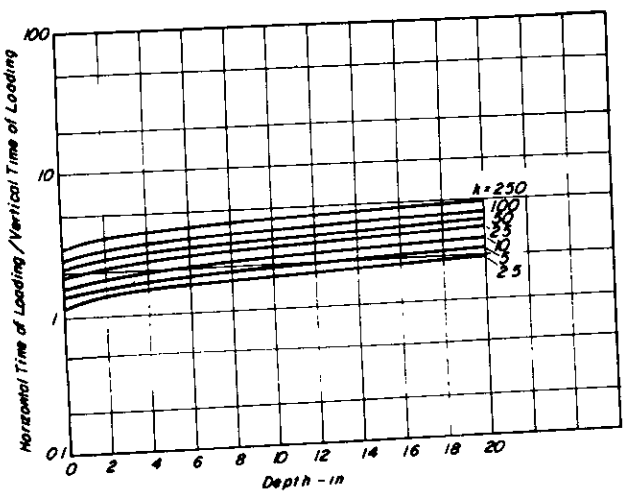

Fig. C19 – Ratio of horizontal to vertical stress time of loading, 60 mph, $k = G_1/G_2$.

ClibPDF - www.fastio.com

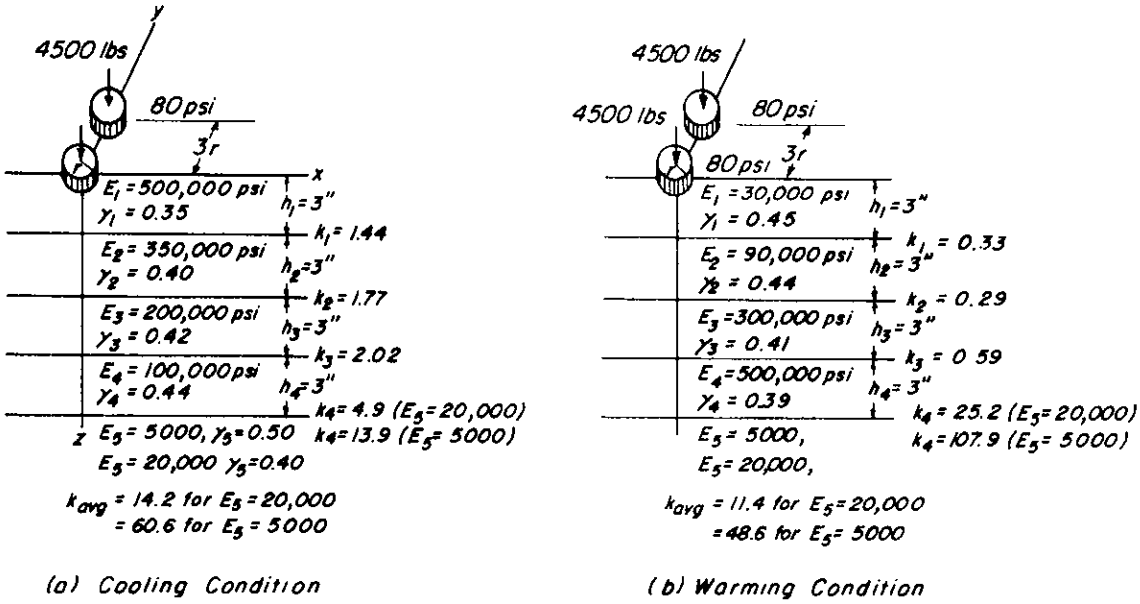

Fig. C20 – Structural sections used to evaluate the effect of temperature gradients on stress-time relationships.

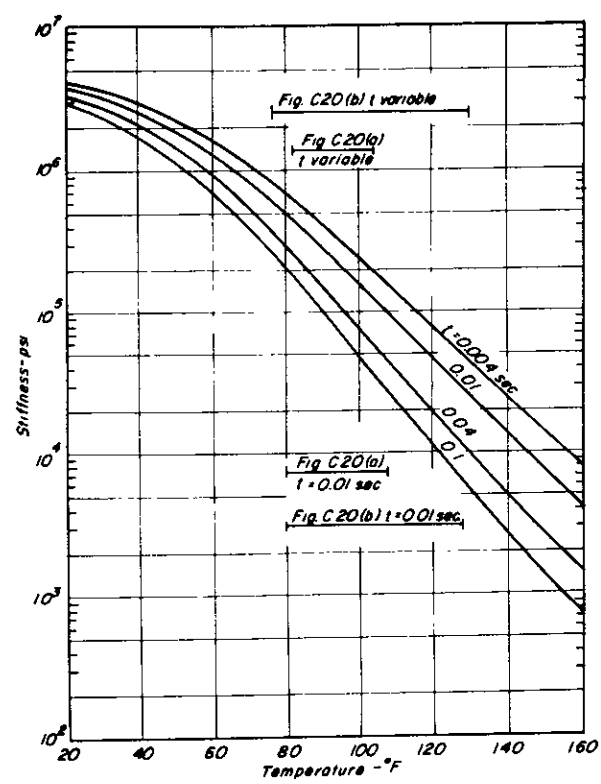

Fig. C21 – Typical stiffness – time of loading – temperature relationship for an asphalt concrete.

ClibPDF - www.fastio.com

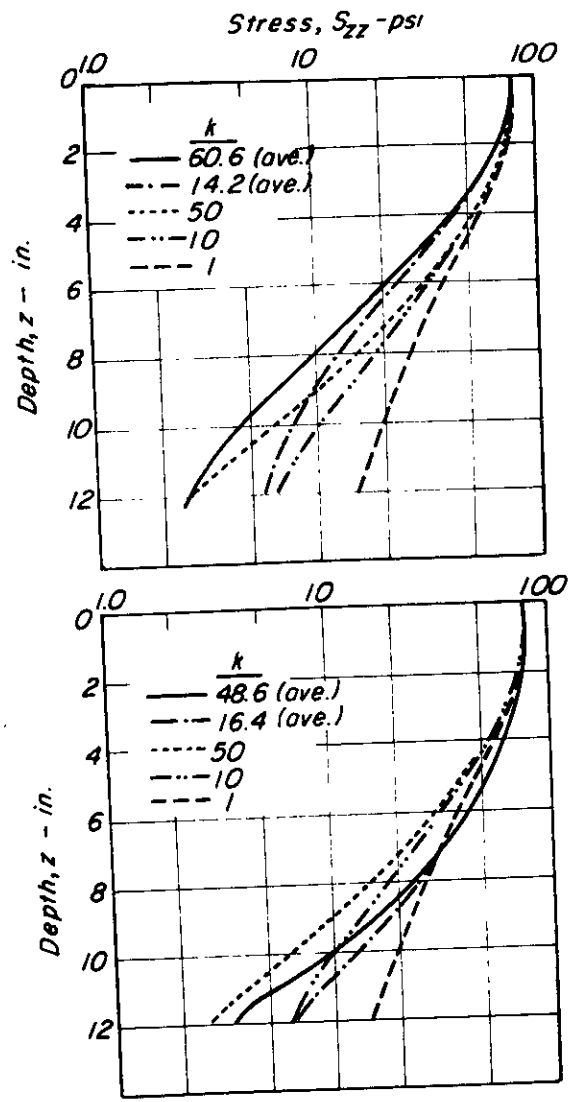

Fig. C22 – Distribution of vertical compressive stresses in a 12-in. layer of variable stiffness compared to a layer of uniform stiffness.

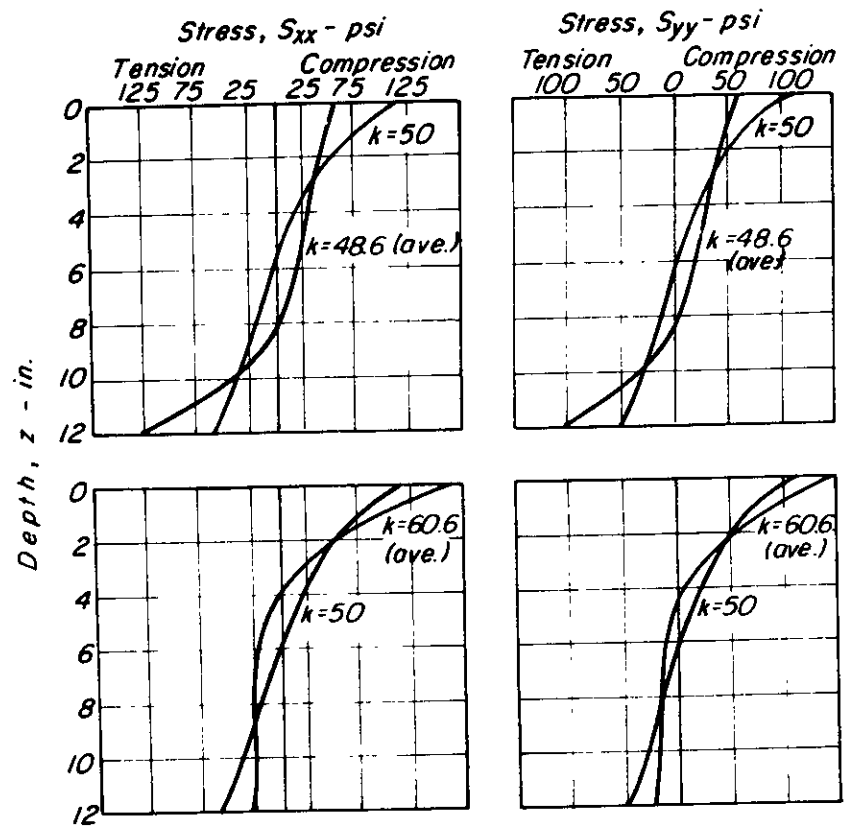

Fig. C23 – Distribution of horizontal stresses in a 12-in. layer of variable modulus (k) compared to a layer of uniform modulus (k).

ClibPDF - www.fastio.com

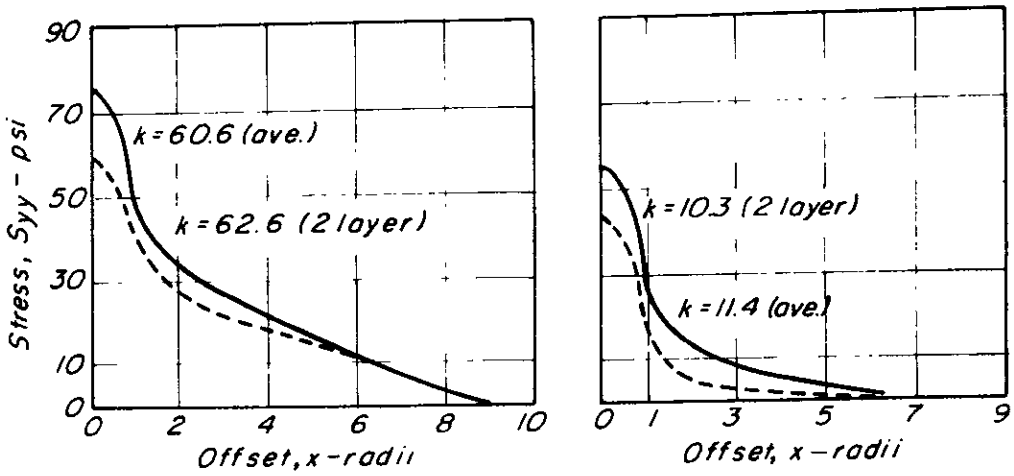

Fig. C24 — Effect of variable stiffness on the vertical stress-time relationship compared to a layer of uniform stiffness, depth = 6 in.

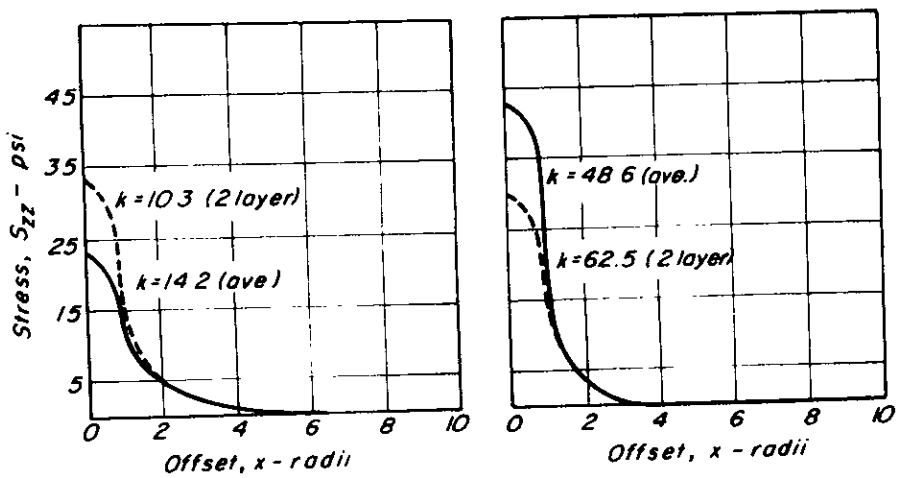

Fig. C25 — Effect of variable stiffness on the horizontal stress-time relationship compared to uniform stiffness condition, depth = 1.5 in.

ClibPDF - www.fastio.com

SUPPLEMENTARY RELATIONSHIPS

ClibPDF - www.fastio.com

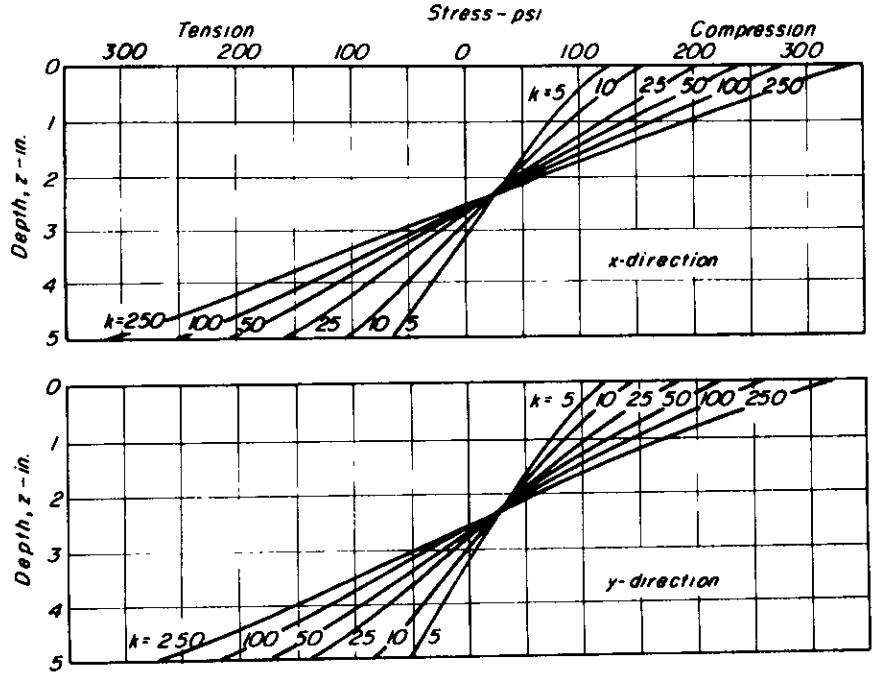

Fig. C26 – Horizontal stresses in layer one at points directly beneath the center of one loaded area, $h_1 = 5$ in., $k = G_1/G_2$.

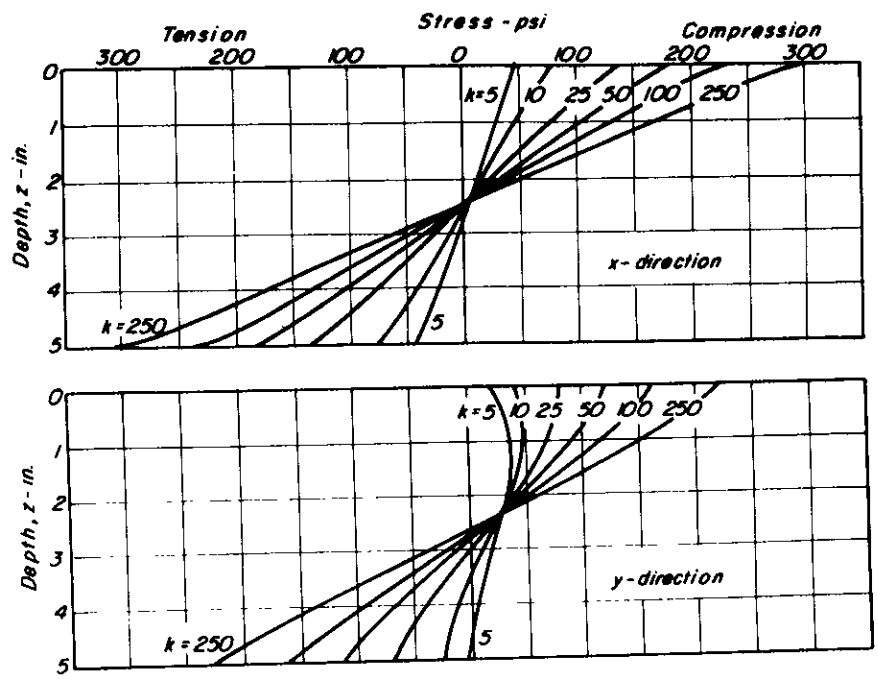

Fig. C27 – Horizontal stresses in layer one at points midway between the loaded areas; $h_1 = 5$ in., $k = G_1/G_2$.

ClibPDF - www.fastio.com

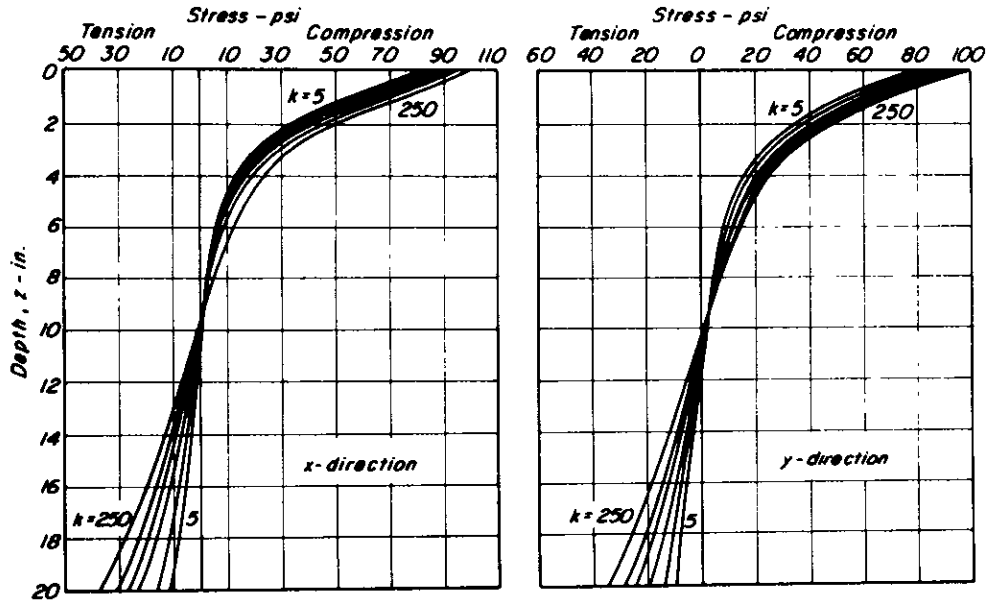

Fig. C28 – Horizontal stresses in layer one at points directly beneath the loaded areas; h_1 = 20 in., $k = G_1/G_2$.

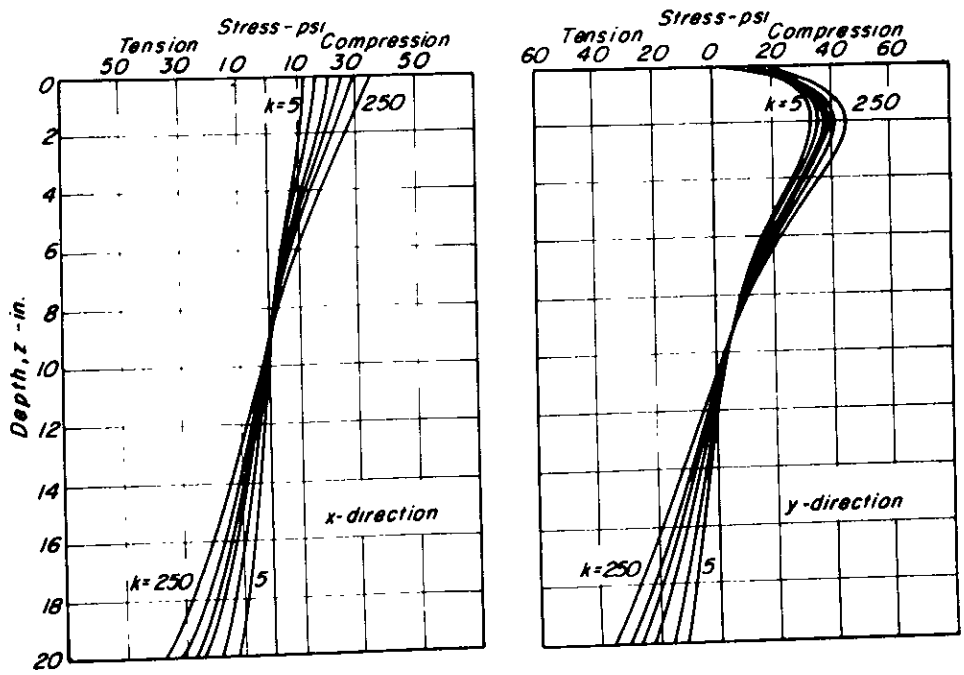

Fig. C29 – Horizontal stresses in layer one at points midway between the loaded areas; h_1 = 20 in., $k = G_1/G_2$.

ClibPDF - www.fastio.com

APPENDIX D

TEST EQUIPMENT AND PROCEDURES

TRIAXIAL COMPRESSION TEST TO MEASURE PERMANENT DEFORMATION OF SUBGRADE SOILS IN REPEATED LOADING

Repeated-load triaxial compression tests similar to those used for determination of resilient moduli (see, for example, detailed description of test procedure to measure stiffness characteristics of subgrade soils contained in Ref. (2)) were used to measure the accumulation of permanent deformation in the subgrade soil specimens. The triaxial cell, shown schematically in Fig. D-1, can accommodate specimens 2.8 in. in diameter by 6 in. high. Air was used for the confining pressure and only one value, 5 psi, was used. Repeated loads were applied pneumatically with a load duration of 0.1 sec. and at a frequency of 20 repetitions per minute.

Both axial and radial deformations were measured by LVDT's attached to the soil specimen as shown in Fig. D-1. Details of the clamps are shown in Figs. D-2a and D-2b. The axial strain device measured the accumulation of permanent deformation over the center 3 in. of the specimens. Measurement of the accumulation of permanent radial strain presented some difficulties intially because of soil creep at the clamps. To overcome this, the strain unit was suspended from springs as shown in Fig. D-1 and bonded to the membrane using an epoxy resin.

Repeated loads were applied over a range in axial stresses and as many as 100,000 stress repetitions were applied to an individual specimen.

Reproducibility of test results is illustrated in Fig. D-3. Comparisons are shown for specimens whose water contents and dry densities

ClibPDF - www.fastio.com

were considered to be reasonably comparable. These data for the numbered specimens shown in Fig. D-3 are:

Specimen No.	Water Content - percent	Dry Density -lb per cu ft
1	16.7	112
37	16.4	113
2	16.8	112
38	15.8	113
3	16.0	113
39	16.4	113

EQUIPMENT TO MEASURE PERMANENT DEFORMATION OF ASPHALT PAVING MIXTURES IN REPEATED LOADING AND IN CREEP

Equipment and Instrumentation

The triaxial compression test system used in this phase of the investigation was developed by Dehlen (11). In this system the axial and radial stresses can be independently applied, Fig. D4. As seen in this figure, this independence is obtained by loading the specimen axially from the bottom with a loading area equal to that of the specimen; a Bellofram is used to seal the axial loading piston. Axial compression or tension is applied by use of a double acting 4 in. diameter Bellofram piston. Radial pressure is obtained by filling the chamber with silicone oil and applying air pressure to it through a Bellofram piston interface.

A pneumatic timer control unit was developed for the system consisting of four pneumatic timer elements and functioning as shown schematically in Fig. D-5. Two elements are activated at the start of the cycle and provide signals of duration t_1 and t_2. Signal t_1 represents the "on-time" signal to either the axial or radial loading system while t_2 introduces a delay time prior to the activation of a third

ClibPDF - www.fastio.com

element. This element provides an "on" signal of duration t_3 to the second loading element. The fourth timer controls the off-load of the system. Times t_1 to t_4 are adjustable from essentially zero to approximately 30 seconds.

Output signals from the timer involve only a small line flow of air, insufficient to operate large air valves. Therefore a booster system was required as shown in Fig. D-6. Using this approach and maintaining short flow distances from air reservoirs to the loading pistons, rise times (time from zero to full load) could be reduced to 0.007 seconds. Where longer load rise times were required, needle valves were introduced to the system to control the air flow rates. Due to limitations imposed by valve response times, the minimum load duration which could be obtained was 0.035 sec.

This equipment was also used for creep tests. For these tests the timer portion of the repetitive loading system was replaced by a digial clock rading to 0.01 min. The main air valves were operated using electric solenoid valves. A main switch activated the solenoid valves and timer simultaneously. System components are shown schematically in Fig. D-7. Use of high air pilot pressures resulted in rapid valve response times with the result that load rise times were less than 0.01 sec. in all tests. Loading times less than one minute were measured using the timer portion of the Sanborn recorder system while times greater than one minute were established from the digital clock.

Deformations in the specimens were measured using linear variable differential transformers (LVDT's) firmly attached to the specimens.

ClibPDF - www.fastio.com

Test Procedures.

Repeated Loading. While many different loading conditions exist in the pavement structure, only three have been chosen for study in the laboratory in part because of limitations of the pneumatic loading equipment to completely simulate the actual conditions. The conditions include:

(1) midway between the loaded areas, horizontal compression (extension tests)

(2) near the point of zero horizontal stress (unconfined compression tests)

(3) at the base of the layer, axial tension and radial compression, both having the same loading time (tension tests)

Due to the time dependent recovery properties of asphalt concrete, the amount of permanent deformation measured would be expected to depend on the time interval between load applications. In preliminary tests it was observed that deformation recovery approached zero at a cycle time of 6 seconds. This value was selected for use in the study.

Table D-1 contains a summary of the tests computed to date.

Creep Loading. Prior conditioning influences the response of asphalt concrete in creep loading. In this study the procedure adopted includes the application of a stress of larger magnitude than that to be used in tests for a period of 10 min. followed by two repetitions of the desired stress applied for a period of 15 min. Recovery times of 1 to 1.5 hours were allowed between each load application. Deformations from the second

ClibPDF - www.fastio.com

TABLE D1

SUMMARY OF REPETITIVE LOAD TEST CONDITIONS

Specimen Number	Temperature °F	Axial Stress psi	Radial Stress psi	Axial Load Time sec	Radial Load Time sec
7	67	0	-80.	--	0.12
8	67	0	-80.	--	0.040
17	67	0	-80.	--	0.040
18	67	0	-80.	--	0.267
12	67	50.0	- 2.5	0.126	0.126
13	67	50.0	- 2.5	0.293	0.293
14	67	50.0	- 2.5	0.075	0.075
15	67	50.0	- 2.5	0.075	0.074
16	67	50.0	- 2.5	0.075	0.076
64	67	-57.5	0	0.116	--
65	67	-57.5	0	0.224	--
68	67	-43.1	0	0.421	--
23	85	0	-60.	--	0.084
24	85	0	-60.	--	0.049
26	85	0	-60.	--	0.049
27	85	0	-60.	--	0.133
56	85	22.2	0	0.292	--
59	85	22.2	0	0.237	--
60	85	22.2	0	0.140	--
61	85	22.2	0	0.140	--
62	85	26.3	0	0.142	--
63	85	26.3	0	0.142	--
51	85	-25.0	0	0.077	--
52	85	-34.6	0	0.097	--
53	85	-25.0	0	0.129	--
54	85	-25.0	0	0.274	--
42	100	0	-30.	--	0.079
43	100	0	-15.	--	0.081
44	100	0	-15.	--	0.126
45	100	0		--	0.083
47	100	0	-15.	--	0.200
32	100	9.0	- 2.0	0.074	0.077
33	100	9.0	- 2.0	0.081	0.077
34	100	9.0	- 2.0	0.148	0.152
35	100	9.0	- 2.0	0.155	0.152
36	100	9.0	- 2.0	0.246	0.243
37	100	9.0	- 2.0	0.238	0.243
40	100	14.0	- 3.0	0.154	0.154
41	100	14.0	- 3.0	0.155	0.154
46	100	-19.75	0	0.112	--
48	100	-14.5	0	0.114	--
49	100	-15.4	0	0.226	--
50	100	-15.4	0	0.089	--

ClibPDF - www.fastio.com

or third application are used for computation of compliance relationships. The two loading conditions utilized are:

(1) unconfined axial compression

(2) axial extension

Table D-2 contains a summary of the tests conducted in this series.

TABLE D2

SUMMARY OF CREEP TEST CONDITIONS

Specimen Number	Temperature °F	Load Type	Cycle 1		Cycle 2		Cycle 3	
			Stress psi	Duration min	Stress psi	Duration min	Stress psi	Duration min
67	67	Axial Comp	23.2	15	36.8	15		
70	67	Axial Comp	36.8	20	23.2	20		
73	67	Extension	30.0	15	15.0	15		
74	67	Extension	21.6	10	9.5	15		
75	85	Axial Comp	20.5	10	10.5	15	9.5	15
77	85	Axial Comp	21.8	10	10.5	15	10.5	15
76	85	Extension	12.0	10	8.0	15	8.0	15
80	100	Axial Comp	8.8	10	5.3	15	5.3	15
81	100	Axial Comp	8.9	10	5.3	15	5.3	15
82	100	Extension	7.1	10	3.0	15	3.0	15

ClibPDF - www.fastio.com

Clib PDF - www.fastio.com

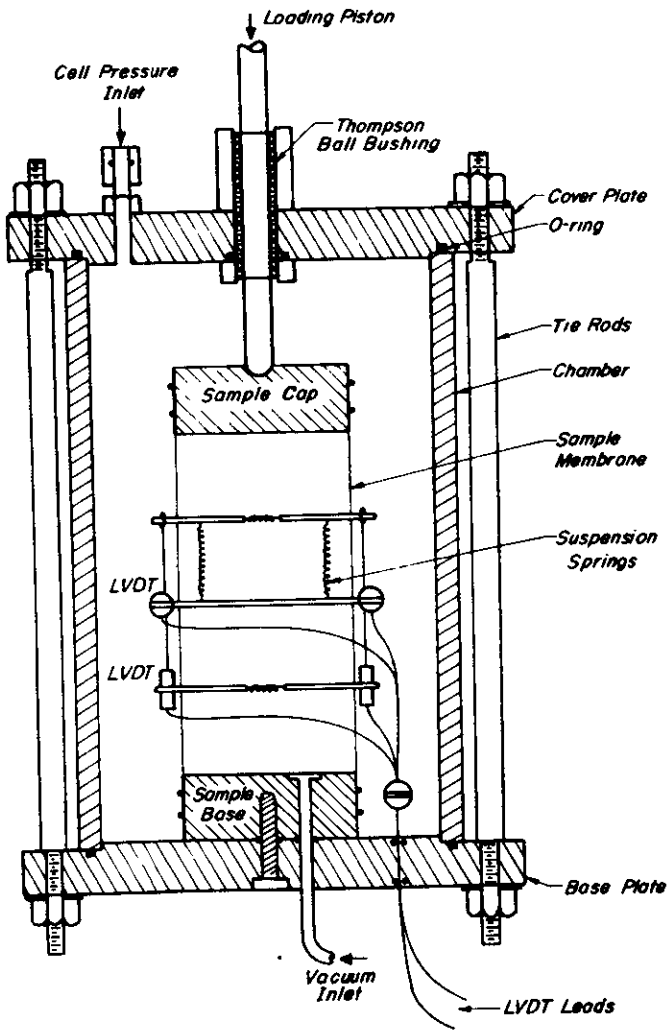

Fig. D1 – Apparatus for repeated load test of soil.

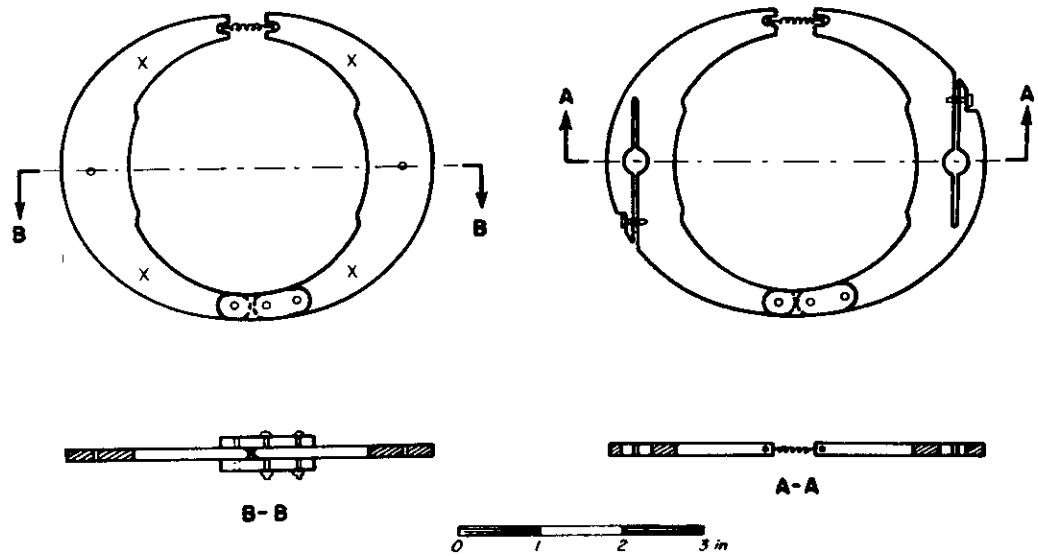

Fig. D2a – LVDT clamps for axial strain measurement.

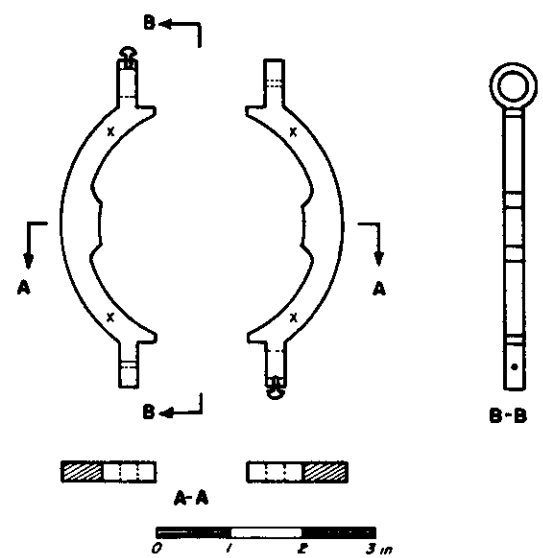

Fig. D2b – LVDT clamps for radial strain measurement.

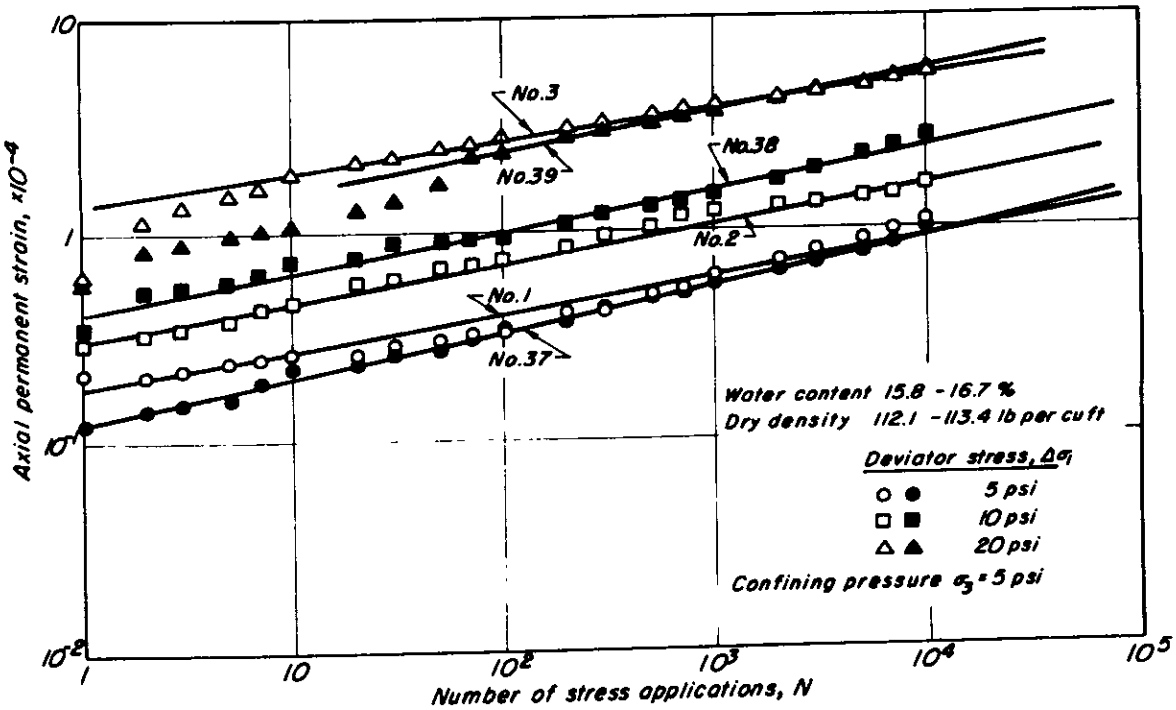

Fig. D3 – Axial permanent strain vs. number of stress applications, Ygnacio Valley subgrade soil.

ClibPDF - www.fastio.com

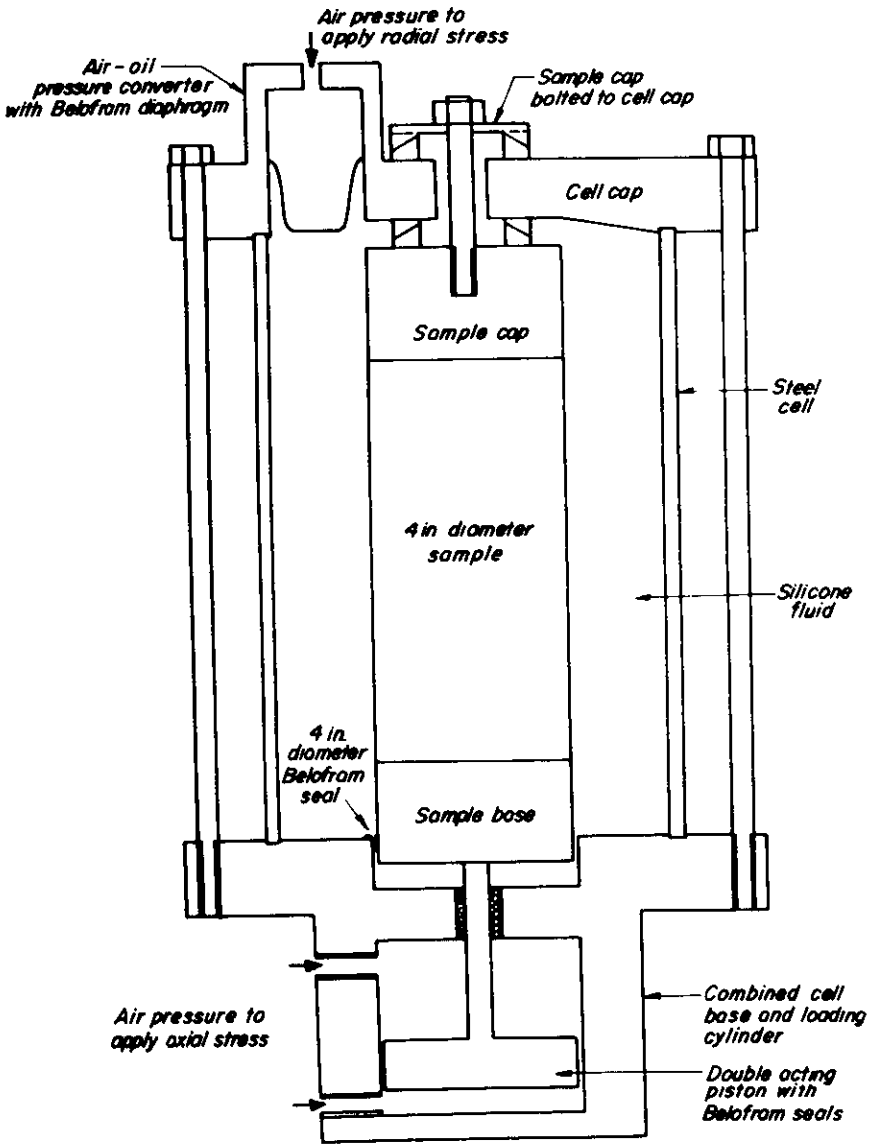

Fig. D4 — Triaxial apparatus permitting independent variation of axial and radial stresses.

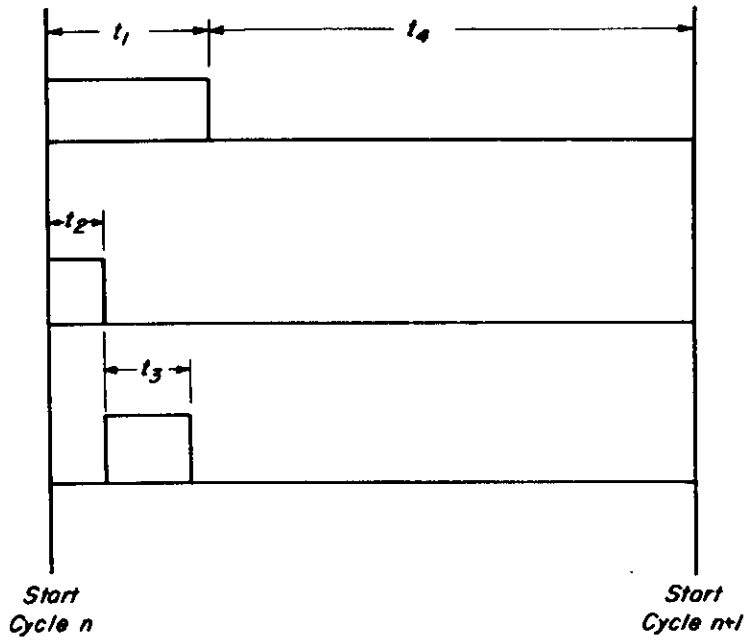

Cycle time = $t_1 + t_4$

$t_2 + t_3 \leq t_1$

Fig. D5 — Timer signal outputs.

ClibPDF - www.fastio.com

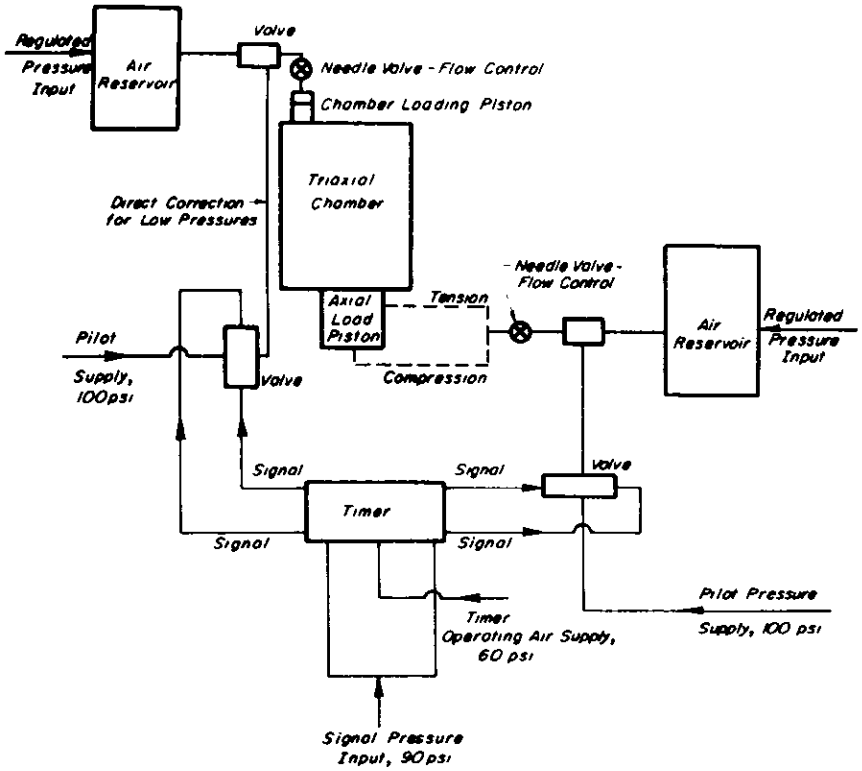

Fig. D6 — Schematic diagram of triaxial loading system for repetitive loading tests.

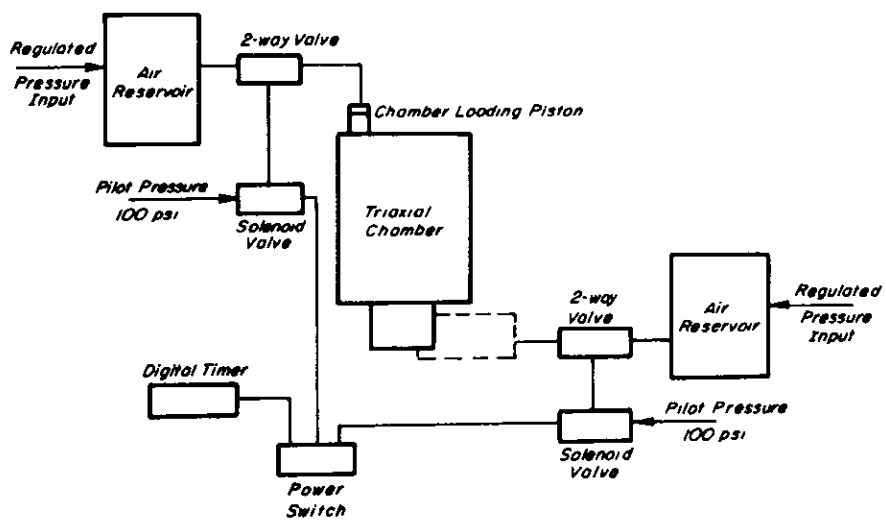

Fig. D7 — Schematic diagram of triaxial loading system for creep tests.

ClibPDF - www.fastio.com